ASPECTS OF THE SYNTHESIS AND CHARACTERIZATION OF DIAMOND AND DIAMOND LIKE CARBON FILMS

Thèse présentée à la Faculté des Sciences

Institut de Microtechnique

Université de Neuchâtel

Pour l'obtention du grade de docteur ès Sciences

Par

Paul Alers

Acceptée sur proposition du jury :

Mme M. Koudelka-Hep,

MM. N. de Rooij (directeur de thèse),

D. Pavuna (EPF Lausanne) et

H. Keppner (HES-ARC Le Locle)

Soutenue le 26 Juin 2007

Université de Neuchâtel

2007

Université de Neuchâtel

FACULTE DES SCIENCES
Secrétariat-Décanat de la faculté
- Rue Emile-Argand 11
- CP 158
- CH-2009 Neuchâtel

IMPRIMATUR POUR LA THESE

Aspects of the synthesis and characterization of diamond and diamond like carbon films

Paul ALERS

UNIVERSITE DE NEUCHATEL

FACULTE DES SCIENCES

La Faculté des sciences de l'Université de Neuchâtel,
sur le rapport des membres du jury

Mme M. Koudelka-Hep,
MM. N. de Rooij (directeur de thèse),
D. Pavuna (EPF Lausanne) et
H. Keppner (HES-ARC Le Locle)

autorise l'impression de la présente thèse.

Neuchâtel, le 23 août 2007

Le doyen :
T. Ward

UNIVERSITE DE NEUCHATEL
FACULTE DES SCIENCES
Secrétariat-décanat de la faculté
Rue Emile-Argand 11 - CP 158
CH-2009 Neuchâtel

■ Téléphone : +41 32 718 21 00 ■ Fax : +41 32 718 21 03 ■ E-mail : secretariat.sciences@unine.ch ■ www.unine.ch/sciences

Mots clés : diamant, DLC, diamond like carbon, carbone, flamme, acétylène, déposition, torche, dépôt, couche mince, tribology, spectroscopie Raman, filament chaud, micro onde, pulsed laser arc, vide, Grüneisen, expansion thermique

Key words : diamond, DLC, diamond like carbon, carbon, flame, acetylene, deposition, torch, coating, thin film, tribology, Raman spectroscopy, Hot Filament, Microwave, pulsed laser Arc, Vacuum, Grüneisen, thermal expansion

Summary

The present thesis is the result of 15 years of continues efforts. The research work started in 1991 and has been completed by a final publication in 2005. The content of the thesis is composed of introductory parts (giving the reader an introduction into the later to be discussed subject) and articles published by the author.

At this point the author would like to draw the attention to the fact that, due to the rather lengthy process of completion of the presented thesis, the references in the first chapters have not been updated with recent new publications on the subjects discussed and therefore reflect the knowledge state at the time the articles were written.

The key subject of the thesis is carbon materials. In order to initiate the reader into the subject to be discussed in the publications of the author, introductory chapters are found at the beginning of the present document.

In the first chapter an historical overview on diamond and DLC is given. The history of diamond, starting with natural diamond and continuing with man made diamonds, is treated and examples of applications of diamond are described. Equally the history of Raman spectroscopy, an analysing method intensively used by the author, is presented.

After the historic introduction, more technical background information is offered on the following subjects:

- Carbon structure and properties.
- Raman spectroscopy.
- Diamond & DLC deposition methods

Following these introductory chapters the scientific work accomplished by the author is presented. This is done introducing the different scientific articles published by the author.

The first article deals with the deposition of diamond using the acetylene flame method. The key innovation presented by the author in this article is the use of a turbulent flame configuration, as the first researcher in this field, which allows for a quicker growth rate of the diamond deposit.

The second article demonstrates the influence of flame turbulence on the growth of mono crystalline diamond. The work presented here is one of the first studies demonstrating the influence of flame morphology on single crystal diamond growth a compared to other deposition parameters such as gas composition, substrate to flame distance and seed crystal orientation.

The third article discusses the interaction of synthetic diamond layers with molybdenum. The interest of this study lies in the potential use of molybdenum as an electrical contact electrode on diamond, as well as in the use of molybdenum as a nucleation initiating substrate for diamond deposition.

The contribution in the fourth and fifth article by the author is in the field of Raman spectroscopy analysis of amorphous carbon films. The paper is a contribution to the, at that time of publication, ongoing work in different international research group aiming at understanding how to use Raman spectroscopy to interpret the structure and composition of carbon materials. In the most recent publication in this thesis, one can see that the results of this research is still being actively used when characterising carbon layers.

Article number six deals with a new innovative method, discovered by the author, which allows to characterize the thermal expansion behaviour of diamond using Raman spectroscopy. The importance of this innovation lies in the fact that the measurement of the thermal expansion of diamond, which is quite difficult using conventional methods, is greatly simplified using the method proposed by the author.

In the last article presented in this thesis the influence of vacuum on the friction and wear properties of carbon films is studied. It is demonstrated that carbon films having good friction and wear properties under atmospheric conditions can degrade quickly when exposed to vacuum. The study has an direct impact on the use of such coatings in for instance satellites or high vacuum production tools.

After the above mentioned presentation of the scientific work accomplished by the author during his thesis, a conclusion and outlook is presented to the reader.

Résumé

La présente thèse est le résultat de 15 ans d'efforts continus. Débuté en 1991, le travail de recherche s'est achevé en 2005 avec une publication finale. Le contenu de la thèse est composé de parties introductives - pour offrir au lecteur une entrée en matière sur le sujet à traiter ultérieurement - et d'articles publiés par l'auteur.

A ce stade, l'auteur souhaiterait attirer l'attention sur le fait qu'en raison du processus d'achèvement assez lent de la présente thèse, les références des premiers chapitres n'ont pas été mises à jour, après les récentes publications de travaux concernant les sujets abordés. Par conséquent, ils reflètent l'état des connaissances à l'époque où les articles ont été écrits.

Le carbone est le sujet-clé de la thèse. Dans le but d'initier le lecteur aux sujets traités dans les publications de l'auteur, on trouvera des chapitres introductifs au début du présent document.

Le premier chapitre offre une vue panoramique sur l'histoire du diamant et du DLC. Il traite de l'histoire du diamant, qui débute avec le diamant naturel, et continue avec le diamant de synthèse et la description d'exemples d'application du diamant. L'histoire de la spectroscopie Raman, méthode d'analyse intensivement utilisée par l'auteur, est présentée selon le même schéma.

Après l'introduction historique, une information à toile de fond plus technique est offerte sur les sujets suivants :

- Structure et propriétés du carbone
- Spectroscopie Raman
- Méthodes de déposition de diamant et de DLC

Suite à ces chapitres introductifs, le travail scientifique accompli par l'auteur est présenté avec les différents articles scientifiques qu'il a publiés.

Le premier article traite de la déposition du diamant avec l'utilisation de la méthode de la flamme acétylène. L'innovation clé présentée par l'auteur dans cet article en tant que premier chercheur dans ce domaine, est l'utilisation d'une configuration de flamme turbulente, ce qui permet une vitesse de croissance plus rapide de la déposition de diamant.

Le deuxième article démontre l'influence de la flamme turbulente sur la croissance du diamant mono-cristallin. Le travail présenté ici est l'une des premières études établissant l'influence de la morphologie de la flamme sur la croissance du diamant à cristal unique, comparée à d'autres paramètres de déposition tels que la composition du gaz, la distance entre le substrat et la flamme, et l'orientation du substrat cristallin.

Le troisième article traite de l'interaction des couches de diamant synthétique avec le molybdène. L'intérêt de cette étude réside dans l'utilisation potentielle du molybdène comme électrode de contact électrique, aussi bien que dans l'utilisation de la nucléation pour initier le substrat à la déposition de diamant.

Dans les quatrième et cinquièmes articles, l'auteur apporte sa contribution dans le domaine de l'analyse spectroscopique Raman des couches de carbone amorphe. A l'époque de sa publication, l'article a contribué au travaux en cours de différents groupes de recherche internationaux cherchant à comprendre comment utiliser la spectroscopie Raman pour interpréter la structure et la composition des matières carbones. Dans les plus récentes publications de cette thèse, on peut voir que les résultats de cette recherche sont toujours utilisés activement pour caractériser les couches de carbone.

L'article numéro six traite de nouvelles méthodes innovatrices découvertes par l'auteur, ce qui permet de caractériser le comportement d'expansion thermale du diamant en utilisant la spectroscopie Raman. L'importance de cette innovation réside dans le fait que la mesure de l'expansion thermale du diamant - relativement difficile avec l'utilisation des méthodes conventionnelles - est largement simplifiée avec la méthode proposée par l'auteur.

Dans le dernier article présenté dans cette thèse, l'influence du vide sur les propriétés de frottement et d'usure des films de carbone est étudiée. Il est démontré que les films de carbone dotés de bonnes propriétés de frottement et d'usure dans les conditions atmosphériques peuvent se dégrader rapidement en cas d'exposition au vide. L'étude a un impact direct sur l'utilisation de tels films, par exemple sur les satellites ou pour la production d'outils pour le vide profond.

Une conclusion et une perspective sont présentées au lecteur, suite à la présentation sus-mentionnée du travail scientifique accompli par l'auteur durant sa thèse.

Preface

The present Thesis is in more then one way unique. The research started in 1991, year in which the Author came to the CSEM (Swiss Centre for Electronics and Microtechnology) as a PhD student after having completed his Chemical engineering studies in the Netherlands.

The research presented in this thesis started at the CSEM in Neuchâtel, Switzerland. The author integrated here in 1991 the Diamond & DLC research group with a key responsibility in the field of Flame diamond deposition and Raman spectroscopy analysis. During the first 3 years, the Author concentrated on the synthesis of mono crystalline diamond using acetylene flame deposition. After 3 years he transferred to the CSEM material analysis department and specialized in Raman spectroscopy.

In this first part of the thesis the major part of research with its resulting publications was completed (publications from 1992-1995). The year 1996 marked the start of what became an extended interruption of the present thesis. In 1996 CSEM Instruments was founded as a spin-off from CSEM. CSEM instruments specializes in the surface mechanical material analysis with instruments measuring the hardness, adhesion, friction and wear properties of surfaces and coatings. The author joined this spin-off as Marketing & Sales manager and joint stockholder of the new company.

The first years of this newly founded company were marked by rapid growth and the implementation of a world wide network of agents and distributors. During this period the author remained active in the scientific field, both by publications as well as by Scientific talks at conferences & client sites (clients of CSEM Instruments are mainly Universities and international research centres). Work produced during this period included research in the field of automotive paint [1] as well as plasma surface treatment methods for tools [2]. During the start of this period (1996-1998) the main part of the thesis document has been written.

In 2003 the author changed from CSM instruments (name changed in 2001) to Vacotec a vacuum equipment manufacturer. In Vacotec the author assumed the function CEO and frequently worked on scientific equipment projects with various Swiss universities. During this period the author decided to complete the present thesis with a new publication related to the prior published work [3]. The scientific work for this publication has been accomplished in a collaboration between Vacotec (la Chaux de Fonds, Switzerland), CSM Instruments (Peseux, Switzerland), the CAFI (le Locle, Switzerland) and the FEMTO-ST/CREST (Montbéliard, France).

Due to a further change of employment at the start of 2005 (the author joined atelier Busch a world wide leading manufacturer of vacuum pumps) a final short interruption of the presented thesis intervened. The present document does reflect this long working process and therefore the references and

scientific findings of especially the first part of this work have to be considered in their historical context.

Finally, the author would like to thank all friends, relatives but especially his wife and 3 daughters for there continues support, helping him to complete the present thesis after over 15 years of more or less continuous effort.

[1] Ulrich Schulz, Volker Wachtendorf, Thomas Klimmasch and Paul Alers, **“**The influence of weathering on scratches and on scratch and mar resistance of automotive coatings”, *Progress in Organic Coatings*, *Volume 42, Issues 1-2*, *June 2001*, *Pages 38-48.*

[2] F. Sanchette, E. Damond, M. Buvron, L. Henry, P. Jacquot, N. Randall and P. Alers**, “**Single cycle plasma nitriding and hard coating deposition in a cathodic arc evaporation device”, *Surface and Coatings Technology*, *Volumes 94-95*, *October 1997*, *Pages 261-267.*

[3] C.Meuniera, P.Alers, L.Marot ,J.Stauffer ,N.Randall ,S.Mikhailov **,** **“**Friction properties of ta-C and a-C:H coatings under high vacuum”, *Surface & Coatings Technology 200 (2005) 1976–1981.*

Table of content

1 Introduction

1.1 Historical overview

Diamond is a fascinating material [1]. It is composed solely of carbon, owing to its crystalline structure, it has many exciting properties. Throughout the history of mankind the beauty of a well-polished diamond gem has provided admiration, and as a result of its great value, it has also revealed less desirable aspects of the human character. The larger diamond gems often have a personal history and a famous name (e.g. Koh-I-Noor, Cullinan, Hope) and can be classed as part of the national heritage of a country.

Koh-I-Noor

Cullinan

Hope

Natural diamond has colours ranging from brown through all kinds of shades of yellow and grey to pure white (colourless). The price of a diamond is closely related to its colour; true white being the most valuable. Other important factors determining its value are its weight, cut and flawlessness. The weight of a diamond is expressed in carat (1 CRT equals 0.2 gram) and the cost per carat increases exponentially with the total weight of the diamond.

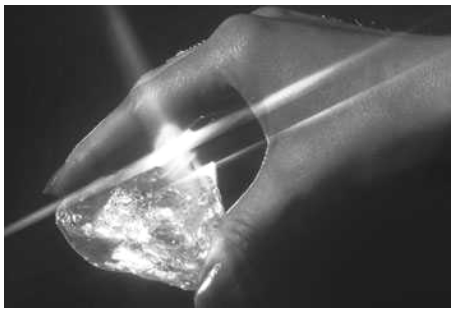

Star of Sierra Leone, rough diamond

Diamond polishing

In the crystalline diamond structure each carbon atom has four covalent bonds to four other carbon atoms in a tetrahedral network. Owing to this structure and its short and very strong carbon-carbon bonds, diamond is extremely hard, and has a high refractive index. It also has a wide range of (optical) transparency and a very high thermal conductivity [4,5]. All these properties make diamond a beautiful gem but also accounts for the great number of technical applications that have emerged.

The annual consumption of industrial diamond is about 100 tons and is used mainly for drilling, sawing and grinding of hard materials [6]. Other technical applications include surgical blades, optical components, high-pressure anvils and heat sinks for electronic chips and power devices. The major volume of the diamond used in industrial applications comes from either natural sources, or manmade synthetic material from high-pressure high temperature cells.

Diamond mine, owned by De Beers in South Africa

There are other technical applications for other forms of carbon, e.g. graphite and the recently discovered form of Buckminster fullerene. Graphite is the most stable form of crystallised carbon and it is often used for its electronic properties and high temperature stability. The non-crystalline forms of solid carbon are also well known. They range from natural materials such as charcoal and soot, to specially prepared materials such as amorphous carbon, glassy carbon and diamond-like-carbon (DLC).

In industry diamond-like-carbon has been readily applied. The mechanical properties, i.e. hardness and toughness can be very close to those of natural diamond. Furthermore DLC can be readily deposited on large areas as a thin protective layer, using synthesis methods developed over the last 10-15 years. Although diamond, using recently developed synthesis techniques, can now also be deposited as a thin layer, DLC is still the industry favourite due to its more reliable, simple and cost efficient production. Applications of DLC range from coatings on machine tools and

bio-compatible layers on medical implants, to decorative “anti scratch” finishing of furniture parts and sun glasses.

1.1.1 The history of diamond synthesis

Nature itself performed the earliest synthesis of diamond about several billion years ago. The dating of diamonds is done by analysing inclusions within the crystals. The oldest, thus classified diamonds are dated to be about 3.2 billion years old, which is almost three quarters of the age of the earth. The process of natural diamond synthesis is not fully understood, but it is deducted that it took place about 100 to 150 km deep in the earth’s mantle. At this depth stable conditions for diamond growth are supposed to be present (pressures of about 50 Kbar at temperatures of approx. 1200°C). The growth rate of diamond under these conditions is rather slow and owing to environmental changes during this process, changes in impurity inclusions can be observed in bigger natural diamonds. The source of carbon needed for the growth of diamond is also still unclear but might have been carbon dioxide, methane or graphite dissolved in silicate magmas. The formed diamonds were then transported to the surface by volcanic activity and are therefore mainly found in old volcanic pipes of the kimberlite type.

It was at the end of the eighteenth century that it was found that diamond was constituted of pure carbon, and many attempts were then made to produce diamond from cheaper carbon sources. The most famous of these were those undertaken by Hannay and Moissan at the end of the nineteenth century. Hannay claimed to produce diamonds by heating iron pipes filled with a mixture of metallic lithium, paraffin and “bone oil distillate” to red heat during many hours. Although diamonds were detected, the results of these experiments could not be repeated by other scientists. It is thought that a laboratory assistant put some natural diamonds in one of the tubes in order to put a stop to such dangerous experiments. These often resulted in the explosion of the iron pipe upon cooling or dismantling. Moissan (who received in 1906 the Nobel price in chemistry for his work on fluorine and the electric arc) used molten ingots saturated with carbon. By quenching the ingots in cold water, Moisson hoped to raise enough pressure to produce diamonds. Some crystals where found after dissolving the iron but none of them still exist to confirm whether they were diamond using modern analytical methods. All attempts to reproduce these results have not succeeded, although other crystals such as silicon carbide and alumina where found.

In the first part of this century a better understanding of the diamond - graphite phase diagram, led in combination with other technical developments to a first suitable method of diamond synthesis. In 1953 the so called HPHT (High Pressure High Temperature) method was developed simultaneously at ASEA in Sweden, and at GE in the USA. The method mimics the formation of natural diamond formation using high pressure (60 Kbar) and high temperatures (1550°C). The HPHT method is now widely used, but the equipment and running costs of this process are high. Metal “catalysts” are used to make the production rate sufficiently high to make the process

economical. About 90% of all industrially used diamond is now produced by the HPHT method. These diamonds contain substantial quantities of metal and nitrogen impurities, which makes the stones unsuitable for jewellery. On the other hand the cost of producing gem stone quality using the HPHT process are too high to compete with natural stones. The largest Gem quality diamond produced so far using HPHT was produced in the De Beers Research laboratories in 1990. The stone, of a yellow brownish colour, and obtained after 500 hours of growth had a weight of 14.2 carat [7,8].

Both natural and HPHT diamonds are grown under conditions where diamond is the stable form of carbon. Attempts have been made beginning at the start of this century to produce diamond under conditions where graphite is normally the stable carbon species. The first successful attempt to produce diamond at pressures of 0.001 bar up to 100 bar were undertaken by Eversole in the second half of the 1950's. His process used a gaseous carbon source (e.g. methane) which he brought in contact with a natural diamond seed crystal at about 1000°C. The pyrolysis of the methane results in the deposition of diamond, but unfortunately also with the associated deposition of graphite. This graphite eventually covers the diamond seed with a film and no further deposition of diamond takes place. The graphite can be then removed by etching using hydrogen at about 50 bar. The resulting cyclic process has an extremely low growth rate of about 0.001μm/h, which makes the method totally uneconomical. A major breakthrough came by the work of Dryanguin, Spitsyn and co workers (USSR). Around 1968 they introduced the use of atomic oxygen species into the process, thus eliminating the need for a cyclic etch step. Although graphite is still deposited, it is preferentially etched away by the atomic oxygen. The higher growth rates of this process, about1μm/h, indicate that the atomic oxygen apparently also acts as a catalyst in the process. An even bigger advantage of this method lies in the fact that it became possible to grow diamond on non-diamond substrates. Thin, but closed, layers of diamond crystallites (1 - 10μm) were deposited on metals like copper or molybdenum and on silicon. Unfortunately these results were not taken seriously outside of the former USSR. Confirmation of the results of Spitsyn in 1982 by Matsumoto and co-workers (Japan) finally made the international scientific community woke up to the benefits of this new method. More than one hundred research groups world wide now are investigating low pressure diamond deposition by chemical vapour deposition (CVD) [2,3]. The large amounts of atomic oxygen needed in the process can be categorised by the method used to produce the atomic oxygen. The main techniques used are the Hot Filament, the microwave, the high power plasma torch and the combustion flame.

The CVD diamond process, was originally seen as a competitor to the HPHT process, has proven in fact useful for alternative applications. The process is too expensive to produce large quantities of diamond abrasive at a reasonable cost, so its applications lie in the special use of thin films deposited over large areas. Although no major economical breakthrough has so far been realised with the CVD diamond process, specialised applications in the cutting tool industry and in the field of diamond coated cantilevers for Atomic Force Microscopes have been introduced successfully. Diamond films are also used for protective windows in laser guided missile systems.

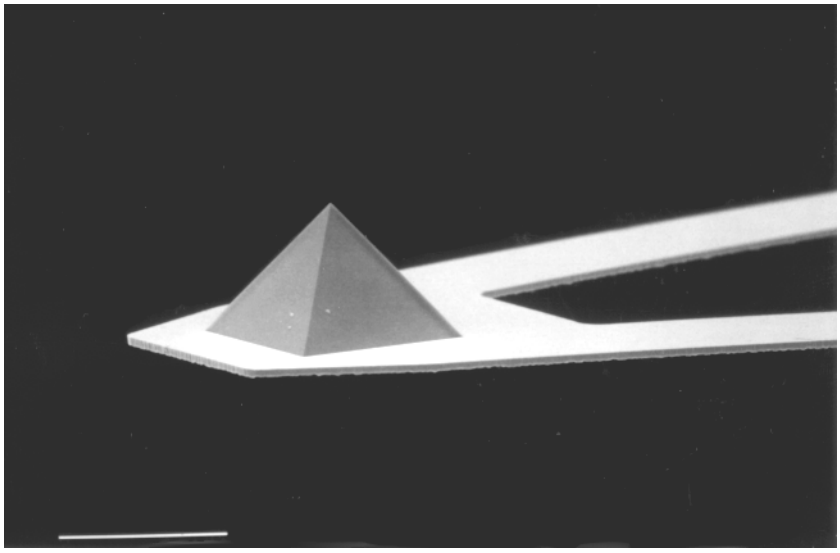

Diamond coated AFM cantilever (source: P Niederman, CSEM SA)

Further applications, using the diamonds high thermal conductivity, include heat sinks for semiconductor applications.

1.1.2 The History of DLC synthesis

Hard carbons based films, later called diamond like carbon (DLC), were reported as early as the last century. These films were usually considered as an incidental feature in plasma discharge and were also observed in acetylene welding [9]. The first systematic studies aiming at producing hard carbon films were reported by Aisenberg and Chabot in 1971 [10]. The deposition resulted from carbon ions produced in a carbon arc in an argon atmosphere. After confirmation of the results of Aisenberg and Chabot by Spencer et al. [11] a substantial rise of research in this field has resulted. Among the most active researches of the early days Holland (1976) and Weissmantel (1979) [12,13] are often cited. The scientific interest for these films is mainly due to their unusual structure and properties. These properties seem to be caused by an unusually large number of tetrahedral (sp^3) carbon-carbon bonds. The detailed film structure is still a subject for study.

Owing to the wide variety of deposition methods used for producing these DLC films they can vary substantially in their properties. These variations are mainly due to differences in structure. In order to classify these variations, Agnus [14] proposed grouping the films according to their gram atom number density, ρ_N, and their atomic composition.

The gram atom number density, ρ_N, is the total number of gram atoms per unit volume:

$$\rho_n = \frac{\rho_m}{\sum x_i A_i}$$

Where ρ_M is the mass density, x_i the atom fraction and A_i the atomic mass of element i. In general it can be stated that films with gram atom number densities greater than 0.2 g-atom/cm^3, are considered to be dense carbon films with diamond like properties. These films may contain hydrogen and can vary in their conductive properties, but are usually amorphous and hard. The hardness usually increases with increasing carbon ions energy impact during deposition.

In present literature these carbon films are being designated by the following nomenclature, amorphous carbon (a-C), hydrogen containing a-C (a-C:H) and metal containing a-C (a-C:Me). Diamond like carbon is part of the a-C and a-C:H group and is named like this owing to its high hardness, which approaches in some cases that of diamond.

Diamond like carbon, has unique properties such as a low friction coefficient combined with a high hardness and wear resistance. This combined with its relative ease of deposition, has helped DLC to find its way into modern industry. Applications ranges from wear protection on computer hard disks, coatings for drills and various tools, to medical prostheses.

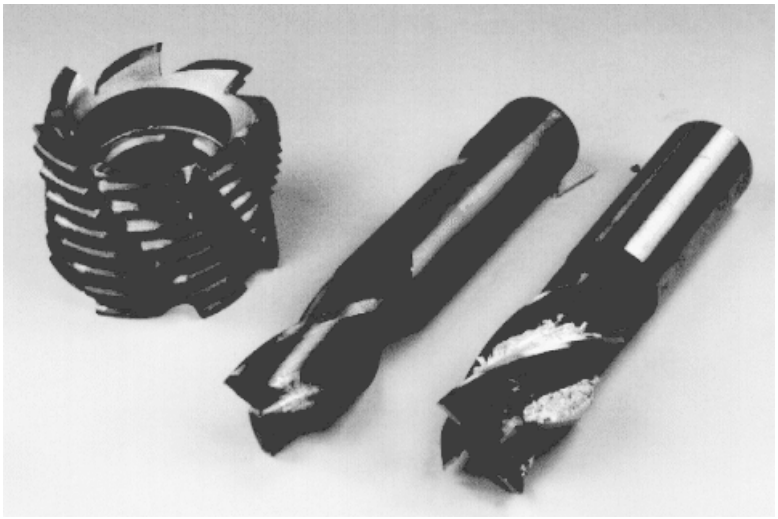

DLC coated drills (source: IWS-FHG)

1.1.3 The History of Raman spectroscopy

The Raman [15,16,17] effect is a vibrational spectroscopy phenomenon and provides information complementary to the IR spectroscopy method. The Raman effect was in fact predicted well before it was first observed and recognised. In 1878 Lommel described certain anomalies to be found in fluorescence, where the colour of the fluorescence depended on the nature of the sample and the exciting radiation used. He suggested the existence of bands with the frequency $\nu \pm \omega$, where ν is the frequency of the radiation source and ω a shift of this frequency due to a damped anharmonic oscillation. Applying quantum mechanics on a molecular level, the

Raman effect was also predicted by Smekal (1923), Kramers and Heisenberg (1925), Schrödinger (1926) and Dirac (1927).

Raman finally confirmed the effect, when his co-workers Krishnan and Vekateswaran detected 'modified scattering' of sunlight, on February 7th, 1928. Raman attributed this result immediately to the Kramers-Heisenberg effect and cabled a short article entitled 'A new type of secondary radiation' to Nature on February 16th, 1928. He received the Nobel price of physics for 'his work on the diffusion of light and for the discovery of the effect which bears his name' on December 11th, 1930.

The polarazibility theory, proposed by Placzek (1934), helped many physicists realise that the Raman effect had a great potential as a tool for qualitative and quantitative analysis and for the determination of molecular and crystalline structures. Up to about 1950, the year when "easy to use" scanning IR spectrometers were introduced, Raman remained more popular then IR for research. After this IR became the choice for routine laboratory analysis. Raman spectroscopy has however undergone a revival again owing to a number of technical improvements. The most important being the Laser, which provided a truly monochromatic high intensity light source for excitation, invented by Maiman in 1960. A further important improvement comes from the use of new detector's (cooled CCD (charged camera device) arrays) and the use of scanning grating spectrometers in combination with holographic laser rejection filters, D.N. Batchelder 1989. The recent addition of near infra red laser radiation sources has furthermore eliminated the problems occurring from high fluorescence levels of certain materials in the visible and UV light range.

Although, for the moment, many more IR spectrometers exist in standard analysis laboratories than Raman spectrometers, an increasingly important role for the latter is foreseeable, as the price improves.

1.1.4 Reference

[1] G. Davies, "Diamond", Adam Hilger Ltd, Bristol (1984). G. Davies, in « Chemistry and Physics of Carbon », vol 13, P.L.

[2] Walker and P.A. Thrower (eds.), Marcel Dekker, New York, 1977, pl. R.C. DeVries, « Synthesis of diamond under metastable conditions », Ann. Rev. Mater. Sci., 17 (1987) pl61.

[3] W.J.P. van Enckevort, "Physical, chemical and microstructural characterization and properties of diamond" in "Synthetic diamond: emerging CVD science and technology", K.E. Spear and J.P. Dismukes (eds.), John Wiley and Sons, (1994) p307.

[4] J.E. Field (ed.), "The properties of natural and synthetic diamond", Academic Press, London (1992).

[5] J.E. Field (ed.), “The properties of diamond”, Academic Press, London (1979).

[6] M. Seal, “Diamonds in science”, Interdisc. Science Rev., 14 (1989) p64.

[7] J.E. Shighley, E. Fritsch, C.M. Stockton, J.l. Koivula, C.W. Fryer and R.E. Kane, « The gemological properties of the Sumitomo gem-quality synthetic yellow diamonds », Gems&Gemology, 22 (1987) pl92.

[8] J.E. Shighley, E. Fritsch, C.M. Stockton, J.l. Koivula, C.W. Fryer, R.E. Kane, D.R. Hargett and C.W. Welch « The gemological properties of the De Beers gem-quality synthetic diamonds », Gems&Gemology, 23 (1987) pl87.

[9] Schmellenmeier, H., Z. *Phys. Chem.,* 205, 349, 1955/56.

[10] Aisenberg, S. and Chabot, R.., *J. Appl. Phys.,* 42, 2953, 1971.

[11] Spencer, E. G., Schmidt, P. H., Joy, D. C., and Sansalone, F. J., *Appl. Phys. Lett.,* 29, 118, 1976.

[12] Holland, L. and Ojha, S. M., *Thin Solid Fi/ms,* 38, L17, 1976.

[13] Weissmantel, C., Schurer, C., Frohlich, R., Grau, P., and Lehmann, H., *Thin solid Films, 61,* L5, 1979.

[14] J.C. Agnus, P. Koidl and S. Domitz, “Carbon Thin Films”, in “Plasma deposited thin films”, CRC Press, 1986, ISBN 0-8493-5119-7

[15] JR Ferrarv and K Nakamoto, “Introductory Raman Spectroscopy”, Academic Press, 1994, ISBN 0-12-253990-7

[16] B Schrader, “Infrared and Raman Spectroscopy: Methods and Applications”, VCH, 1995, ISBN 3-527-26446-9

[17] NB Colthup, LH Daly and SE Wiberley, “introduction to infrared and Raman Spectroscopy”, Academic Press, 1990, ISBN 0-121-82554-X

1.2 Carbon materials

In this chapter the author would like to give an overview of the most common carbon materials. Their structure and properties as well as their nomenclature will be discussed. Only materials composed of pure carbon will be described, in order to help the reader to understand better the two forms of carbon (diamond and diamond like carbon) which are the subjects of this thesis.

Carbon [1] is the 6 Th element in the periodic table. It is rarely present as a single atom and usually found in association with other atoms. The properties of this "associated" bulk of atoms depend on the nature of the atoms present and on the nature of their physical and/or chemical interactions. The physical interactions are the van der Waals forces, which attract atoms if they are close enough and repulse them when further away. The chemical interaction is the bonding between atoms. For the case where only carbon atoms are present these physical and chemical interactions will determine the properties of the resulting material. For example, in the case of soot, a carbon material produces for instance in a match flame, the nature of interaction is mainly physical and the resulting material is soft and loosely held together. The opposite of this example is diamond, which has only chemical interactions and is hard and tough.

Between these two extremes, soot and diamond, most other pure carbon materials have a mixture of physical and chemical interactions between their carbon atoms, and offer therefore a wide variety of resulting properties. The different carbon materials can however be devised in two groups referring to their structure, crystalline and amorphous.

1.2.1 Crystalline carbon materials

Crystalline carbon materials are highly structured forms of carbon. Their structure is mainly chemically bonded and resulting materials have defined physical and chemical properties. Their crystalline matrix is composed of the two stable carbon bonding orientations, sp_2 and sp_3 (fig 1).

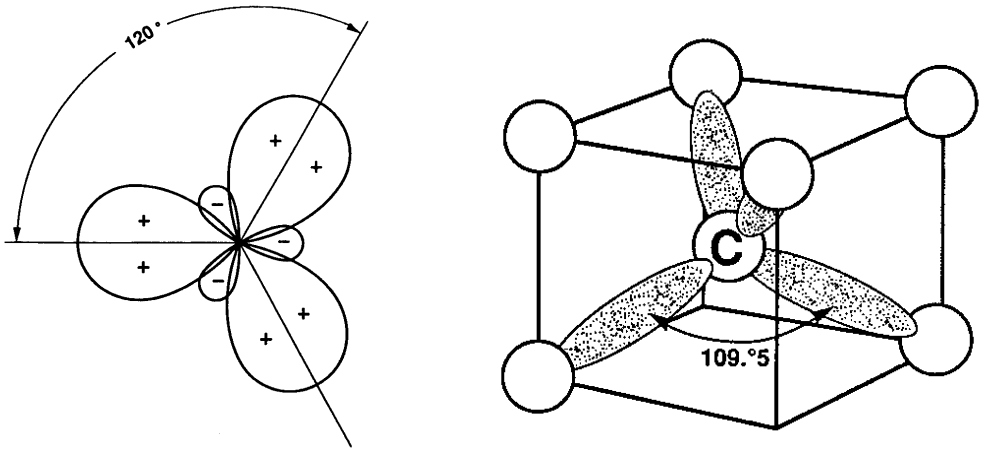

Figure 1 Bonding structures of carbon (left sp_2, right sp_3)

Graphite is a sp_2 bonded form of carbon. It is composed of planes of sp_2 bonded carbon held together by van der Waals forces (fig 2).

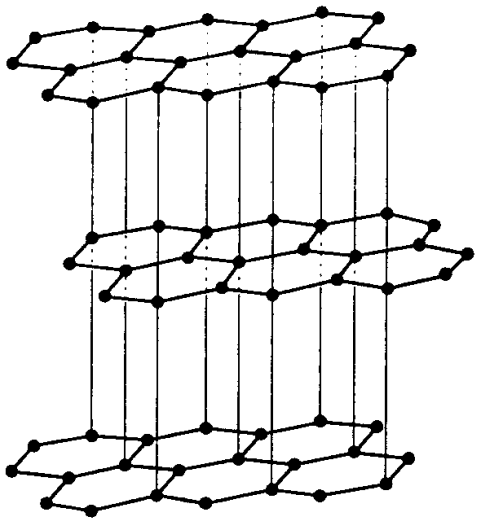

Figure 2 Graphite structure.

The graphite crystal has a hexagonal structure.

Diamond has a sp_3 bonding structure. Its structure also presents planes, which are in this case chemically bonded (fig 3).

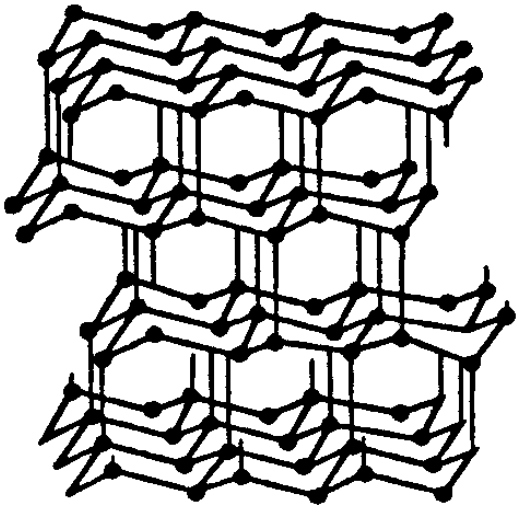

Figure 3 Diamond structure

The crystalline structure of diamond includes the cubic, octahedron, dodecahedron and more complicated forms. The crystalline planes of a simple cubic diamond crystal are shown below (fig 4).

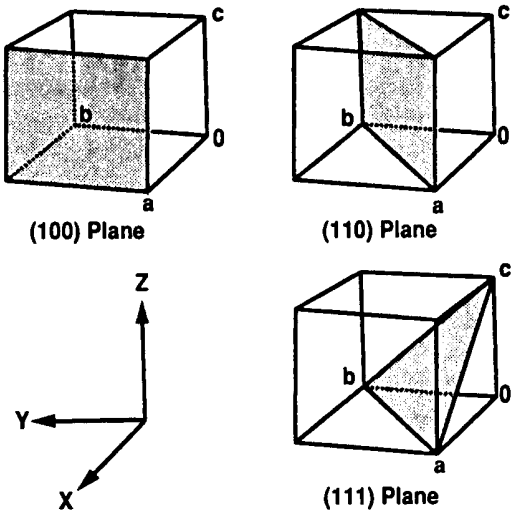

Figure 4 The indices of some simple planes in a cubic diamond crystal.

The simple planes shown above correspond to the three major crystal forms of diamond: the {100} cubic, the {110} dodecahedral and the {111} octahedral (fig 5).

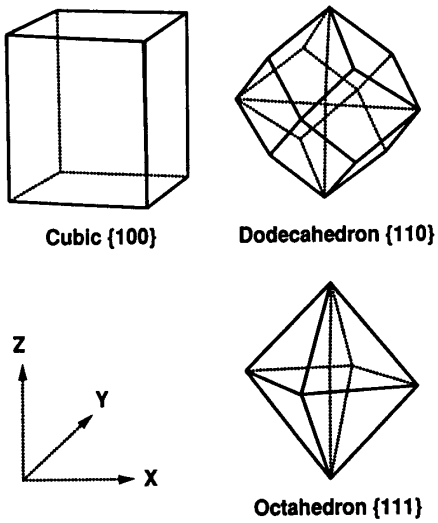

Figure 5 The major crystal forms of diamond.

In CVD diamond, the {111} octahedral and the {100} cubic surfaces predominate and cubo-octahedral crystals combining both of these surfaces are commonly found.

1.2.2 Amorphous carbon materials

By amorphous forms of carbon materials the authors mean, apart from soot, the technical forms of carbon indicated by a-C, a-C:H and a-C:Me. These terms stand for amorphous carbon (a-C), hydrogen containing a-C and metal containing a-C. In general DLC is part of the a-C (produced by solid carbon targets) or a-C:H (using hydrocarbon sources) group.

In the case of a-C DLC, the structure consists of a sizeable portion of small (5-10 nm) sp_3 (diamond) bonded carbon crystals combined with amorphous areas. The hydrogen content of these materials is less than 1 atomic percent.

Hydrogenated DLC (a-C:H) contains up to 50 atomic percent of hydrogen. Its structure is essentially amorphous with isolated clusters of sp_2 (graphite) and few sp_3 (diamond) bonded areas.

1.2.3 Properties of diamond and DLC

The main physical properties of diamond and DLC are presented in the table below.

Property	Natural Diamond	CVD Diamond	DLC
Density, g/cm^3	3.515	3.40 ± 0.10	1.8 –2.8
Thermal conductivity at 25°C, W/m.K	2200	> 1300	400 -1000
Bandgap, eV	5.45	5.48	0.8 -3
Index of refraction at 10 µm	2.40	2.34 – 2.42	1.8 –2.4
Electrical resistivity, Ωcm	10^{16}	10^{12} - 10^{16} *	10^5 - 10^{15}
Dielectric constant (45 MHz – 20 GHz)	5.70	5.6	8 -12
Vickers Hardness, Kg/mm^2	5700 - 10400	5000 - 10000	2000 - 9000
Coefficient of friction (varies with humidity)	0.05 – 0.15	0.05-015	0.01 –0.3

Boron doping of CVD diamond can reduce the electrical resistivity to < 10^4 Ωcm.

1.2.4 Reference

[1] Hugh O. Pierson, “Handbook of carbon, graphite, diamond and fullerenes”, Noyes Publications, 1993, ISBN 0-8155-1339-9

1.3 Raman spectroscopy

When light quantum with an energy of $h\nu_0$ (were h is the Planck constant and ν_0 is the frequency of the entering light) hits a molecule, most of it will return with an energy $h\nu_0$ due to elastic scattering (Rayleigh scattering). A much lower part of the light will scatter inelastically and exchange vibrational energy during this process. This effect is called Raman scattering and results in light being returned with energies of $h\nu_0 \pm h\nu_s$, were $h\nu_s$ is a shift in energy linked to the material properties of the molecule hit (fig. 1).

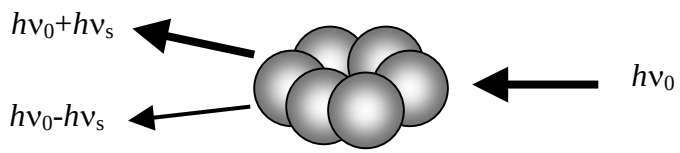

Figure 1: The principle of Raman scattering.

At room temperature, according to Boltzmann's law, most molecules are in their vibrational ground state (S_0). Only few will be in a vibrationally exited state. Therefore the Raman process which transfers vibrational energy to the molecule, and emits light quantum of a lower energy ($h\nu_0-h\nu_s$), is more probable than the reverse (fig. 2).

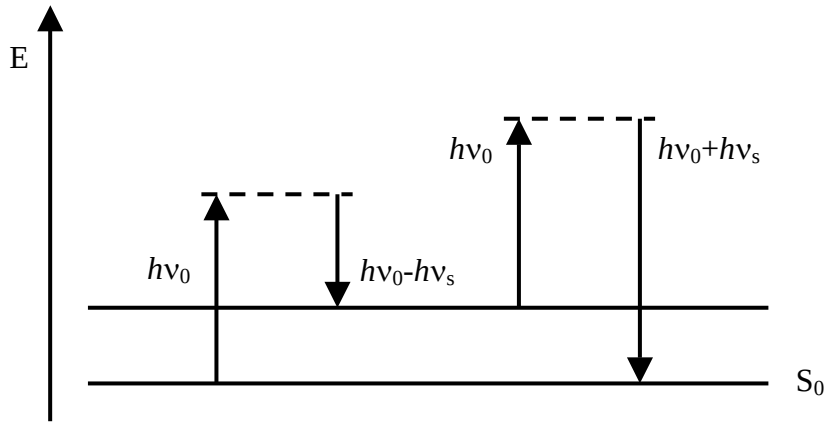

Figure 2: Energy level diagram.

Wood (1928) proposed to call these lower energies, in analogue to the postulate on fluorescence by Stokes (1880), Stokes lines and the reverse process anti-Stokes (Fig 3). At room temperature the process emitting light quanta of lower energy than the exciting light is more probable, therefore the Stokes lines have a higher intensity than the anti-Stokes. Fore this reason the Stokes part of the Raman Spectrum is more easily recorded than the anti stokes part and therefore usually only this part of the Raman spectrum is acquired.

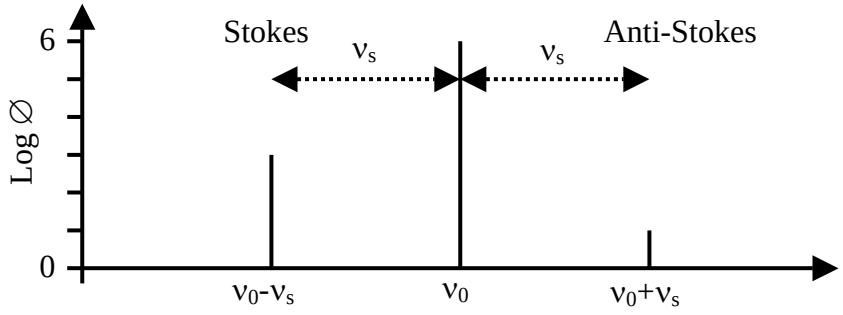

Figure 3: Intensity of Stokes and anti-Stokes Raman lines at room temperature.

The position of a Raman line does give information on the molecule's structure. The intensity ratio between its Stokes and anti-Stokes line allows the determination of the materials temperature.

A Raman spectrum is usually recorder in frequency shifts, defining the exciting radiation as having a zero frequency shift. The reason for this is that the Raman lines are not linked to an absolute frequency but to a shift with respect to the exciting radiation. Therefore, expressing the Raman spectrum in absolute wavelengths or wave numbers is not very practical. The most common way of expressing Raman spectra is therefore in wave number shift's (cm^{-1}).

A Raman line is not of a single frequency but a Gausian distribution around a central frequency ω_s (fig. 4).

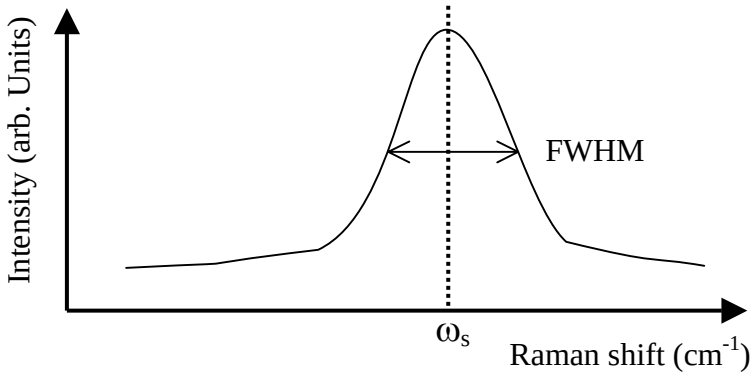

Figure 4: Typical shape of a Raman peak.

The Raman peak reflects the molecular bonding of a material. Every bonding length is linked to a specific frequency and therefore the Raman peak reflects the distribution of bonding length's in a material. The mean bonding length is represented by the central frequency ω_s. If a Raman peak is large, e.g. its FWHM (Full Width at Half Maximum) is big, the number of possible bonding length's present in the

molecule is big. The material has in this case an amorphous nature. In conclusion, the central frequency ω_s reflects the bonding's mean length and the FWHM reflects the molecule's degree of crystallinity.

The Raman peak position can also be used to evaluate the stresses present in a crystalline material. Since the bonding length changes when the material is compressed or elongated, the central frequency of the Raman Peak will also change. The Raman peak will shift to higher wave numbers if the material is in tensile stress and to lower wave numbers in the reverse case (fig. 5).

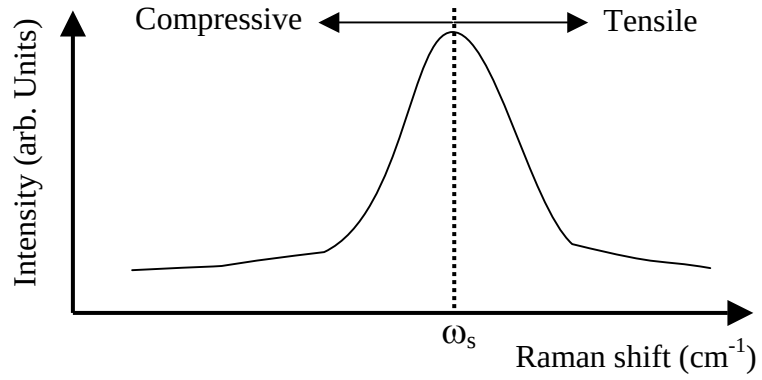

Figure 5: Raman peak shift due to material stress.

However, the above is only valid if the temperature of comparison is constant. If the temperature of a material increases, its bond length will also increase owing to the thermal expansion of the material. This will also result in a shift of the Raman peak to higher wave numbers.

The evaluation of stresses and thermal expansion of a material using the Raman peak shift is not always easy. One of the complications arises in non-symmetric crystalline structures. Since these structures have different mean bonding length's in all axis one can not simply use the Raman shift to calculate an uni-axial stress or a thermal expansion. A possible solutions to this problem lies in the use of polarised Raman spectroscopy, which allows to separate the Raman shifts resulting from different crystal axis. Owing to the complicated nature of polarised Raman spectroscopy, the analysis of thermal expansions and uni-axial stresses, is in practice only possible for symmetric crystals, which show the same Raman shift behaviour in all crystal axis.

1.3.1 The Raman analysis of diamond

Raman spectroscopy is a common way of determining the quality of natural and man made diamond [2,3]. Quality is in this case a measure of 3 parameters obtainable by analysing the Raman spectrum of the diamond material (fig 6). A first parameter is the FWHM of the diamond peek. The FWHM indicates the crystalline nature of the diamond and is small (about 1-2 wave numbers) for high quality natural and man made diamond. A second parameter is the position of the diamond peak. If this position is shifted with respect to its normal room temperature value (1332 cm^{-1}) the diamond is under tensile or compressive stress [1,5]. This is not so much the case in natural diamond but often occurs in thin film diamond layers deposited onto a substrate with a different thermal expansion coefficient. The third parameter is the ratio between the diamond peek intensity (I_{peak}) and the Raman spectrum's background ($I_{background}$). Mainly impurities and growth imperfections incorporated in the crystalline structure cause the Background in a Raman spectrum of diamond. If the Raman background becomes intense as compared to the actual diamond peek, the diamond quality is judged to be poor. This last parameter is mainly used if the optical, thermal or electrical properties of the diamond are of importance, since the impurities and growth imperfections causing the background spectrum are not influencing the diamond's mechanical behaviour.

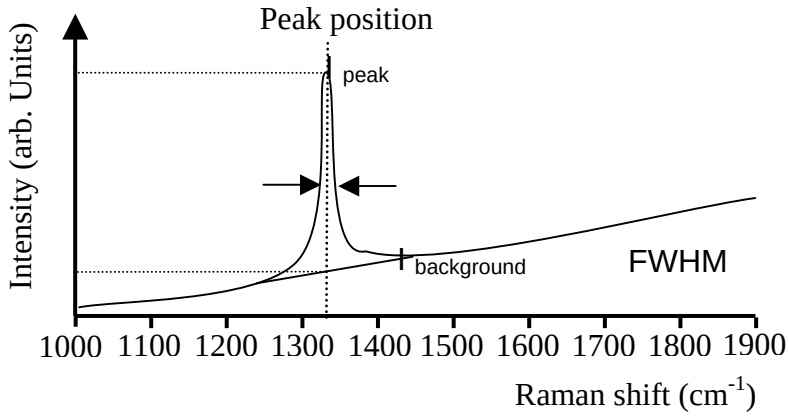

Figure 6 Typical diamond Raman spectrum.

Examples of using Raman spectroscopy for evaluating diamond quality is give in the chapters "A comparative study of …", "Single crystal diamond …" and "The behaviour of the molybdenum ...".

Raman spectroscopy is not only used to evaluate the quality of diamond. The authors have developed a simple theory based on a modified Grüneisen equation allowing the evaluation of the thermal expansion behaviour of diamond. This method uses the shift of the diamond peek at different temperatures as a measure for uni-axial thermal expansion. The Raman method offers, in this application, an easy access to a physical property of natural and man made diamond. Especially in the case of thin diamond films deposited on silicon, the method allows to obtain thermal expansion data, which are normally not accessible through classical measuring methods.

An example of such an analysis is given in the chapter “Correlations between Raman scattering and thermal expansion behaviour for CVD and natural diamond”.

1.3.2 The Raman analysis of DLC

Raman spectroscopy is use to evaluate the diamond likeness of DLC films [4]. The Raman spectrum allows to evaluate the amount and size of graphite bonded clusters (sp^2, threefold co-ordination) and diamond bonded clusters (sp^3, fourfold co-ordinated carbon atoms). The spectrum of DLC is composed of broad unsymmetrical bands in the 900 cm^{-1} to 1800 cm^{-1} region. It is composed of two peaks, originating from the graphite “G”-line at about 1580 cm^{-1} and the diamond “D”-line near 1350 cm^{-1} (fig. 7).

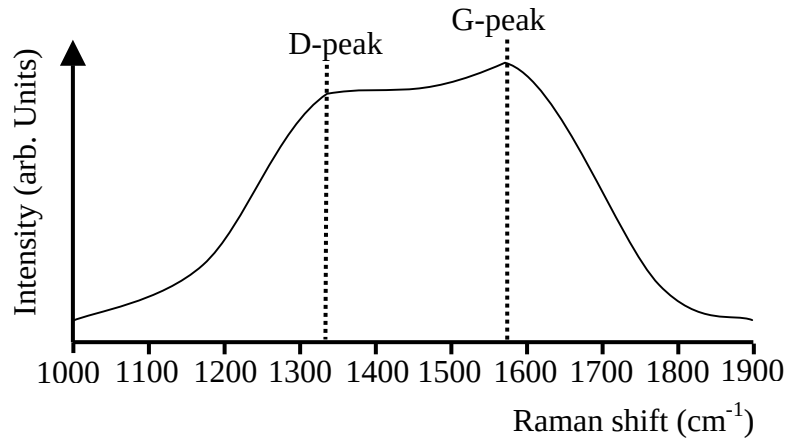

Figure 7: Typical shape of a DLC Raman spectrum.

The evaluation of the intensity ratio of the D and the G-line and their FWHM allows to determine the diamond likeness of the film. An example of use is given in the chapter “Raman characterization of amorphous carbon films”.

A further way of using Raman spectroscopy on DLC type films is the evaluation of particles, which are sometimes incorporated in these films owing to the nature of the deposition process. The Raman analysis are performed by a using a micro Raman set-up which allows to focus the excitation laser light trough a microscope onto a small (1 μm^2) area. The highly localised Raman data obtained in this way allow analysing the incorporated particle’s composition without the influence of the bulk material.

An example of such an analysis is given in the chapter “Morphology and structural characterization of plasma-assisted prepared carbon films”.

1.3.3 The influence of laser excitation frequency

The choice of excitation frequency of the laser source used to obtain a carbon Raman spectrum does influence the resulting spectrum. The laser frequency does influence in particular the intensity and position of sp^2 bonded species. This effect can be used to enhance the signal of this carbon species or alternatively to reduce its intensity if the sp^3 species need to be studied more carefully.

An example of using different excitation laser energies is give below (fig. 7) for a nano crystalline diamond film and a a-C:H (DLC) film.

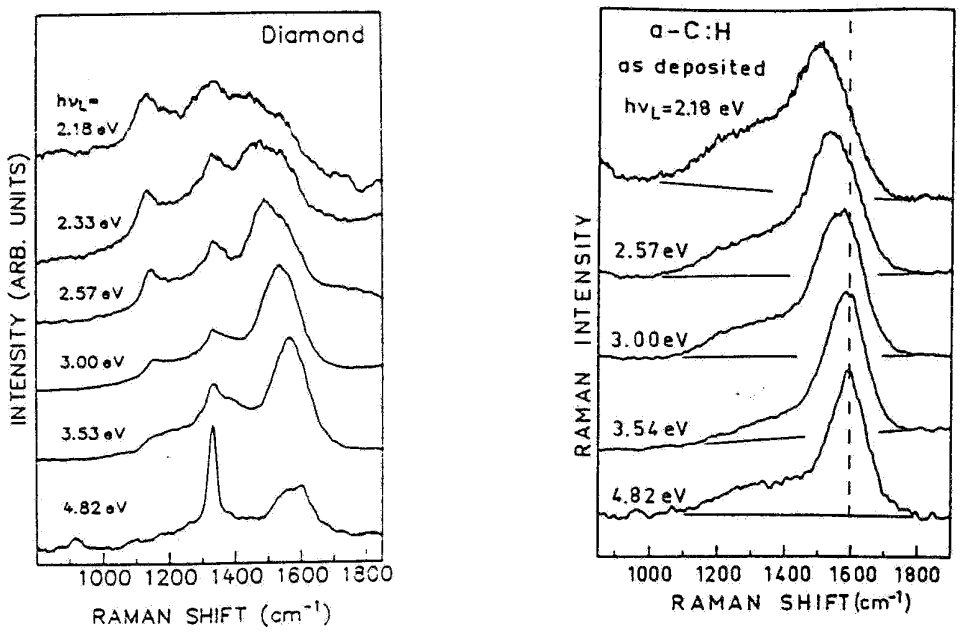

Figure 7 Examples of Raman spectra from diamond and a-C:H (DLC) films acquired at different laser excitation energies (reproduced from Wagner et al. [6,7])

The above spectra show that the choice of laser frequency does influence the Raman spectra of diamond and DLC films in an important manner. This influences the results when using Raman for quality evaluation. Since in the case of diamond the ratio between background and diamond peek is used, this parameter is only valid if comparing spectra acquired with the same laser frequency. A similar reasoning applies to the quality assessment of DLC.

In the diamond case the most commonly used laser source is the 514 nm line of an argon ion laser. In the case of DLC film, the 633 nm line of a helium neon laser is often preferred, owing to the fact that the sp_2 species are enhance in intensity at this excitation frequency.

1.3.4 Reference

[1] K H Chen, Y L Lai, J C Lin, K J Song, L C Chen and C Y Huang, “Micro-Raman for diamond film stress analysis”, Diamond and Related Materials 4, 460 (1995)

[2] T Grögler, O Plewa, S M Rosiwal, R F Singer, “CVD diamond films as protective coatings on titanium base alloys”, To appear in Proceedings of the 14th International Plansee Seminar -May 12-16, 1997

[3] G Heinrich, T Grögler, S M Rosiwal, R F Singer, “CVD diamond coated titanium alloys for biomedical and aerospace applications”, To appear in Surface and Coatings Technology

[4] W N Wang, N A Fox, P W May, M P Knapper, G Meaden, P G Partridge, M N R Ashfold, J W Steeds, I P Hayward, and G D Pitt., “Laser Raman studies of polycrystalline and amorphic diamond films”, Phys. Stat. Sol. 154, 255 (1996)

[5] C D O Pickard, T J Davis, A Gilmore, J W Steeds, “Calculation of the stress in large square facets of MPCVD grown diamond from cathodoluminescence and Raman spectroscopy measurements and comparison to stress predicted from finite element models”, Diamond and Related Materials 6 (1997) 1062-1066

[6] J. Wagner, C. Wild and P. Koidl, “Resonance effects in Raman scattering from polycrystalline diamond films”, Appl. Phys. Lett., Vol 59, No. 7 (1991) 779-781

[7] J. Wagner, M. Ramsteiner, Ch. Wild, and P. Koidl, “resonant Raman scattering of amorphous carbon and polycrystalline diamond films”, Physical Review B, Vol. 40, Nr. 3 (1989) 1817-1822

1.4 Low-pressure synthesis of diamond

Low-pressure diamond synthesis [2] (pressures up to 1 atm.) takes place by chemical vapour deposition (CVD). The process involves a gaseous mixture of hydrogen and a hydrocarbon source within a reactor system. The gases are exposed to a source of energy, which activates this mixture and creates large quantities of atomic hydrogen as well as a number of stable hydrocarbon species and/or radicals. This mixture is then transported to the surface of a suitable substrate, by natural gas diffusion and/or forced flow. The hot gas mixture (about 2000°C) reacts with the surface of the substrate (typical at 800°C) to form diamond and a variety of other carbon species. The large amounts of atomic hydrogen, which must be present for the process to work, will preferentially etch away the non-diamond carbon species.

Although a large number of methods exist to generate an effective gas mixture, a few parameters seem to be fairly independent of the technique to be employed. This has first been described by Bachmann et al. 1991 [1], who noticed that for a given temperature and pressure, a deposition diagram can be constructed describing those combinations of carbon, oxygen and hydrogen (C/O/H) which will result in diamond formation.

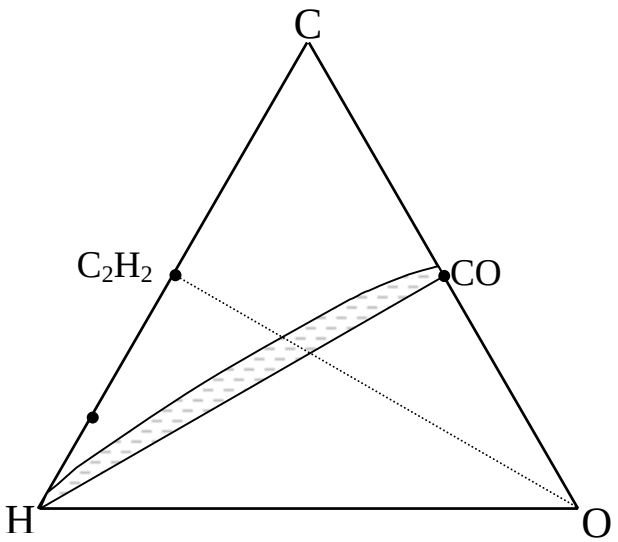

Figure 1: Deposition diagram as proposed by Bachmann et al. 1991. Some pure compounds used in diamond deposition are indicated. The dotted line refers to flame deposition. The axis between H and CH_4 reflects the hot filament deposition. (The principle of the flame and hot filament method are described in more detail in the following chapters)

In this diagram three areas can be distinguished. The first area is enclosed under the H/CO connection line and no carbon growth can take place in reactive mixtures for these compositions. The second, shaded, area gives the narrow band of compositions, which are needed for the growth of a good quality diamond. The area above the diamond growth zone normally indicates the growth of graphite or highly contaminated diamond. The limit between the diamond growth zone and the graphite

growth area is difficult to define owing to the vague definition of “good quality diamond”. More recently the quality has been defined by the Raman spectrum of the deposit. Typical criteria used in this method are peak position, peak width and background intensity (details are described in the chapter on Raman which is found earlier in this thesis).

Although the diagram does not provides a direct measure of the quality of the diamond, generally it decreases the further conditions diverge from the H/CO connection line. Although the actual diagram is determined by thermodynamic considerations, temperature and pressure do not influence the area in a major way. The area can however be enlarged by varying the amount of activation energy present in the gas mixture. At higher activation energies the diamond-graphite boundary shifts upwards. Also higher deposition rates can be detected approaching the diamond-graphite separation line. This is also the case for reactive mixtures of compositions situated in the middle of the diagram.

In the now following part of the chapter an introduction into the deposition methods used is given. The first part will deal with the Oxygen-Acetylene flame method, the second part will describe the hot filament deposition method.

1.4.1 Reference

[1] P.K. Bachmann, D. Leers and H. Lydtin, Diamond and Related Materials 1 (1991) 1.

[2] J.J. Schermer, J.E.M. Hogenkamp, G.C.J. Otter, G. Janssen, W.J.P. van Enckevort and L.J. Giling, Diamond and Related Materials, 2 (1993) 1149.

1.5 Oxygen-Acetylene flame deposition

This method was first reported by Hirose and Kondo in 1988 [1]. An Oxygen-Acetylene Flame provides in this process a gas plasma containing activated carbon species. A substrate is then placed inside the flame and is cooled in order to maintain a sufficiently low temperature (below approx. 1100 °C) for diamond to be deposited (fig 1). Although simple, the flame deposition method results in high quality diamond at high growth rates [4]. Its major disadvantages lie in its limited deposition area and high heat production (complicated substrate cooling).

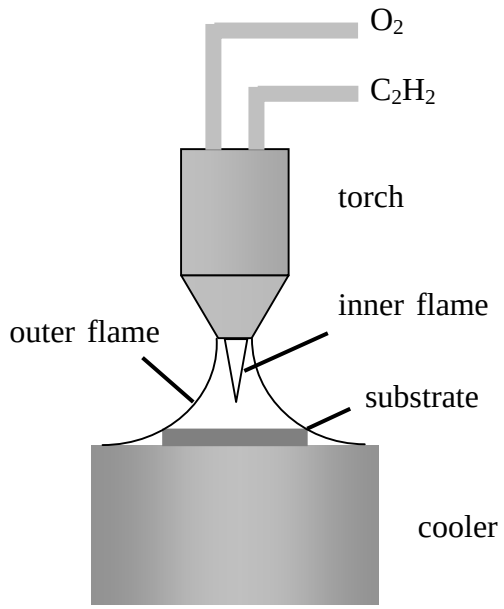

Figure 1 Schematic drawing of a flame diamond deposition set-up.

The deposition of diamond in the flame depends mainly on the oxygen/acetylene-mixing ratio and total flow rate, as well as the substrate temperature. In general it is found that at higher substrate temperatures, up to an optimum of about 900° C, the diamond quality and growth rate will increase, if the oxygen/acetylene-mixing ratio and total flow rate stay constant.

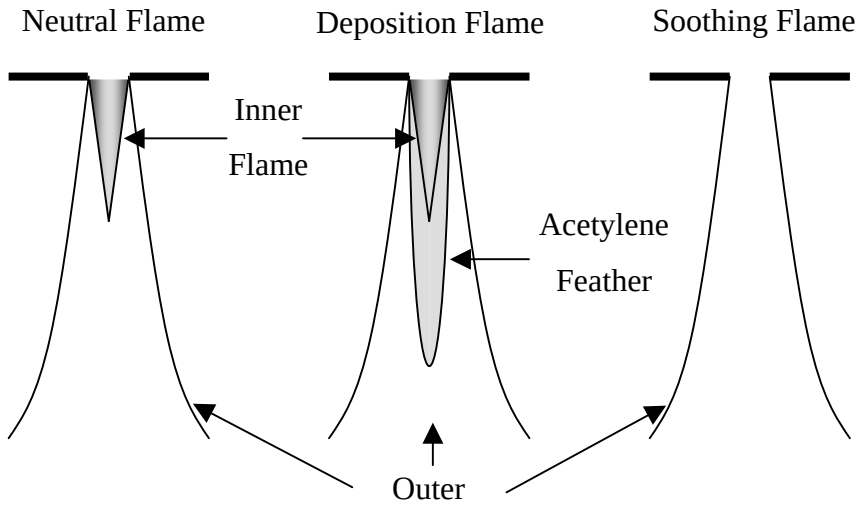

Figure 2 Flame shapes at changing oxygen-acetylene-mixing ratio's [5,6].

The mixing ratio will determine the shape of the flame (fig. 2). The oxygen/acetylene flame will consist of an inner flame and an outer flame if oxygen is present at a higher level than acetylene. In such a flame no diamond can be deposited. As soon as the quantity of acetylene versus oxygen becomes sufficient a third flame area will appear, called the acetylene feather. Diamond will be deposited if the cooled substrate is placed in this feather. Increasing the amount of acetylene further will change the flame into a yellow-orange coloured soothing flame, which has only one (not well-defined) flame area.

In order to deposit diamond, not only is the flame gas mixture important, but other factors. The most important are: substrate temperature and composition, the distance between the flame's inner core and the substrate and the flame turbulence. One further practical factor, the acetylene gas purity, also influences the final result. The influence gas purity has been studied in more detail and the results will be given in the sub chapter entitled "The influence of Acetylene purity".

The surface temperature of the deposition area has a large influence on the deposition quality and rate. In general higher deposition temperatures result in better diamond quality and higher deposition rates. The optimum deposition temperatures are between 900°C and 1100°C. At higher temperatures an increase in deposition quality is still observed, but the growth rate starts to drop due to an increase etching of the deposited diamond. At lower surface temperatures the diamond becomes increasingly contaminated by other carbon species and is therefore no longer of use.

The choice of substrate is important in many ways. Owing to the high temperatures, needed to get acceptable diamond quality and deposition rates, not all substrates will be sufficiently stable. The composition of the substrate also influences the ease at which diamond can be nucleated at its surface and determines also the initial crystal growth direction. Substrates of choice are molybdenum for polycrystalline deposits and natural single crystalline diamond for epitaxial deposits.

The distance between the flame's inner core and the substrate will determine the energy density (closer to the inner flame the flame plasma energy becomes higher)

and thus the amount of activated deposition species which reach the substrate's surface. If the inner core is too close to the substrate, the amount of energy reaching the surface can no longer be eliminated by the substrate cooling in a homogeneous way. This will result in an inhomogeneous diamond deposit. If the inner core is too far away from the surface the surrounding acetylene feather will no longer cover the deposition area, and thus the result will also be an inhomogeneous deposit.

The flame turbulence results from the combustion gases coming out of the burner. In general a burner will start its operational range with laminar flow conditions. These conditions will result in a so called laminar flame (figure 3). Increasing the flow rates in the burner will create turbulence. If this turbulence becomes fully settled the resulting flame will also be turbulent (figure 3).

The influence of the flame turbulence on the deposition lies in the efficiency of the combustion and thus the amount of activated species produced [2]. It can be noticed that a turbulent flame results in higher deposition rates due to the fact that its turbulence creates a more efficient combustion. A second effect noticed is the fact that a turbulent flame is broader and shorter than a laminar flame. This can result in a larger deposition area using the same burner.

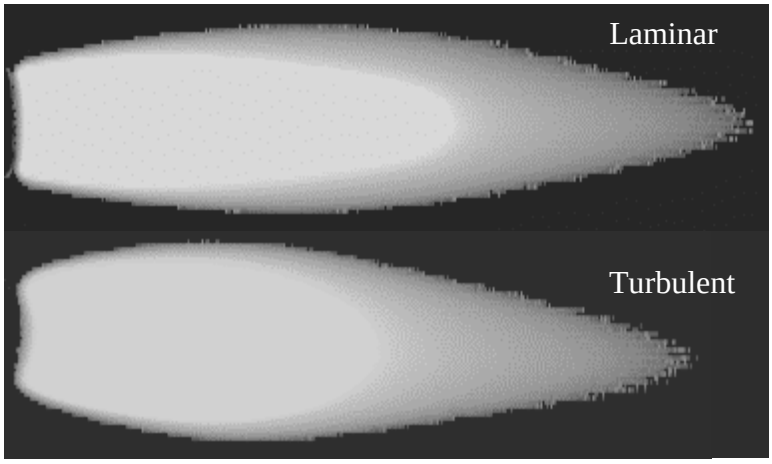

Figure 3: Laminar and turbulent flame shapes.

Usually going from a laminar to turbulent flow behaviour involves an increased gas flow. Therefore it can be argued that the increased deposition rates and area are due to an increased combustion gas flow. The reason why this is not the case is explained in the Chapter "A comparative study of laminar and turbulent oxygen-acetylene flames for Diamond Deposition". Further results obtained by turbulent flame deposition are given in the chapter "Single crystal diamond deposition by laminar and turbulent acetylene-oxygen flames".

1.5.1 The influence of Acetylene purity

The influence of acetylene purity [3] on the torch diamond deposition process has long been neglected. Although the gas quality used for diamond deposition is 99.6% pure, this purity only applies to the acetylene gas before filling in its gas container. Owing to the explosive nature of acetylene at high pressures (above 6 bar) one cannot simply put the gas into an empty cylinder. In order to stabilise the acetylene for transport, the gas cylinder is filled with a porous mass. The porous mass material acts in much the same way as clay is used to stabilise tri-nitro glycerine, a highly explosive liquid, into dynamite. In this way one can safely store pure acetylene with pressures up to 24 bar. Unfortunately at this cylinder pressure one can only store a very limited amount. In order to increase the quantity, acetone has also been added to the porous mass. Acetone has the property of easily dissolving large amounts of acetylene and in this way and at 24 bar cylinder pressure, about 5-10 times more acetylene can be stored.

The acetylene normally used in diamond torch deposition is of the type, which has been dissolved in acetone. The presence of acetone however has a number of inconveniences. For instance it is released at its vapour level concentration during the use of the acetylene cylinder. This means that at high cylinder pressures (full bottle) only a limited amount is released, but as soon as the bottle pressure drops the amount increases rapidly (figure 4).

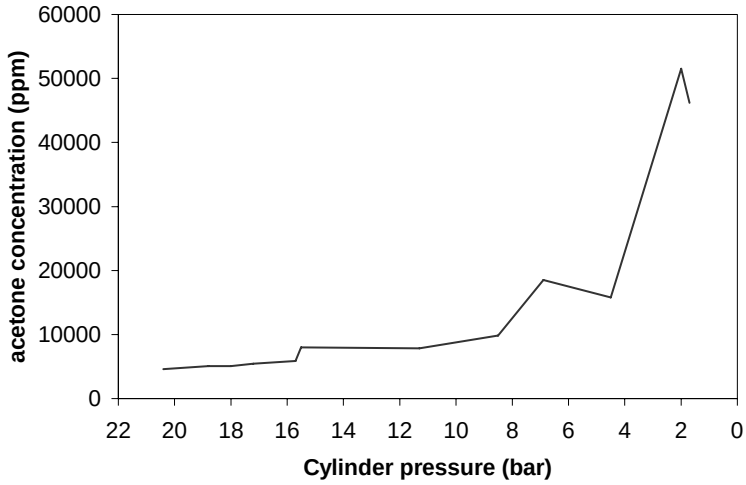

Figure 4: Acetone release at different acetylene cylinder pressures.

The effect of the acetone on the diamond deposition process is twofold. First, a changing C/H/O balance of the mixture will occur when keeping the volume mixture of oxygen and acetylene constant during the use of a total acetylene cylinder. This causes a change in deposition conditions and thus a change in the quality of the diamond and the deposition rate reached. Second, the acetone present will gradually decrease the energy produced during combustion. Acetone burns, producing less energy than acetylene, thus decreasing the energy available for diamond deposition and therefore the efficiency of the process. How the diamond growth rate depends on the cylinder pressure (for a constant acetylene/oxygen mixing ratio) is given in figure 5. From these data it can be concluded that the growth rate is only stable during the

first 3 to 4 bar of cylinder pressure use. One might be able to compensate this by continuously changing the acetylene/oxygen-mixing ratio. This, however, not only complicates the deposition procedure, but also does not take into account the energy loss caused by the increasing amount of acetone.

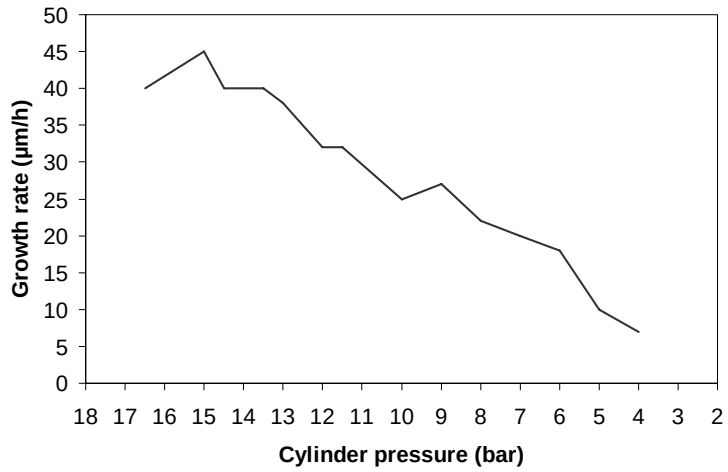

Figure 5: Diamond growth rate at constant acetylene/oxygen volume ratio vs. cylinder pressure.

A further problem is linked to the acetone used to dissolve the acetylene. The acetylene contains 0.4 % impurities before it is stored in its transport cylinder. These impurities consist mainly of nitrogen, but also of oxygen, hydrogen, methane and water. Such impurities, with the exception of water, do not dissolve well into acetone compared with acetylene. Therefore the impurities are released from the acetone before the acetylene and high release rates of these impurities are noticed at the start of the cylinder use. The nitrogen present is typically released at rates of 4000 ppm when starting to use the cylinder. This level rapidly decreases to below 10 ppm after using only 5% of the cylinder's content. The presence of nitrogen during the diamond deposition influences the quality in terms of growth defects. Although these so called nitrogen defects do not influence the mechanical properties of the deposited diamond, they do cause a very strong luminescence and therefore limit the optical applications possible.

A similar effect is observed with the oxygen, hydrogen and methane impurities (fig 6). Their release level does however not completely fall after using 5% of the cylinder content and hydrogen especially stays present at levels of 4000 ppm falling to 1000 ppm during total cylinder usage.

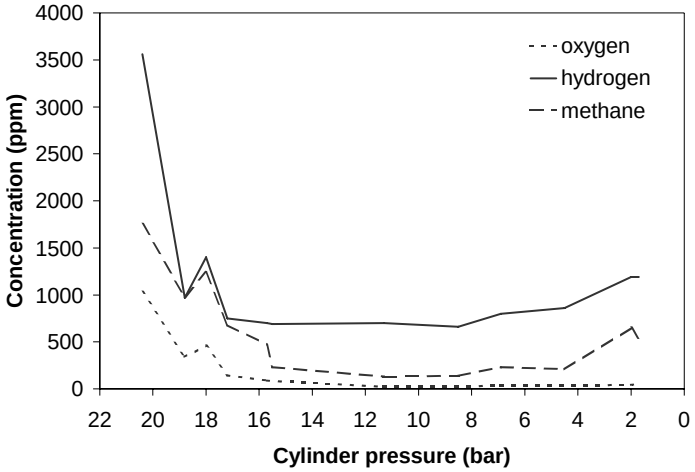

Figure 6: Oxygen, hydrogen and methane concentrations.

All of the above impurities, apart from oxygen, can cause growth defects resulting in optical defects similar to those caused by nitrogen. The total luminescence caused by these impurities as function of the cylinder pressure in shown below (fig 7).

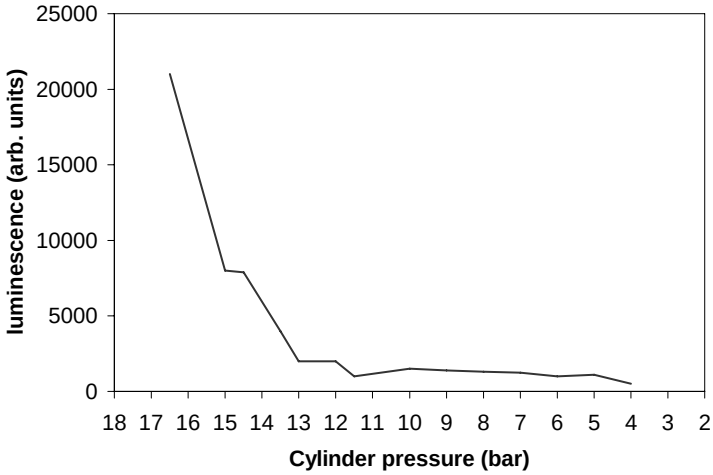

Figure 7: Diamond luminescence (at 690 nm) intensity vs. cylinder pressure.

Using a standard bottle of acetylene, it becomes clear that no stable high quality diamond deposition is possible. In summary, during the first 5 bar of bottle pressure, the acetone quality stays relatively stable, but the amount of other impurities is at its peak. Going to lower bottle pressures the impurity amount becomes lower but the acetone amount starts to increase rapidly.

Different solutions to this problem have been proposed. Active carbon filters between the acetylene cylinder and the burner can be used. The effect of this filter is to stabilise the acetone and the impurity concentrations. Due to the fact that all components present in the cylinder gas mixture absorb rather well to the active carbon, their concentration after this filter become constant as soon as the filter saturates. Although this is a rather elegant way of stabilising the impurity levels, it does not eliminate the fundamental problem of the impurities. Furthermore it can

pose a safety problem owing to the rather high amounts of acetylene absorbed in the active carbon mass. If no proper precautions are taken this mass might explode during filter change or spontaneously heat and ignite due to auto combustion of the acetylene.

An alternative method consists of passing the gas through a liquid nitrogen cooled trap. The acetone will be frozen out during the passage. Again this method does not eliminate the release of other impurities during the first 5 bar of bottle pressure. At the same time the frozen acetone will contain a substantial amount of acetylene and therefore poses a safety problem as soon as this cold trap is cleaned.

The safest and most effective method at present is to use acetylene cylinders containing no acetone. An obvious disadvantage lies in the low quantity of acetylene contained in such a cylinder. The cost of the process as well as the frequent bottle change does pose a practical and economical problem. Ideally the deposition process should be integrated next to an acetylene production plant.

Although the above described problems are not often mentioned in torch deposition related literature, they provide serious drawbacks for the process, preventing it from being scaled up to a commercially viable level.

1.5.2 Reference

[1] Y. Hirose and N. Kondo, Extended Abstracts, 35th Jpn. Appl. Phys. Spring Meet., March 1988, p 434.

[2] L.M. Hanssen, W.A. Carrington, J.E. Butler and K.A. Snail, Mater. Lett., 7 (1988) 289.

[3] P. Alers, “Impurities in acetylene an their influence on oxygen-acetylene flame diamond deposition”, paper presented at Diamond Films ‘93, sept. 1993, Albufeira, Portugal.

[4]

[5] G. Janssen, “Flame deposition of diamond”, paper presented at Diamond Films ‘93, sept. 1993, Albufeira, Portugal.

[6] A.G. Gaydon and H.G. Wolfhard, “Flames, their structure, radiation and temperature”, 4th edition, Chapman and Hall, London (1979).

[7] W.C. Gardiner Jr. (Ed), « Combustion Chemistry », Springer, New York (1984).

1.6 Hot Filament deposition

The Hot filament deposition process [1-12], or to be more precise, the hot filament assisted chemical vapour deposition process (HF-CVD), was originally developed by Matsumoto et al. . The basic set-up of the equipment (fig 1) consists of a filament, usually made out of tungsten or tantalum, which is heated up to 2000 °C by an

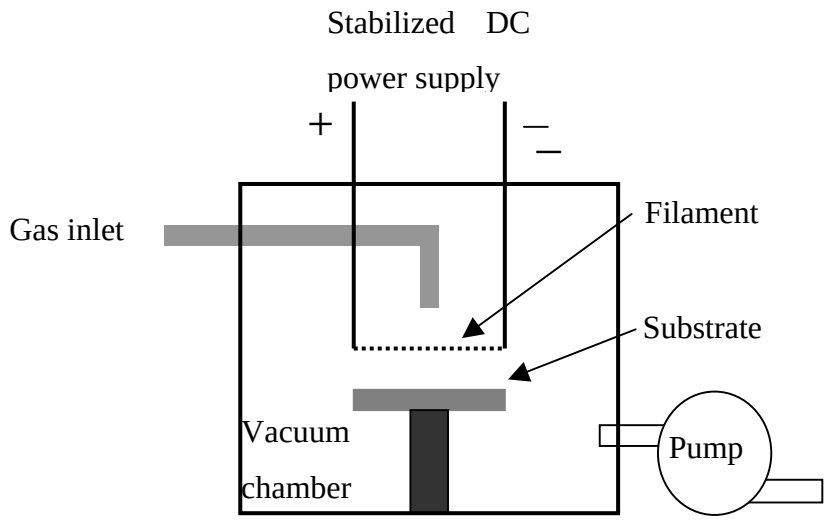

electrical current.

Figure 1: Basic Hot Filament activated CVD set-up

The hot filament serves as the activation source of the reactive gas mixture, which is usually composed of hydrogen with a few percent of methane. The gas mixture is flowing in the direction of the substrate, and passes the hot filament approx. 1 cm before reaching the substrate's surface. The substrate is controlled in temperature and the whole set-up is placed in a vacuum chamber operating at a pressure of approx. 10 to 200 mbar.

Typical deposition rates obtained with such a set-up are < 1μm/h for good quality diamond. The main problems encountered in this method are directly linked to the filament. If the reactive gas mixture passes a single filament the resulting deposit on the underlying substrate will be quite inhomogeneous (figure 2). This is because the filament will inhomogeneously heat the substrate's surface by radiation. This causes a temperature gradient (up to 200 °C), and will result in a variable distribution in the diamond deposit thickness, quality and morphology.

A further reason for this effect lies in the difference in travel distance of the, at the filament activated, reactive species to the different deposition sites on the underlying substrate. The longer these species have to travel, i.e. the border of the substrate, the less reactive they become. The resulting diamond deposit tends to be therefore less thick and of worse quality at the borders of the substrate.

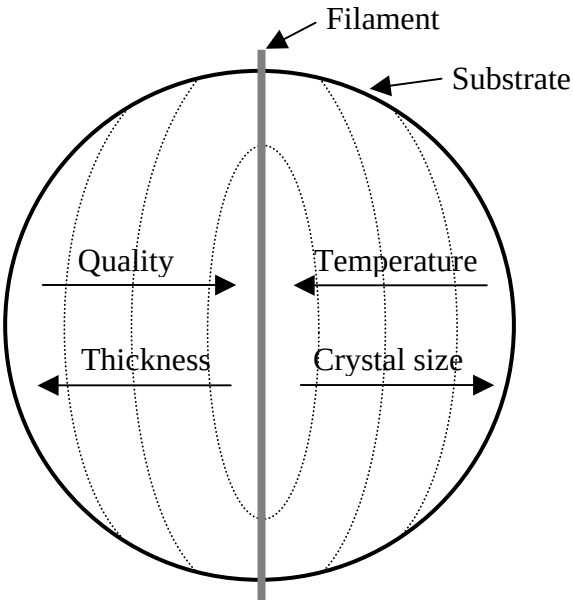

Figure 2: Influence of the filament on the substrate and diamond deposit (the arrows indicates the direction of increase).

The solution to the above-described problem lies in the use of a filament array in order to cover the total substrate area in a homogeneous way. The use of an array requires an extremely accurate control of the filament's dimensions and power supply, in order to guaranty a homogeneous activation over the whole substrate surface area. Furthermore, the reactive gas feed nozzle has to be adapted in order to spread the gas over the total filament array. Although the correct implementation of the above is technically not easy, good results are obtainable.

A further parameter influencing the process stability is again linked to the filament. Due to the presence of activated carbon in the gas mixture the filaments commonly used (Tungsten, Tantalum..) tend to form carbides. These carbides have two effects. First, they change the electrical resistance of the filament and thus the power provided to the filament has to be constantly adapted to maintain appropriate deposition conditions. Second, the carbides tend to be brittle and therefore fragilise the filament. In order to reduce the problems linked to the above, adequate filament suspension are used, and in general the filament is preconditioned into by heating it in an appropriate gas mixture of hydrogen and methane to stabilise it. The latter procedure has to be repeated on a regular basis, in order to maintain a good filament quality.

The filament will evaporate slowly during the deposition and therefore will contaminate the diamond deposit. Although this effect can be greatly reduced by proper control of the filament's stabilisation, the resulting films will never obtain the purity which can be reached by other methods like microwave or flame deposition.

The advantages of the method lie in the fact that the deposition area can be scaled up and that it can be adapted to wafer technology, using alternating sample holders and vacuum passages. The main application area of the HF-CVD technique lie in this field. This is also due to the fact that its low growth rates do limit its application in

other fields. HF-CVD is therefore seldom used for bulk diamond deposition, unless large deposition areas are required.

In the next chapter, results obtained by the HF-CVD method are discussed.

1.6.1 Reference

[1] S. Matsumoto, Y. Sato, M: Tsutsumi and N. Setaka, J. Mat. Science, 17 (1982) 3106.

[2] H. Matsubara and T. Sakuma, J. Mater. Sci. 25 (1990) 4472.

[3] G. Janssen, W.J.P. van Enckevort and L.J. Giling, “CVD growth of diamond: the multiple role of atomic hydrogen”, in Proc. First Int. Symp. on Diamond and Diamond like Films, J.P. Dismukes (ed.), The Electrochemical Society, Pennington (1989) p508.

[4] Y. Hirose, S. Amanuma, N. Okada and K. Komaki, in “Proc. First Int. Symp. on Diamond and Diamond like Films », J.P. Dismukes (ed.), The Electrochemical Society, Pennington (1989) p80.

[5] D.G. Goodwin, Appl. Phys. Lett. 59 (1991) 277.

[6] M. Frenklach and H. Wang, Phys. Rev. B 43 (1991) 1520.

[7] D.G. Goodwin and G.G. Gavilet, J. Appl. Phys. 68 (1990) 6393.

[8] W.L. Hsu, Appl. Phys. Lett. 59 (1991) 1427.

[9] L.R. Martin and M.W. Hill,lJ. Mat. Sci. Lett., 9 (1990) 621. M. Frenklach, J. Chem. Phys., 97 (1992) 5794

[10] J.E. Butler and R. L. Woodin, Phil. Trans. R. Soc. Lond. A 342 (1993) 209.

[11] C.J. Chu, R.H. Hauge, J.L. Margrave and M.P. D Evelyn, Appl. Phys. Lett. 61 (1992) 1393.

[12] Y. Muranaka, H. Yamashita and H. Miyadera, J. Appl. Phys. 69 (1991) 8145.

1.7 The Deposition of DLC

Diamond like carbon (DLC) [1-4] is a form of carbon which is not crystalline (ie diamond or Graphite) but neither is it completely amorphous like soot. DLC can have a wide variety of properties depending on the mode of deposition. Unlike diamond deposition, hydrogen is not required but can be added to change the properties of the resulting DLC film.

The carbon source used in DLC deposition is either solid, in this case usually composed of graphite, or a gas (methane is mainly used). The activation energy used to make the carbon reactive is provided by a wide variety of energy sources. The most common are the microwave and the plasma arc.

1.7.1 Microwave deposition

The basic equipment for a microwave system consists of a vacuum reaction chamber where the sample is mounted on a temperature controlled substrate holder and a microwave source, which is used to generate plasma in the chamber (fig. 1).

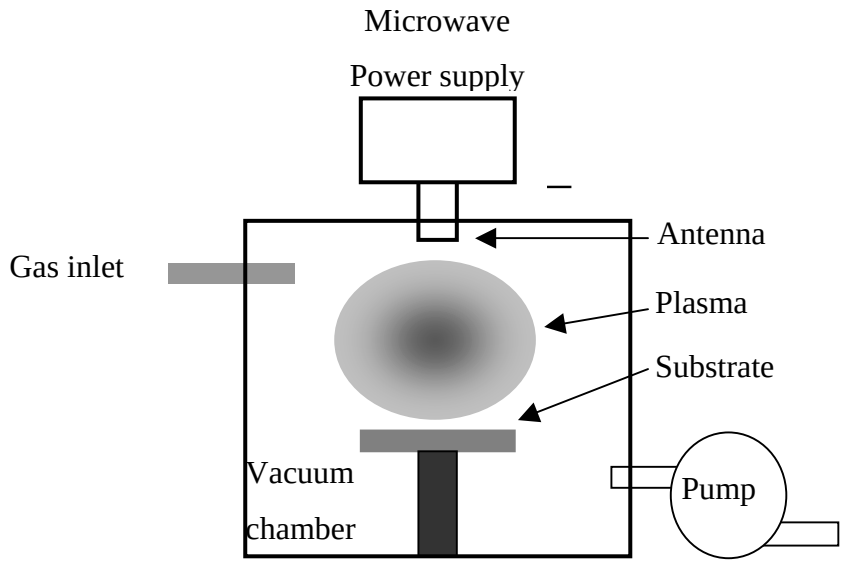

Figure 1: Typical Microwave DLC deposition equipment.

The addition of argon and/or hydrogen is mostly required to stabilise the reactive plasma. In order to activate the acceleration of the ionised carbon from the plasma towards the substrate a bias voltage is often used. This voltage is applied by a DC source to the sample and is usually between 50 and 250 V.

The microwave deposition method has only a limited deposition area. Owing to the rather low ionization energies which are obtained using microwaves, the properties of the films deposited are closer to graphite than to diamond. For the same reason the deposition rates obtained are rather low (typically 1 μm/h). The advantage over other methods lies in the low contamination of the deposited film. Therefore the application

of microwave deposited DLC is highly suited to those applications requiring small areas, for example in microelectronics and magnetic storage devices, where the purity and the homogeneity is of importance.

1.7.2 Arc deposition

The Arc deposition [5] principle requires the creation of an electric arc between an electrode and a deposition material. In the case of DLC deposition this target is usually composed of graphite. The electric arc activates the graphite surface and ionized carbon atoms are emitted. These ions recombine on the substrate, placed in the reaction chamber, to form a DLC film (fig. 2).

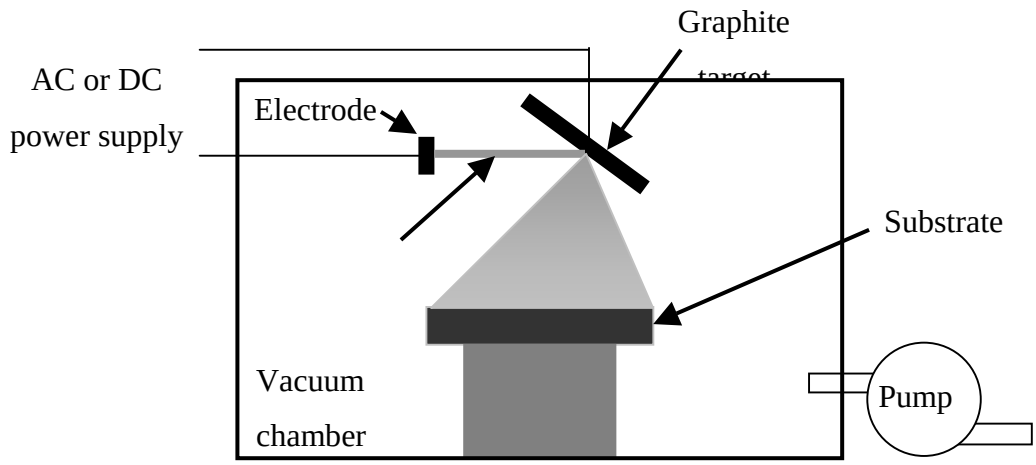

Figure 2: Typical Microwave DLC deposition setup.

As in microwave DLC deposition, a bias voltage is applied in order to accelerate the ionized carbon towards the substrate.

The advantage of the arc method lies in the large deposition areas that can be achieved. The method allows also a high activation of the carbon atoms by either a high-tension arc or by adding additional energy from, for example, a laser source. The resulting DLC deposited can have properties that are very close to those of actual diamond. The deposition rates obtained by this method are in general also higher than those obtained by microwave deposition (> 5 µm/h). A disadvantage of the method lies in the fact that carbon particles can be detached from the graphite target and create inhomogeneous inclusions in the DLC film. The technique is therefore mainly used for large area deposition where the anti wear properties of DLC are required, e.g. drills, moulds and other tools. DLC coated glass for bar code scanners are now found in super markets

Typical examples of the results obtained by such an Arc deposition method can be found in the chapters “Morphology and structural characterization …” and “Raman characterization of amorphous carbon films”.

1.7.3 Reference

[1] Moravec, T. J. and Orent, T. W., *J. Vac. Sci. Technol., 18,* 226 1981

[2] Berg, S. and Andersson, L. P., *Thin Solid Films, 58,* 117 1979

[3] Enke, K., Dimigen, H., and Hubsch, H., *Appl. Phys. Lett.,* 36 291, 1980

[4] Y. Lifhitz, S. R. Kasi and J. W. Rabalais, “Carbon sp3 film growth from mass selectioned ion beams: parametric investigation and subplantation model”, Materials Science Forum 52 and 53, 1990, 237.

[5] H.J. Scheibe, B. Schultrich, “DLC-film deposition by laser-Arc and properties study”, Thin Solid Films, 246, 1994, 92.

2 Publications

2.1 A comparative study of laminar and turbulent oxygen-acetylene flames for Diamond Deposition

In the early years of diamond CVD development, the oxygen-acetylene flame method has known a great success among research groups. The low initial investment required and the good quality of diamond at high growth rates, which was obtained in an uncomplicated manner, made the method the ideal candidate for numerous applications. When the author joined the CSEM diamond research group the flame method was part of the ongoing research.

In a permanent effort of up scaling the flame diamond growth method both in covered deposition area and in growth rate, the differences between laminar and turbulent flames was studied. After solving the problem of stabilising a fully settled turbulent flame at similar total gas flow rates as used in laminar flames, significant improvement in growth rate was found when using turbulent flames. The following publication reports the first published results of this study. The following publication is the first in the field showing a comparison of turbulent and laminar flames under identical operational conditions. All other related work showing results produced in a turbulent flame had the drawback of using substantially higher total gas flow rates then laminar burners of the same size. The contribution of the author lies in the design of the turbulent burner, which allowed the use of identical conditions as similar size laminar burners.

However, after having improved the growth rates, further research showed that enlarging the deposition area was less obvious. The energy flux developed by a relatively small flame (covering 1 cm^2 of deposition area) reach already 10KWh. The use of turbulent flames concentrates this energy flux more to the substrate than a laminar flame (hence the higher growth rates). Creating and handling such high energies poses some technical problems. In up scaling the most important are how to cool the substrate and how to construct burner systems capable of creating large flames safely.

Owing to both of the above-mentioned reasons the maximum obtainable deposition area, using a single flame burner, is about 3 cm^2. Since other rapid diamond deposition methods, like for instance plasma torch deposition, did not suffer from this limitation, the flame diamond deposition method became less popular. Presently the oxygen-acetylene deposition method is only a marginal part of the ongoing diamond deposition research. It is mainly applied as demonstration method in teaching and therefore still exploiting its prime merits, being cheap and easy to implement.

A comparative study of laminar and turbulent oxygen–acetylene flames for diamond deposition

P. Alers, W. Hänni and H. E. Hintermann
CSEM, Centre Suisse d'Electronique et de Microtechnique SA, CH-2000 Neuchâtel (Switzerland)

Abstract

Free-standing polycrystalline diamond films have been deposited using pre-mixed laminar and turbulent oxygen–acetylene flames. The use of new burners which had been developed at CSEM has made it possible to compare the performance of laminar and turbulent oxygen–acetylene flames produced by burners with the same exit opening size using the same total gas flow amount and gas mixing ratio.

The quality of the as-deposited films was measured by electron microscopy and Raman spectroscopy. A marked difference in growth rate was observed. Films grown in a turbulent flame grow twice as fast as in the laminar case.

1. Introduction

The deposition of diamond by laminar and turbulent pre-mixed oxygen–acetylene flames has been studied by a number of research groups. Although both types of flame give good results [1, 2], a fair comparison between laminar and turbulent flames has not been made (because of differences in gas flow rates and burner exit opening sizes). The reason for this lies in the limitations of the commercial burners used so far.

The onset of turbulence in a commercial burner requires, as stated before by Snail and Craigie [3, 4], a sufficiently high Re number in the burner exit opening. It is furthermore shown to be impossible to stabilize a laminar and a turbulent flame on the same commercial burner using the same total gas flow. It is argued here that these limitations of commercial oxygen–acetylene burners are a direct consequence of their design.

The easiest way to demonstrate this is to look closer at this design and to do some Re number calculations for the different flow sections of this commercial burner. In principle a commercial burner consists of a tube (diameter D_t) ending in a small exit opening (diameter D_e) on which the flame will burn (Fig. 1).

A No. 0 standard welding torch was measured to have a D_t of 4 mm and a D_e of 0.89 mm. The Re number in a tube can be defined as $\mathrm{Re}=4V/\pi Dv$, where V is the total gas flow amount, D the diameter of the tube and v the kinematic viscosity of the gas mixture which is equivalent to the viscosity μ of the gas mixture, divided by the gas mixture density ρ. The kinematic viscosity v was calculated [5] to be 0.129 $\mathrm{cm^2\ s^{-1}}$ for an oxygen–acetylene mixture with an oxygen-to-acetylene ratio of 1 at 300 K. On the assumption of a total gas flow amount of 2.8 standard $\mathrm{l\ min^{-1}}$, often used for a No. 0 torch [2, 3], Re numbers for the burner inlet tube (of diameter D_t) and the burner exit opening (of diameter D_e) are 1152 and 5175 respectively. When we take into account that the onset of turbulence in a tube starts at $\mathrm{Re}>2320$ [6, 7], it can be deduced from the Re numbers calculated earlier that, for a No. 0 burner, the flow in the burner inlet is laminar, and the flow in the burner exit opening is turbulent. However, in order to change a laminar flow into a turbulent flow, not only is a sufficiently high Re number necessary, but also a sufficiently long tube section is required. The length L needed for this flow settling is given by $L/D=50$ for smooth tubes, where D is the tube diameter, and $L/D\approx 40$ for rough tubes [6, 7]. If one looks now at the exit opening of a commercial burner, it is no longer than a few millimetres and one can see that the length of this opening section is not sufficient to change a laminar flow into a turbulent flow. This means that for a No. 0 burner the flame burning on it under the flow conditions described earlier will be laminar, although the Re number calculated for the exit opening is in the turbulent region.

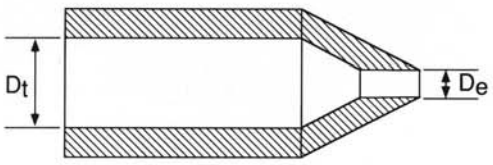

Fig. 1. Design principle of a commercial oxygen–acetylene burner.

It can now be seen that, if one wants to compare a laminar and a turbulent flame on burners with the same exit opening size under the same flow conditions, one

0925–9635/93/$6.00

has to modify the classical design used in commercial burners. A turbulent flame on a No. 0 burner can, for instance, be achieved by making the diameter of the burner inlet tube so small that a turbulent flow already exists in this section.

The solution chosen in this study involves the use of the classical burner design to achieve a laminar flame, and the addition of a turbulence-creating step in this design just before the burner exit opening to achieve a turbulent flame.

2. Experimental details

The flame deposition equipment used for the experiments consists of a water-cooled torch, mass flow controllers for the process gases and a 5 mm molybdenum rod mounted in a water-cooled copper block as a substrate. The burner tips used in the torch have an exit opening of 0.8 mm and were made out of stainless steel. The purities of the process gases were 99.99% for oxygen and 99.6% for acetylene. The temperature of the substrate was measured by a thermocouple mounted just under the molybdenum surface. The substrate was diamond polished before each deposition and kept 1–2 mm under the inner flame during a deposition. In order to obtain free-standing diamond films, the substrate temperature was kept at 800 °C, thus preventing adhesion with the molybdenum substrate surface.

Two sets of experiments were done to compare the performance of a laminar flame with that of a turbulent flame. In the first series the acetylene flow was kept constant at 1.00 standard l min^{-1} and the oxygen–acetylene ratio was varied between 1.07 and 1.10. In the second series the oxygen-to-acetylene ratio was kept constant at 1.09 and the total gas flow amount was varied between 1.67 and 2.30 standard l min^{-1}. Each set of experiments was done using a laminar burner and copied using the turbulent burner developed in house.

The crystalline structure and the thickness of the as-produced films were examined by electron microscopy. The diamond quality was assessed by Raman spectroscopy. In these Raman measurements an He–Ne laser at 633 nm was used, thus allowing excellent sensitivity for carbon species [8].

3. Results and discussion

By using burners with the same exit opening size under the same total flow conditions, it was possible to compare the deposition performance of laminar and turbulent flames and also the physical properties of these flames. The first difference noted between a laminar and a turbulent flame was the loud hissing sound that the turbulent flame produced, compared with the almost-quiet laminar flame. After a closer look at both flames (Fig. 2), the obvious difference in shape became apparent. Under the same flow conditions, the inner flame of the turbulent burner was much shorter and more rounded than the inner flame of the laminar burner. The total length of the acetylene feather, however, stayed the same under equal flow conditions. A further difference noticed was the heat distribution in both flames. The adjustments to the substrate cooling system required when changing from a laminar to a turbulent flame indicated that the heat production just under the flame front of the turbulent flame was much higher than the heat production at the same height in the laminar flame. A similar experiment using the end zone of the outer flame of both flames showed that the heat production of the laminar flame was much higher than the heat production of the turbulent flame in this zone. A reason for this phenomenon could be the more efficient mixing in the flame front of the turbulent flame, leading to a faster combustion and consequently a higher heat production in this part of the flame.

These physical differences between the laminar and the turbulent flames also led to a substantial difference in growth performance. Although the homogeneous deposition zone for both flames was the same, 3 mm, the growth in a turbulent flame is twice as fast as in a laminar flame (Figs. 3 and 4). In the first series of experiments, the influence of the oxygen–acetylene mixing ratio on the film growth was studied (Fig. 3). At an oxygen-to-acetylene mixing ratio of 1.07, the film growth rate of the turbulent flame was almost 2.5 times that of the laminar flame. This difference gradually decreased to 1.7 times for a mixing ratio of 1.10. The film growth rate also decreased when going from a mixing ratio of 1.07 to 1.10 for each case. These effects

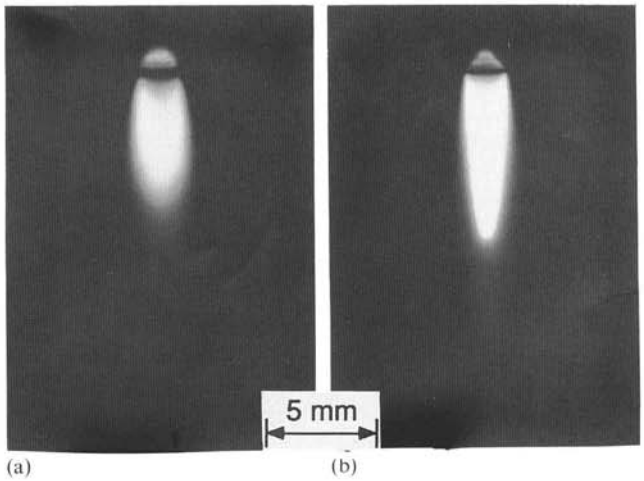

Fig. 2. Flame shape of (a) a turbulent and (b) a laminar oxygen–acetylene flame.

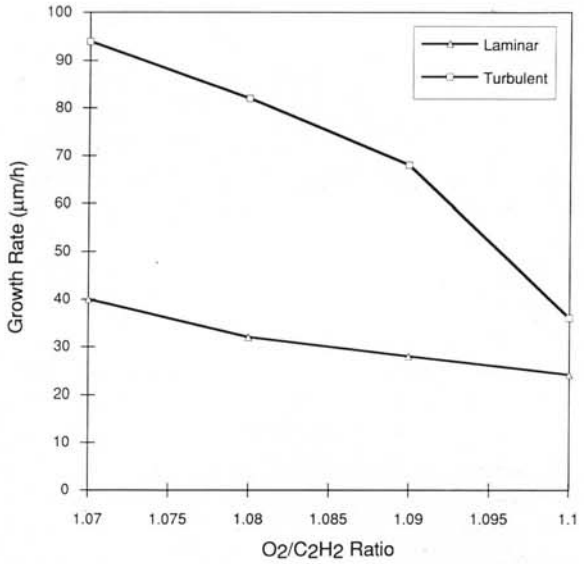

Fig. 3. The influence of the oxygen-to-acetylene mixing ratio on the growth rate in turbulent and laminar flame diamond deposition.

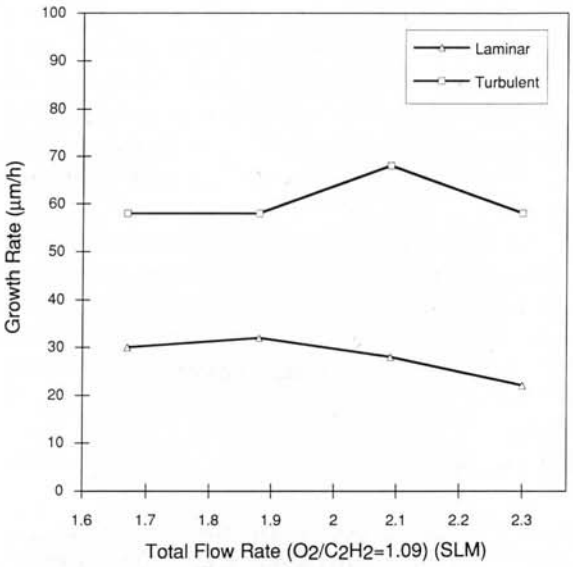

Fig. 4. The influence of the total gas flow rate on the growth rate in turbulent and laminar flame diamond deposition.

for both flames are probably due to the decreasing size of the acetylene feather in which the deposition takes place, which makes it harder to place the substrate in this feather and still to keep a sufficiently large gap between the substrate and the inner flame. Another explanation for the decreasing growth rate might be a decreasing amount of active growth species at higher oxygen-to-acetylene mixing ratios.

In the second series of experiments the oxygen-to-acetylene mixing ratio was kept constant at 1.09 and the total gas flow was varied between 1.67 and 2.30 standard $l\,min^{-1}$ (Fig. 4). The film growth rate for both flames stayed almost constant in this total flow range at about 60 $\mu m\,h^{-1}$ for the turbulent flame and about 30 $\mu m\,h^{-1}$ for the laminar flame. The Re number in the 0.8 mm burner exit opening varied from 3472 at 1.67 standard $l\,min^{-1}$ to 4781 at 2.30 standard $l\,min^{-1}$. It can be concluded that this change in Re number, which is an indication of the extent of turbulence in the flow, did not have an influence on the film's growth rate. This probably means that the mixing in the turbulent flame is already perfect at Re numbers as low as 3472, indicating that one might as well use the lower total gas flow rate of 1.67 standard $l\,min^{-1}$ and so economize on the cost of the process gases.

An important conclusion to be drawn from both series of experiments could be that the oxygen–acetylene flame deposition process is transport limited [3] (the high mixing rates in the turbulent flame giving a more efficient reactive species transport and therefore a higher growth rate). This conclusion can, however, not be drawn with certainty because the higher growth rate in the turbulent flame may also be due to the observed higher heat production rate in the deposition part of that flame.

Examination of the films produced in these experiments shows that the influence of the different flame types on the film quality is less obvious than the influence on the film growth rate. The electron microscopy photographs (Figs. 5 and 6) indicate no significant crystalline shape differences apart from the obvious differences in crystal size and layer thickness due to the faster growth rates in the turbulent flame. In particular, in the cross-section photographs, one can see clearly that the turbulent layer (Fig. 6(a)) is in fact a continuation of growth on features already present in the laminar layer (Fig. 6(b)). Both films exhibit the crystalline structure shown in top view in Fig. 5, over a homogeneous zone

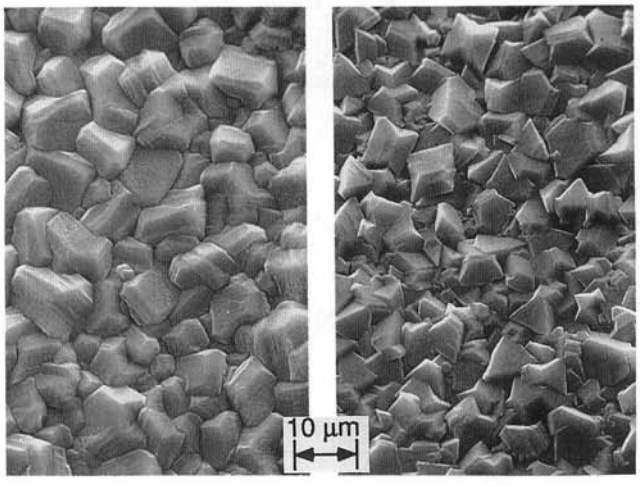

(a) (b)

Fig. 5. Top views of the flame-grown polycrystalline free-standing diamond films: (a) turbulent; (b) laminar.

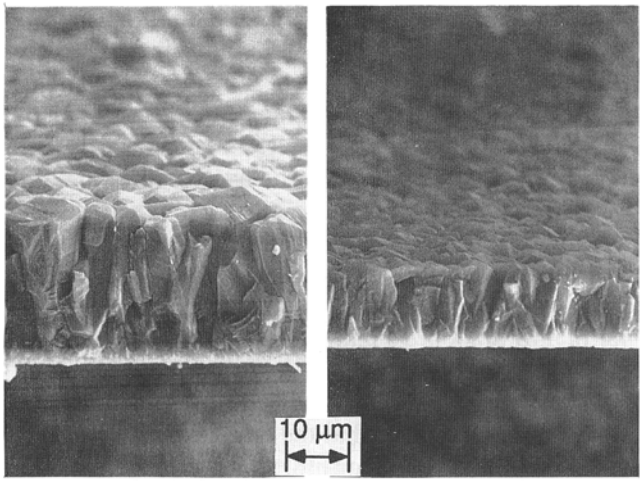

Fig. 6. Cross-sections of the flame-grown polycrystalline free-standing diamond films: (a) turbulent; (b) laminar.

of 3 mm diameter. It is believed that these similarities in growth features for both films arise because in both cases the same reaction principle is involved.

The only difference found in film quality is shown in the Raman microspectra for films grown with a laminar flame and a turbulent flame under the same conditions (Figs. 7 and 8). Here one can see that the luminescence background and the amount of carbon species present in the laminar-flame-grown film are higher than in the turbulent-flame-grown film. One should, however, be careful with the Raman microspectroscopy data, because these measurements where done using an He–Ne laser at 633 nm, where the sensitivity for carbon species is much higher than for a measurement done with an Ar laser at 514.5 nm. Reference measurements done on similar films with an Ar laser at 514.5 nm showed almost no carbon species and also a lower luminescence background.

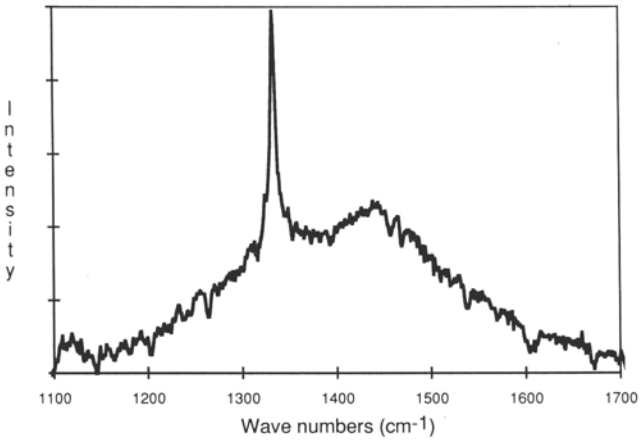

Fig. 7. The Raman microspectrum of a polycrystalline free-standing diamond film grown in a turbulent flame (He–Ne; 633 nm).

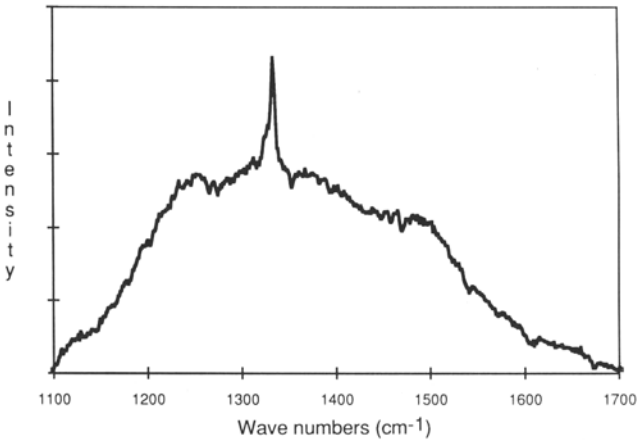

Fig. 8. The Raman microspectrum of a polycrystalline free-standing diamond film grown in a laminar flame (He–Ne; 633 nm).

4. Conclusions

The growth of polycrystalline diamond films is twice as fast in a turbulent flame as in a laminar flame, using burners with the same exit opening sizes, the same total gas flow amounts and the same substrate positions within the flames. This difference might be due to the higher transfer rate of reactive species in the turbulent flame arising from the better mixing, or to the observed higher heat density in the deposition zone of the turbulent flame.

The crystalline structure of the films produced from both types of flame are essentially the same, although a higher amount of carbon species and luminescence background was found for the laminar-flame-grown film with Raman microspectroscopy measurements.

Acknowledgment

This work was supported by the Swiss National Research Foundation under Contract 21-30089.90.

References

1 J. W. Glesener, A. A. Morrish and K. A. Snail, *J. Appl. Phys., 70* (9) (1991) 5144.
2 G. Janssen, W. J. P. van Enckevort, J. J. D. Schaminee, W. Vollenberg, L. J. Giling and M. Seal, *J. Cryst. Growth, 140* (1990) 752.
3 K. A. Snail and C. J. Craigie, *Appl. Phys. Lett., 58* (17) (1991) 1875.
4 K. A. Snail, C. L. Vold, C. M. Marks and J. A. Freitas, Jr., *Diamond Relat. Mater., 1* (1991) 180–186.
5 G. Vogelpohl, in *Landolt–Börnstein, New Series*, Vol. 6, 6th edn., Springer, Berlin, 1955, p. 586.
6 H. Brauer, *Grundlagen der Einphasen- und Mehrphasenströmungen*, 1st edn., Sauerländer, Aarau, 1972
7 B. C. Sakiadis, *Perry's Chemical Engineers' Handbook*, 6th edn., McGraw-Hill, New York, 1984, p. 5–1.
8 M. Yoshikawa, *Appl. Phys. Lett., 55* (25) (1989) 2608.

2.2 Single crystal diamond deposition by laminar and turbulent acetylene-oxygen flames

The interest of this publication lies in the detailed study of the effects of flame turbulence on the deposition of single crystalline diamond films. As demonstrated in the previous article, turbulent oxygen acetylene flames can increase the diamond deposition rate substantially for polycrystalline deposits. One of the research topics in the CSEM diamond group involved the deposit of single crystalline films on natural diamond seed crystals. The aim of this study was to use the oxygen acetylene flame as a rapid deposition method in order to create thick windows of optically pure diamond. For this reason it was of importance to verify if the use of a turbulent oxygen acetylene flame can increase the diamond growth rates when depositing on natural diamond seed crystals.

The following study shows that the differences in growth rate using a turbulent flame are not very significant. Although no disadvantages in using a turbulent flame are found, no great benefits are detected either. Since the use of turbulent flames poses some technical complications (easier flash back of the flame in the burner, hence a lower intrinsic security than in a laminar burner and a higher heat development requiring therefore a more powerful cooling substrate cooling system) it can be concluded that turbulent flames are not the best choice when depositing single crystalline films.

This publication furthermore shows the influence crystalline orientation of the diamond seeds has on the subsequently grown single crystalline diamond films. It is demonstrated that not all orientations are equally well suited for subsequently stable growth of thick single crystalline diamond films. These important findings have been used in the next step of the single crystalline diamond film growth project, which was the growth on mosaics of aligned natural diamond seeds. The right choice of crystalline orientation of the seed crystals has allowed for the deposition of a continuous single crystalline diamond film starting with two separate seed crystals (BRITE EURAM project). A subsequent up scaling of the demonstrated principle to large mosaics has so far not been demonstrated. One of the reasons for this lies in the limited deposition area up scaling possible using an oxygen acetylene flame (to large not stable burners). Other rapid diamond deposition methods, like for instance the plasma torch, have not been used successfully yet due to the deposition impurities included in the films, which make the unsuitable for optical applications.

In conclusion, the subjects presented in the publication have contributed in the better understanding of both turbulent flame deposition behaviour and single diamond growth conditions.

Single crystal diamond deposition by laminar and turbulent acetylene-oxygen flames

J. J. Schermer and L. J. Giling
Research Institute of Materials (RIM), University of Nijmegen, Toernooiveld, 6525 ED Nijmegen, The Netherlands

P. Alers
CSEM Centre Suisse d'Electronique et de Microtechnique S. A., CH-2000 Neuchâtel, Switzerland

(Received 5 December 1994; accepted for publication 27 April 1995)

The homoepitaxial deposition of diamond layers on {111} and {001} type-IIa natural diamond substrates, by both laminar and turbulent acetylene-oxygen flames, is described. Using the same gas flows, temperatures, and supersaturations of 4%, a higher growth rate was obtained on a {001} substrate with a turbulent flame than with a laminar flame. Layers grown at the same temperature on {111} substrates with a supersaturation of 3% show no significant difference in growth rate. Due to the large differences in geometry between both types of flames it is not possible to relate the substrate positions in the acetylene feathers to each other and compare the growth results at any location. However, it is shown that the application of turbulent flames for single-crystal growth does not lead to a dramatic change in quality of the diamond as was previously reported in the literature. It is demonstrated by microscopic and spectroscopic techniques that the crystallographic orientation of the substrates, the deposition temperature, and the gas velocity all have a larger influence on the crystal morphology and impurity incorporation of the grown single crystals than the introduction of turbulence.

I. INTRODUCTION

In recent years the homoepitaxially deposition of diamond crystals from a laminar acetylene-oxygen combustion flame has only been studied by a limited number of research groups,[1,2] despite the fact that with this relatively simple and inexpensive deposition technique good quality single crystals comparable to type-IIa natural diamond can be obtained at high growth rates.[3] Snail and Craigie argued that the growth rate could be increased significantly by the introduction of turbulence if diamond growth in laminar flames is transport limited.[4] The laminar or turbulent nature of a gas flow in a tube is within certain limitations determined by its dimensionless Reynolds number (Re) defined as $\mathrm{Re}=4f_{\mathrm{tot}}/\pi D\nu$, with f_{tot} the total gas flow, D the tube diameter, and ν the kinematic viscosity of the gas mixture. For a mixture at 300 K with an acetylene-to-oxygen ratio close to 1, which is used in flame deposition, ν can be calculated to be 0.129 cm^2/s.[5] Reynolds numbers below 2300 are associated with laminar flows and above 3200 with turbulent flows.[6] Between these two limits the flow is regarded to be in a transition state. As argued before by one of the authors,[7] it is hard to obtain a turbulent flame with a commercial burner since the exit tube is by far not long enough to establish a turbulent flow. Although the Reynolds number calculated at the exit opening is well above 3200, the flame obtained is still laminar. Therefore, in this case Re should be related to the diameter of the gas tube leading to the tip; however, a turbulent flame can be obtained with a commercial burner by the use of extremely large flow rates and larger exit openings as compared to the laminar situation. A diamond layer deposited in a turbulent flame obtained in this way[8] was shown to have a better quality but a lower growth rate than specimens grown in a laminar flame.[4] This gain in quality at the cost of growth rate is a common phenomenon in crystal growth by chemical-vapor deposition (CVD); see, e.g., Ref. 9.

Recently, researchers at the CSEM succeeded in designing a burner for which a fully turbulent flame is stabilized at the same total gas flow as for a laminar flame obtained by a commercial burner with the same exit diameter. Alers and co-workers[7] reported that in such a turbulent flame the polycyrstalline diamond deposition rate on molybdenum substrates is twice as high as in a laminar flame under similar conditions. In the present study an upscaled burner tip of the same design with an exit opening of 1.4 mm in diameter is used to generate a turbulent flame. The results of homoepitaxial deposition on {111}- and {001}-oriented natural diamond substrates with this burner are compared with those obtained by a commercially available laminar burner with the same exit opening. The {111} samples are discussed in detail, while the {001} samples are considered briefly as the growth of these samples by the flame technique was previously described.[3]

II. EXPERIMENTAL DETAILS

The flame deposition setup has been described in detail in previous work.[3,10] The cooling system developed at the University of Nijmegen allows regulation of the deposition temperature to within ±20 °C absolute and ±10 °C relative. The flows of the high-purity source gases oxygen (99.995%) and acetylene (99.6%) are regulated by mass flow controllers within ±0.05 standard liter per minute (slm). A commercially available welding torch equipped with a 1.4-mm-diam orifice tip was used to generate the flame. Whenever a turbulent flame was required this tip was exchanged by a CSEM-designed turbulent tip with the same exit diameter.

 0021-8979/95/78(4)/2376/9/$6.00

The turbulent burner, which basically consists of a turbulence-inducing orifice mounted inside a commercially available burner tip a few millimeters before the exit opening, was designed for total gas flows around 6 slm. Because diamond deposition takes place in a narrow composition region around a 1:1 mixture of acetylene and oxygen,[11,12] the oxygen flow during all experiments was fixed at 3 slm. The deposition temperature T_d was kept around 1150 °C for most experiments. At such high temperatures good quality diamond single crystals with growth rates up to 130 μm/h were obtained with a laminar flame before.[3] The position of the sample in the acetylene feather is determined by the distance d from the inner cone of the flame or the distance b from the burner tip (see Sec. III). The gas composition is defined by the acetylene supersaturation (S_{ac}) or the acetylene-to-oxygen ratio R.[13] The deposition times varied between 2 and 3 h. The growth conditions and a number of characteristics of the samples are listed in Table I. The samples grown in the turbulent and laminar flame are denoted T and L, respectively. The second character in the notation indicates whether the type-IIa natural diamond substrate has a cubic (C) or octahedral (O) top face. These (within ±4°) {001}- and {111}-oriented substrates are cylindrically shaped with a diameter of 2 mm and a thickness of 250 μm. To ensure a good thermal contact during deposition the substrates were soldered onto the water-cooled substrate holder.

After flame deposition the surface morphology of the single crystals was investigated by scanning electron microscopy (SEM) and optical differential interference contrast microscopy (DICM). The orientations of the facets developed along the sides of the samples were determined by measurement of their angles θ relative to the top face of the sample using a two-circle optical-reflection goniometer. The diameter of the in-drawn circle of these faces is used as a measure of their morphological importance (M) relative to each other. In addition the differences in crystalline perfection of the deposited layers were analyzed by various techniques such as cathodoluminescence (CL) topography, and Raman and photoluminescence (PL) spectroscopy. The PL spectra presented in this study were obtained at 87 K using the 514.5 nm line of an Ar^+ laser as the excitation source. The luminescence was dispersed by a 0.6 m double monochromator with 1200 lines/mm gratings and detected by a cooled photomultiplier tube with a GaAs photocathode.[14] The equipment used for Raman spectroscopy and CL topography have been described elsewhere.[3,15]

III. FLAME CHARACTERISTICS

An important feature of a premixed flame is the flame front. For the acetylene-oxygen flame this is the zone in which the primary combustion of the premixed gases and oxygen to CO and H_2 takes place.[6] This reaction zone propagates opposite to the outflowing source gases with the burning velocity v_b which equals the gas flow component normal to the zone. For a laminar flame the primary combustion process is reasonably well understood and the burning velocity and the shape of the flame front can be described in terms of gas composition, total flow rate, and the dimension of the burner orifice.[6] The flame fronts in Fig. 1 can be recognized

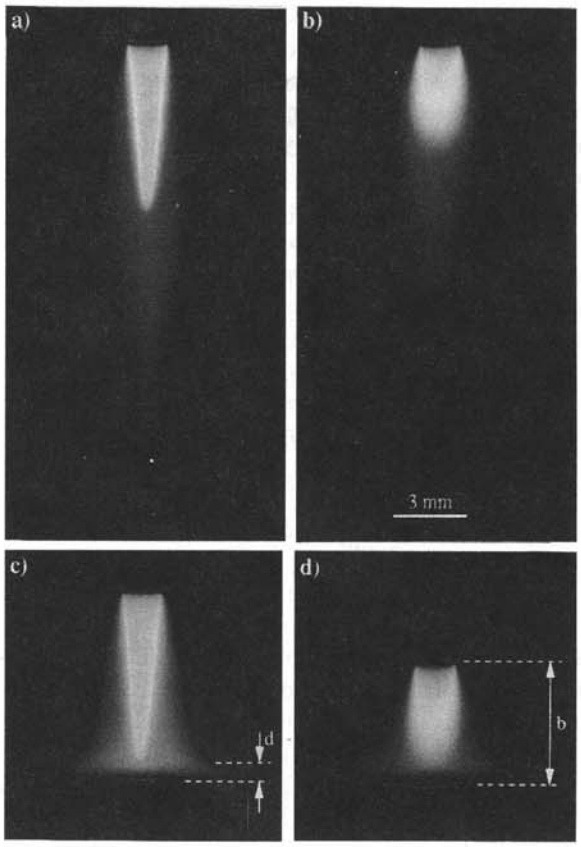

FIG. 1. Free-burning (a) laminar and (b) turbulent acetylene-oxygen flames obtained with the same gas composition (f_{ox}=3 slm, R=1.005, S_{ac}=5%) and burner opening which is 1.4 mm in diameter. The same (c) laminar and (d) turbulent flames directed on a cooled substrate.

as the brightest parts of the flames due to emission of thermally or chemically excited C_2 and CH radicals. Figure 1(a) shows that the front of a laminar flame (Re≈2000) is a conically shaped zone with a thickness of about 40 μm. Inside this cone the gas mixture is heated up slightly but does not react. Apart from side effects at the rim and the rounded tip of the cone, v_b is constant over the flame front. Therefore, the burning velocity of a flame can be determined from the measurement of the area of the flame from A_f and the total gas flow f_{tot} by $v_b = f_{tot}/A_f$.[6] Approximating the flame front of the flame in Fig. 1(a) by a cone with height h and base radius r, which in general is about 10% larger than the radius of the burner opening. $A_f = \pi r\sqrt{r^2+h^2}$ and v_b is found to be 5.8 m/s.

Outside the cone the combustion proceeds in a diffusion flame in which the CO and H_2 formed in the flame front react to CO_2 and H_2O by in-diffusion of oxygen from the ambient. In case an excess of acetylene is present in the gas mixture, this reacts outside the flame front in the diffusion flame forming the acetylene feather [see Fig. 1(a)]. This feather, in which all kinds of hydrocarbons exists, is visible due to radiation of C_2 and CH radicals.[16] If the excess of acetylene is diminished the feather decreases until a neutral flame is obtained as the feather just disappears. This situation can be clearly recognized in a laminar flame and defines the zero point in the acetylene supersaturation (S_{ac}=0%).

The turbulent nature of the CSEM-designed burner (Re ≈7000) was confirmed by the loud hissing sound of the burner[4,6] and the shape of its flame front which is shorter and more rounded than the laminar one [see Fig. 1(b)]. The center of the front is not sharply defined but is blurred and therefore usually referred to as the flame brush. In contrast to the center, the rim of the flame front remains steady indicating that the amount of turbulence decreases radially with the distance from the center of the flame. For turbulent flames obtained with commercial burners by the application of high flow rates,[17] the flame front is more elongated and the part which remains well defined is larger than for the turbulent flame which is used in the present study. The appearance of such a flame is a kind of intermediate between the laminar flame and the turbulent flame shown in Fig. 1. The brush appears to be a time average of a rapidly fluctuating wrinkled and sometimes even fragmented flame front, as was also confirmed by Marks *et al.*[18] using dark-field shadow photography. These fluctuations indicate that the burning velocity varies both in time and with the position of the flame front. This is caused by turbulent eddies of the same dimensions as the thickness of the flame front leading to sharp curvatures in the front and an increased transfer of heat and radicals.[6] Approximating the mean area of the front by a truncated cone with a hemispherical top, the average value of the burning velocity of the flame in Fig. 1(b) is estimated to be 7.5 m/s.

Not only the flame front but also the acetylene feather of the turbulent flame is smaller. This shows that the combustion of the excessive acetylene proceeds faster by the enhanced in-diffusion of oxygen from the ambient due to the turbulence. Diamond deposition takes place if a cooled substrate is placed in the reducing acetylene feather [see Figs. 1(c) and 1(d)]. Outside the feather in the oxidizing outer flame, diamond will be etched rather than grown. In previous studies[3,10] the quality of the deposited material among others appeared to be dependent on the excess of acetylene used to create the feather and the position of the substrate in it. Using a laminar flame these features were described by S_{ac} and d [see Fig. 1(c)], for which the flame front directly or indirectly is used as a reference. However, as the turbulent flame front is not sharply defined the accurate determination of the values for d and S_{ac} in a turbulent flame is not possible. This problem is "solved" by using the substrate to burner distance b [see Fig. 1(d)] and the acetylene-to-oxygen ratio R in a turbulent flame as an alternative reference for d and S_{ac}, respectively.

IV. GROWTH RESULTS AND DISCUSSION

Due to the specific graphitelike appearance of the {111} surface and its easy disturbance of stacking order,[19] crystal volumes grown via this face usually suffer from several defects such as stacking faults, graphitelike inclusions, and, perhaps most of all, microtwinning. These defects obstruct the step growth mechanism of the face, which therefore easily becomes polycrystalline after growth of a few micrometers.[15] Janssen *et al.* demonstrated the occurrence of this phenomenon for a flame-grown specimen at a temperature of approximately 940 °C.[20] Results of a recent study on flame-grown polycrystalline diamond layers indicate that the occurrence of these defects increases with a decreasing activation level of the gas phase.[13] Samples grown at a distance larger than 2 mm from the flame front or with supersaturations above 6% show a fast deterioration of the {111} facets. It was discussed that this is probably related with the formation of larger hydrocarbon compounds and possibly soot in the gas phase which, upon deposition easily induces the formation of twins or other defects. To avoid these problems the {111} samples in the present study were grown at about 1 mm from the flame front using a somewhat lower value for R (S_{ac}) than the {001} samples (see Table I). This strategy appeared successful because the single-crystal nature of the samples was maintained, although the deposition rate was much lower than that of the {001} samples. Table I shows that for the {111} samples grown at 1150 °C the introduction of turbulence did not result in an increase in growth rate; however, the {001} sample grown by the turbulent flame was obtained with a higher deposition rate than the one grown by the laminar flame. Polycrystalline layers grown on molybdenum substrates, using the same flames as described in the present study, reveal a similar behavior of the growth rate as a function of the supersaturation. At low S_{ac} diamond layers grow faster in the laminar flame in the turbulent flame, at high S_{ac} the layers grow faster in the turbulent flame. This phenomenon could be described by the higher mixing rates in the turbulent flame, resulting in a less localized flame front and a smaller acetylene feather due to a faster completion of the combustion process.[13] Compared to the total length of the turbulent feather, growth proceeds relatively close to the flame front for high S_{ac}. For low S_{ac} growth proceeds relatively close to the periphery of the turbulent feather where the combustion of excessive acetylene is almost completed. A more detailed description of this process is given in Ref. 13.

TABLE I. Growth conditions and results.

Sample	LO	TO1	TO2	LC	TC
Burner tip	laminar	turbulent	turbulent	laminar	turbulent
Substrate	{111}	{111}	{111}	{001}	{001}
T_d ±20 (°C)	1150	1150	1250	1150	1150
f_{ox} ±0.03 (slm)	3.0	3.0	3.0	3.0	3.0
S_{ac} ±0.5 (%)	3.0	···	···	4.0	···
R ±0.005	0.985	0.985	0.985	0.995	0.995
d ±0.1 (mm)	1.0	~1	~1	1.0	~1
b ±0.3 (mm)	8.0	5.0	5.0	8.0	5.0
h_d ±5 (μm)	43	38	58	85	97
v_d ±3 (μm/h)	14	13	21	34	49

Besides diamond deposition on the top faces, a number of facets and curbed bands were developed along the sides of the substrates. To simplify the discussion, the locations of the observed bands (bold lines) and faces (grey markers) on the {111} specimen are indicated in a stereographic projection shown in Fig. 2. For the side faces θ and M, both averaged over the three symmetry equivalent faces, are given in Table II. The crystallographic orientations indicated by the white markers are subject to discussion but were not observed on the samples. The goniometer measurements revealed that in general the {001} and {111} side facets at all specimens are

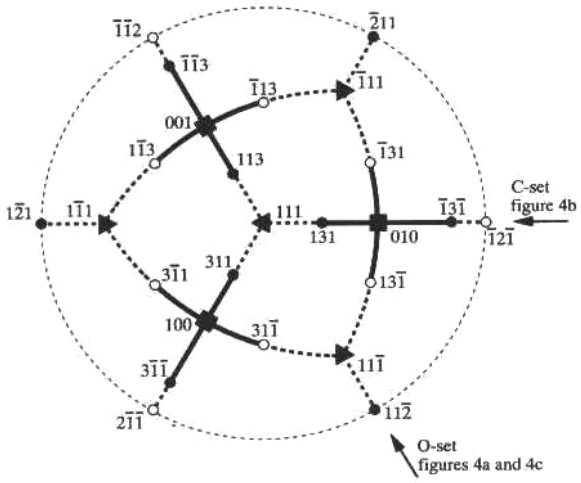

FIG. 2. Locations of the observed faces (grey markers) and curved bands (bold lines) on the {111} samples in a stereographic projection on the (111) plane. The faces indicated by the open markers were not observed but are subject to discussion. The solid and dashed bold lines indicate a difference in stabilization observed for the orientations in the curved bands. Note that all the orientations which show evidence of some kind of stabilization coincide with the $\{hhk\}_{h\leq k}$ parts of the ⟨110⟩ zones. The periphery of the projection is outlined by the dashed thin line.

well developed and give clear reflections. Other faces are still somewhat curved resulting in a diffuse reflection or a band of reflections in the optical goniometer telescope, giving values of θ with an accuracy not better than within 2°. The curved faces with orientations between {113} and {117} at the {111} samples are referred to as $\{11X\}$ $(3<X<7)$. The final form of these faces in general is {113} since these are the only facets other than {111} and {001} observed on previously reported {110} samples[3,21,22] and on the {001} specimens discussed in the present study, which due to higher growth rates are in a further stage of development than the {111} specimen. However, it should be noted that for silicon CVD a relatively low supersaturation, as used for the growth of the {111} samples, resulted in the development of a wealth of additional facets such as {337}, {7 7 13}, and {9 9 19}.[23]

A. Morphology of specimen grown on {111}-oriented substrates

Sample LO grown using a laminar flame shows a number of interesting features which are discussed in detail followed by a comparison with the characteristics of the {111} samples grown with a turbulent flame. Figure 3(a) shows that the (111) top face of the sample is covered by triangular hillocks. These elevations are bounded by vicinal faces of the "positive"[24] form $\{111+\delta\}$ with $0<\delta\ll 1$ which are stepped toward the $[\bar{1}\bar{1}2]$, $[\bar{1}2\bar{1}]$, and $[2\bar{1}\bar{1}]$ directions. The inclination of the vicinal faces with the exact (111) face is 4° as was determined by the goniometer. Close examination with DICM reveals that most of the large elevations consist of two individual hillocks with closely spaced (between 5 and 15 μm) summits which have one slope in common. The summits are connected by a peculiar line-shaped feature typically 2 μm wide, perpendicular to the in-plane ⟨112⟩ directions. Several of them could be identified as penetration twins.[25,26] Accumulation of steps generated by contact nucleation at both ends of the low inclination side (twin plane) of the twins[27] can account for the observed appearance of the "double" growth hillock. Alternatively, the triangular features might be generated by extended dislocations along ⟨112⟩, consisting of two closely spaced partial dislocations with a stacking fault in between.[28] In that case the twins between the summits of these elevations could be formed at any time during the deposition process. The relatively small number of hillocks compared to the dislocation density of type-IIa natural diamond (10^6 cm^{-2}) is explained by the fact that most of the smaller hillocks from individual dislocation sources are overgrown by larger ones generated by twins or extended, more active, dislocation sources. The presence of the triangular hillocks indicates that the growth rate is limited by integration of growth units into the kink positions in a step. The slopes of the hillocks are opposite to those expected from a first-order periodic bond chain (PBC) analysis,[29] but can satisfactorily be explained by the assumption of step reconstruction by dimer formation.[30] In the center of the sample the triangular features are somewhat less distinct and the hillocks are a bit rounded. There are two

TABLE II. Angles of the side faces with the top face of the {111} specimens and the smallest lateral width of these faces as an indication of their morphological importance.

Sample LO		Sample TO1		Sample TO2		Calculated	
$\theta\pm2$ (deg)	$M\pm3$ (μm)	$\theta\pm2$ (deg)	$M\pm3$ (μm)	$\theta\pm2$ (deg)	$M\pm3$ (μm)	θ (deg)	Indices
			Faces in the O sets				
71.2	140	70.4	150	70.5	200	70.5	111
89.5	40	87.5	80	...	...	90	112
...	...	...	...	107.2	50	100–113.8	113–117
127.1	50	126.0	50	123.3	65	125.3	001
			Faces in the C sets				
35.6	38	36.4	40	30.2	50	29.5–43.2	131–171
56.2	30	56.2	15	...	...	54.7	010
71–76	95	72–82	145	65–77	175	65.3–80	171–131
109.9	70	110.3	75	110.0	100	109.5	111

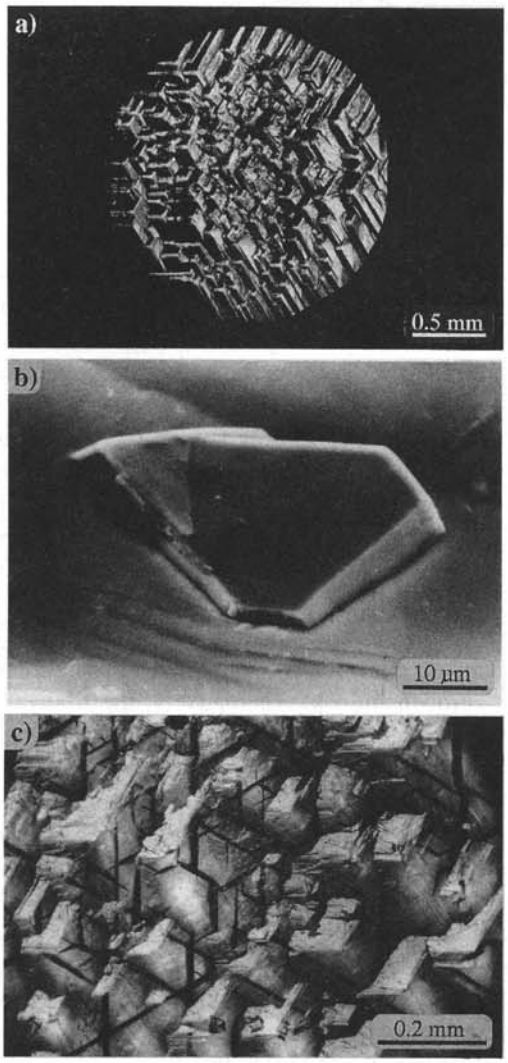

FIG. 3. (a) DICM overview perpendicular to the {111} top face of a flame-grown single crystal (sample LO) and (b) and (c) detailed pictures of crystallographic imperfections on it. (b) SEM picture of a twofold twin. (c) Cracks along the {111} crack planes in the deposited layer revealed by DICM. The orientation of the sample on photographs (a) and (c) is along the same direction as the stereographic projection shown in Fig. 2.

complementary explanations for this effect. First, the hillocks can be bounded by $\{1\,1\,1+\delta\}$ as well as $\{1\,1\,1-\delta\}$ vicinal faces ($0<\epsilon\ll 1$), which gives the crystal a more rounded hexagonal appearance.[31] The occurrence of these additional faces is to be expected in a gas atmosphere containing many active molecules the adsorption of which partly hampers the step reconstruction of the {111} face.[30] Second, round hillocks will occur if instead of the integration of growth units at the kink position of a step the surface diffusion of these units toward the step plays the limiting role in the growth velocity of the crystal face.[27,30] The diffusion rate of growth units along the surface will be less if diffusion is hampered by the presence of adsorbed species, which is consistent with the first picture. Note that growth of {111} faces is not limited by gas-phase transport because {110} faces grow several times faster under similar circumstances[3] so local differences in supersaturation of the gas phase cannot account for the described phenomena.

In addition to the triangular features the top face exhibits about ten clearly distinguishable parallel twins[26] of approximately 30 μm in diameter [see Fig. 3(b)]. None of these twins is perfectly shaped, they all show evidence for additional twinning due to the increased local strain in the diamond lattice. This process eventually leads to the complete deterioration of the octahedral surface since the growth steps cannot pass the twin boundary. At the same time it is clear from their limited appearance that formation of twins can be suppressed by deposition close to the flame front using a relatively low supersaturation and a high deposition temperature. From the fact that their presence does not seem to interfere with the macrosteps located nearby on the crystal surface, it can be deduced that they were nucleated in a final stage of the growth experiment. Whatever induced their appearance, which is not restricted to a certain part of the octahedral top face, in this stage remains unclear.

Inspection of the sample by DICM reveals that the center of the sample exhibits a large number of cracks along the octahedral cleavage planes [see Fig. 3(c)], i.e., perpendicular to the $\langle 112\rangle$ directions in the plane of the top face. The cracks are confined to the grown layer and were formed after growth since the cracks do not interfere with the growth features at the surface. Van Enckevort *et al.*[32] reported similar crack patterns which are a manifestation of stress release of homoepitaxial {111} samples grown by the hot filament technique. The stresses arise from a lattice mismatch between the grown layer and the substrate. Near the rim of the top face the sample is not cracked since the strains in this region are expected to be released by elastic deformation of the side faces of the crystal. This picture is supported by the fact that previously investigated flame-grown samples on {110} substrates show an increasing amount of cracks along the {111} cleavage planes with increasing lateral dimensions of the crystal.[3]

Along the rim of the top face a curved band of macrosteps has developed which is interrupted by six sets of broad connected facets more or less vertical along the sides of the sample [see Fig. 4(a)]. Some of the faces are not shown in the stereographic projection of Fig. 2 because their angle with the top face is more than 90°. These faces have developed in spite of the fact that they are not directly facing the main gas flow. The faceted sets, which are of two different types, are shown in detail in Figs. 4(b) and 4(c). The large side facet visible in Fig. 4(c) is identified as a {111} face since it shows exactly the same growth features as described for the top face. Together with the top face the position of this side face completely fixes the orientation of the sample. The arrows in Fig. 2 indicate the direction in which the photographs of Fig. 4 were taken. The goniometer measurements reveal that the faces in the set shown in Fig. 4(b), and to be referred to as the (cubic) C set hereafter, are {11*X*}, {001}, {11*X*}, and {111} from top to bottom. The other set [see Fig. 4(c)], to be referred to as the (octahedral) O set, exhibits {111}, {112}, and {001} faces from top to bottom. Figure 4(d) is a schematic representation of both sets showing the relative dimensions of the observed faces averaged over the three symmetry-equivalent counterparts (also see Table II). From the cross section it becomes clear that, al-

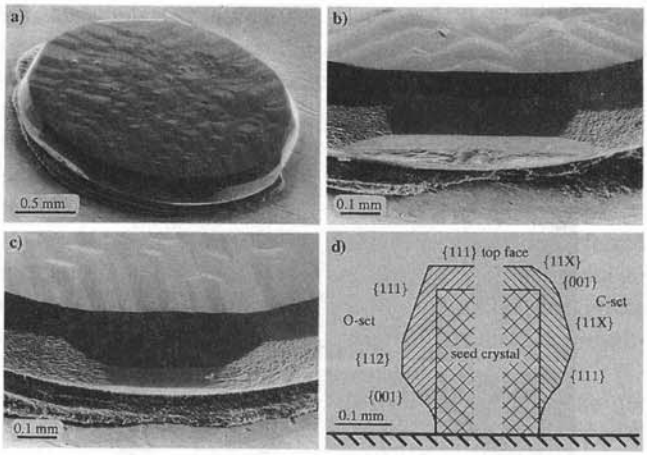

FIG. 4. (a), (b), and (c) SEM photographs and (d) a schematic cross section of a diamond single crystal (sample LO) grown on a {111} natural diamond substrate. The overview (a) and detailed pictures of a faceted C set (b) and O set (c) were taken in the directions indicated by the arrows in Fig. 2 at an angle of ≈55° with the top face. Note the difference in the curved band close to the two faceted sets and the rough appearance of all orientations other than $\{hhk\}_{h\leq k}$.

though reported by others,[33] the observed {112} faces in the O sets most probably are the "translated" sides of the original cylindrical substrate which have not grown out of the crystal form yet. The morphological importance of the {112} faces in the three O sets of the specimen differ significantly (between 17 and 60 μm). Because the angle between both faces adjacent to the {112} orientation in the C sets (≈37°) is smaller than in the O sets (≈55°) (see Table II), the face has already disappeared from all C sets. The gradual transition to the rough, cobbled orientations on both sides of the {112} faces [see Fig. 4(c)] illustrates their relatively low degree of stabilization compared to the other side faces. In addition the cross section shows that the morphological importance of more stable faces with equivalent Miller indices in both sets changes with their distance from the top face. This is related with the typical gas-phase geometry of the flame technique of which the composition changes significantly between the top and the bottom of the samples.

A comparison between Figs. 4(b) and 4(c) reveals that close to the O sets the curved band shows a high density of macrosteps parallel to the ⟨110⟩ PBCs, while it exhibits more flattened features close to the C sets. This indicates that most of the surfaces with orientations in the curved band are stabilized in one direction (parallel to the in-plane PBCs) but that close to the C sets a discrete number of them are stabilized in two directions. The difference in stabilization, indicated by the solid and dashed lines in Fig. 2, can be described by a model based on an orientation-dependent broken bond analysis of the surfaces, with additional considerations about dimer formation perpendicular to the ⟨110⟩ PBCs which is presented elsewhere.[34] The model shows that due to the formation of dimers, stabilization in at least one direction is expected for orientations corresponding to Miller indices $\{hhk\}_{h<k}$ in the ⟨110⟩ zones which, according to the PBC theory, should be rough (kinked) K faces.[35] Except for the {111} facets which are stabilized by three connected ⟨110⟩ PBCs, all the faces and the curved bands with macrosteps observed in the present study belong to these zones. Other orientations, including the $\{hhk\}_{h>k}$ which should be stepped S faces according to the PBC theory, have a rough appearance [see Figs. 4(b) and 4(c)]. From this it can be concluded that the presence of ⟨110⟩ PBCs, consisting of nearest-neighbor covalent bondings only,[35] in one direction is not sufficient to stabilize the surface.

About half of the (111) top face of the substrate used to grow sample TO1 in the turbulent flame was misoriented toward $[11\bar{2}]$ resulting in a strong elongation of the growth hillocks in that direction. The other half of the top face has approximately the same density of triangular hillocks as observed for sample LO although most of them do not reveal the described line-shaped features at their summits. The phenomena observed along the sides of sample TO1 are less pronounced but also similar to those on sample LO (see Table II). This shows that the application of turbulence does not lead to large differences in the crystallographic habit of the grown samples. Sample TO2, which is grown in a turbulent flame at a 100 °C higher deposition temperature, shows some remarkable differences compared to the other two {111} samples and is therefore discussed in more detail Figure 5(a) shows that the top face of the sample is covered by a small number of large growth hillocks which have overgrown all the others. The summits of most of them are badly shaped showing steep irregular pits [see Figs. 5(a) and 5(b)]. Possibly similar inclined twins as observed on sample LO have locally hampered the growth of the {111} top face inducing the pits. No twins are observed on the final surface which is cracked although to a lesser extent that sample LO.

Figure 5(c) shows that for sample TO2 the occurrence of {112} faces in the O sets is "obscured" by the development of faces with {11X} orientations (see also Table II). The C sets, of which one is shown in Fig. 5(b), differ completely from those of the other {111} samples. The {001} faces have disappeared and at the positions they would be expected the width of the sets perpendicular to the plane of the cross section is strongly reduced. The {11X} faces closest to the top face of the sample now definitely are identified as {113} facets. In contrast to this, the {11X} facets further away from the top have shifted toward the {117} orientations. The shallow rim indicated by the arrow in Fig. 5(b) shows that these {11X} faces even tend to break up into two separate facets, most probably {113} and {115} or {117}. At both sides of the waist in the C set, flat faces started to develop which likely correspond to the {11X} faces originally laying in the curved band along the rim with the top face of the sample (see Fig. 2). These faces just started to develop from this band and were not observed on the other {111} samples. This is explained by the fact that in the band with a relatively low curvature (radius≈1 mm), the {11X} faces and orientations close to them, which are only slightly less stabilized, hardly hamper each others development. In regions of higher curvature as between the {111} and {001} within the faceted sets (radius≈0.2 mm) the more stable {11X} faces have a pronounced appearance since they have competed and survived their neighboring orientations. The {11X} faces in the C sets originating from the straight corner between the top and the

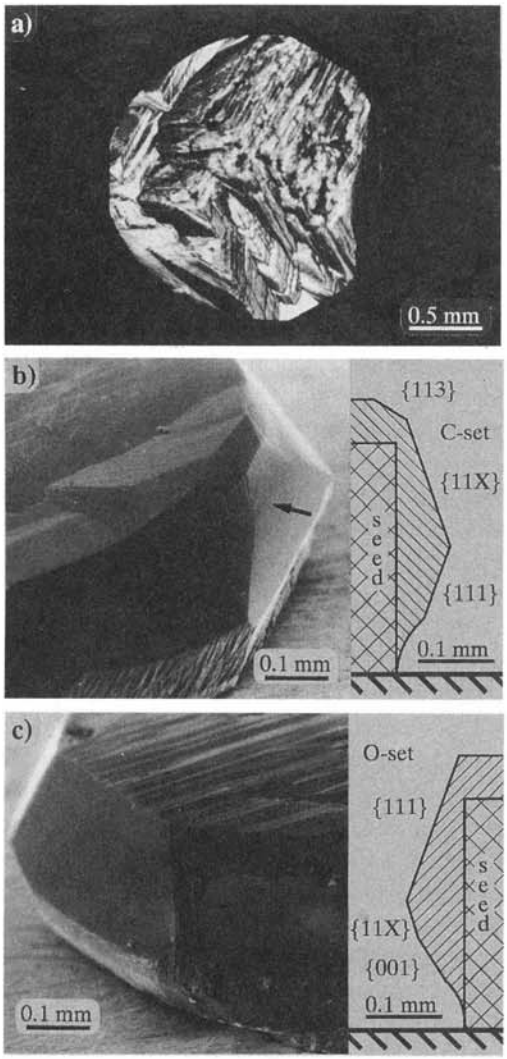

FIG. 5. Photographs and schematic cross sections of a diamond single-crystal (sample TO2) grown on a {111} natural diamond substrate. The overview (a) was taken by DICM perpendicular to the top face. The detailed side views of the faceted C set and O set (b) and (c), respectively, were taken by SEM at an angle of ≈55° with the top face.

side wall of the substrate have the most pronounced appearance.

In addition to the large curved band along the top face, a smaller but similar band has developed along the octahedral bottom face of the sample [see Fig. 5(c)]. Note that this band also shows flattened areas close to the ⟨001⟩ orientation in the O set just as the band along the top face does close to the ⟨001⟩ orientation in the C set.

B. Morphology of specimen grown on {001}-oriented substrates

Diamond layers grown in a laminar flame on cylindrically {001}-oriented type-IIa natural diamond substrates were thoroughly investigated in a previous study.[3] These samples, referred to as C series are compared with the samples investigated in this study. They {001} top faces of the samples in the C series are flat and grow via steps due to the (2×1) surface reconstruction.[36,37] They show no sign of twinning or

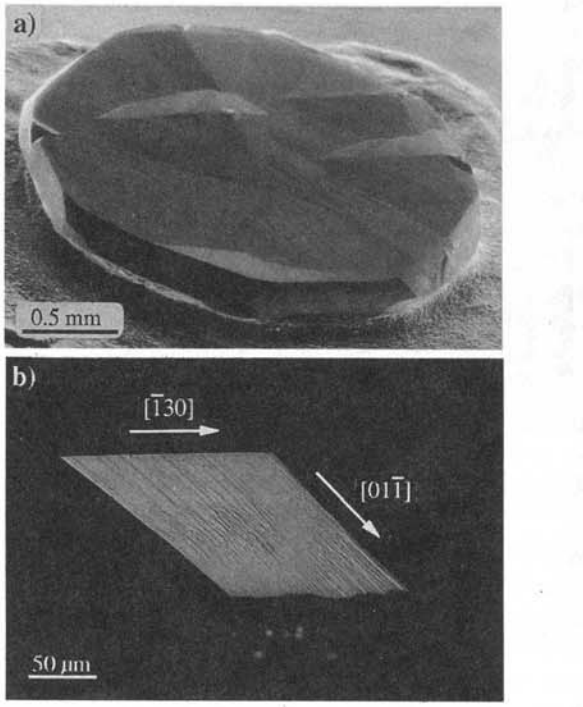

FIG. 6. Photographs of a diamond single crystal (sample TC) grown on a {001} natural diamond substrate. The SEM overview (a) was taken at an angle of ≈55° with the (001) top face. The picture of the (311) facet was obtained by DICM more or less perpendicular to the facet.

crack formation. Along the rim {111} and {001} side faces have developed giving the samples an octahedral shape as was also reported by Snail and Hanssen.[2]

The top and side faces of both {001} samples presented in this study reveal the same features, except for some occasional cracks on the LC samples related with minor inclusions that were induced by inappropriate cleaning before growth. Because of this, sample TC—grown in the turbulent flame—looks somewhat smoother and has sharper boundaries with its side faces than sample LC. Figure 6(a) shows that several square growth hillocks have developed on sample TC with macrosteps aligned along the ⟨011⟩ directions as expected from the 2×1 surface reconstruction.[36] DICM reveals that the hillock located more or less in the center of the sample originates from a three-dimensional nucleus or penetration twins.[27,38] Such features which are common for hot-filament-grown {001} single crystals[32] are rarely observed on flame-grown specimens. Like the other hillocks on sample TC they generally have sharp point-shaped summits which are usually located near the rims of the top face. These hillocks are most probably generated by bundles of screw dislocations originating from the substrate. In addition to the {111} and {001} facets, eight {113} facets are observed on the perimeter of the samples [see Fig. 6(a)]. Figure 6(b) gives a detailed view of one of these facets. The rims of this (311) facet are parallel to the [01$\bar{1}$] and [$\bar{1}$30] directions. The features shown in the photograph with steps parallel to the in-plane [01$\bar{1}$] PBC might be considered as extremely elongated hillocks which were able to expand rapidly along ⟨011⟩ since in this direction no energy barrier exists for the addition of growth species. Possibly these hill-

ocks are nucleated in the central region of the facets by dislocations originating from the straight corner of the cubic top face with the side wall of the substrate. In that case the hillocks might coalèsce further away from the center causing the decreased step density observed toward the top and bottom of the facet [see Fig. 6(b)]. An alternative explanation of this effect is that the hillocks are generated at the rims of the facet which for {001} facets were found to be preferred nucleation sites during flame deposition.[27] Hillocks nucleated at the top and bottom rims of the {113} facets interfere with each other somewhere in the middle of the facet resulting in a higher density of macrosteps in this region.

Surprisingly, in the first instance {113} facets were not observed on the previously examined samples of the C series.[3] Reinspection of these samples revealed that only the sample with the thinnest epitaxial layer of these specimens exhibits very small {113} facets. For this sample the average growth rate of these {113} faces (v_{113}) relative to that of the {111} side faces on the sample (v_{111}) was found to be about 2.2. For the other samples it could be deduced that $v_{113}/v_{111}>1.9$ since no {113} facets were present any more. This indicates that under the applied growth conditions, the minimum in the surface energy of the {113} face is only local.[34] Finally, the diamond crystal will be bounded by the more stable {111} and/or {001} faces, dependent on their relative growth rates.[25,26,39] For the samples LC and TC, which are grown at a 50 °C lower temperature than the previous obtained samples,[3] v_{113}/v_{111} is 1.7 and 1.6, respectively. Apparently relatively small differences in the deposition temperature influences the crystallographic appearance of the samples to a larger extent than the introduction of turbulence in the flame. The wealth of growth features observed on the {111} samples is not present on the {001} samples because they are overgrown by the (under the applied growth conditions more stable) {111}, {001}, and {113} facets.

C. Impurities

The main impurities expected in flame-grown diamond single crystals are nitrogen, nondiamond carbon phases such as graphitic inclusions, and hydrogen which is chemically bonded to carbon as CH_2.[1] Previously investigated {110} samples, flame deposited at 1200 °C, show that an increase in hydrogen concentration is reflected by an increase in background fluorescence as well as in the full width at half-maximum (FWHM) of the diamond peak in the Raman spectrum (see Table I of Ref. 3). However, similar to the {001} samples of the C series (see Sec. IV B) investigated in the same study all the {111} and {001} samples presented in the present study show Raman spectra that are identical to the natural type-IIa substrates with a FWHM$\leq$3 cm^{-1}. This indicates the absence of nondiamond carbon phases and incorporated hydrogen.

The PL spectra of the flame-grown diamond layers are usually dominated by two vibronic systems that have been attributed to nitrogen-vacancy pairs with their zero phonon lines at 2.156 eV (575 nm) and 1.945 eV (638 nm).[1,40] The spectra of the samples considered in the present study, however, are dominated by their Raman lines (indicated by R) to which they are normalized (see Fig. 7). The spectra reveal an

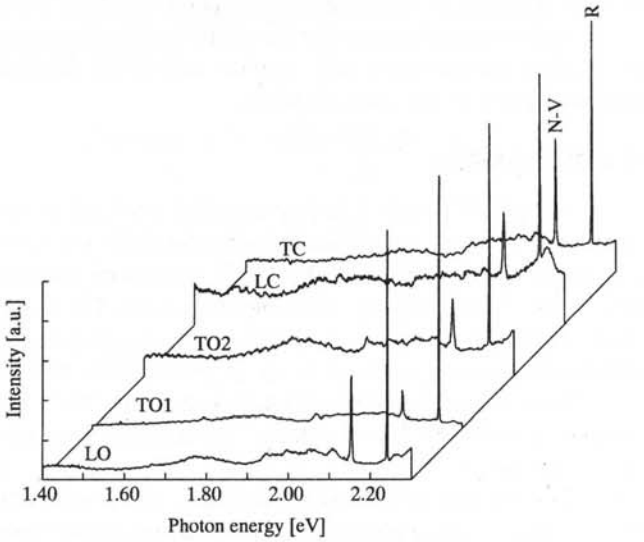

FIG. 7. PL spectra of the flame-grown diamond single crystals normalized to the first-order Raman phonon line (R). The peak indicated by N–V is the zero phonon line of the nitrogen-vacancy-related 575 nm system. The spectra are not corrected for the system response and the increasing intensity observed at the high-energy end of several of them is caused by reflections of the laser light.

extremely low density of luminescent defects with a marginal presence of the 575 nm (indicated by N–V) system and almost no sign of the other nitrogen-related system mentioned above. Therefore, it can be concluded that, under the present growth conditions, incorporation of nitrogen as nitrogen-vacancy pairs from the ambient in the crystals, which grow via the *F* faces {111} and {001}, is low. No significant differences are observed between samples grown by a laminar and a turbulent flame.

This picture is supported by CL topographic investigations: All samples reveal blue-band *A* luminescence characteristic for natural type-IIa diamond. In contrast to this, the previously investigated samples from the C series revealed some orange luminescence from the 575 nm system, indicating a small amount of nitrogen incorporation. However, these small amounts could not be detected by infrared spectroscopy[3] so the grown diamond layers have to be classified as type IIa. It is well possible that the decrease in signal of the 575 nm system is caused by higher gas velocities used in the present experiments. The samples of the C series were grown using a burner orifice of 1.6 mm in diameter and a total gas flow of 6.8 slm giving a gas velocity v_0 of 56 m/s at the burner opening, while the specimens in this study were grown at v_o=65 m/s. The high quality of the {001} diamond single crystal grown with a turbulent flame as reported by Snail *et al.*,[8] in our opinion, is mainly caused by the same effect, i.e., improved shielding from the ambient air due to a high gas flow rate, which can be calculated to be 127 m/s in their experiment (20.5 slm total flow with an 1.85 mm burner opening). This shows that the incorporation of nitrogen in flame-deposited single crystals in the first place is determined by the applied gas flows. Obviously the generated turbulence is not sufficient for a significant increase of the amount of nitrogen mixed in from the ambient up to the center of the feather where the single crystals are located.

Results obtained by a detailed investigation of the influence of the applied supersaturation at the position of the sample in the feather for turbulent and laminar flames on diamond growth,[13] point in the same direction.

V. CONCLUSIONS

In the present study it is demonstrated that laminar and turbulent flames can be obtained using the same gas flows and burner openings by the addition of a turbulence-inducing step inside a commercially available burner tip. The flames show significant geometrical differences due to a higher reaction rate (burning velocity) in the turbulent flame as a result of the enhanced mixing of heat and radicals. The flame front of the turbulent flame is blurred and more rounded than that of the laminar flame.

Due to the large differences in geometry it is not possible to relate the positions in the acetylene feathers of both flame types to each other and compare the growth results at any location in the flames. In order to determine which type of flame is better suited for diamond deposition, the performance of both over a large range of growth conditions should be compared. Recently, the influence of the growth parameters S_{ac} and d, which are most closely related to the gas-phase geometry, on diamond deposits grown by both flame types has been investigated. The results of this study are presented elsewhere.[13] However, this preliminary study already shows that the application of turbulent flames for single-crystal growth does not lead to a dramatic change in quality of the diamond as previously reported in literature. The crystallographic orientation of the substrates, the deposition temperature, and the gas velocity have a larger influence on the crystal morphology and impurity incorporation of the grown single crystals.

In addition it was demonstrated that the single-crystalline nature of diamond layers exceeding 50 μm thickness deposited on {111} substrates can be maintained in a highly activated gas phase. This is obtained by deposition with the substrates close to the flame front at a high temperature and a relatively low supersaturation. All faces and the curved bands with macrosteps, observed on the {111} and {001} single crystals, belong to the $\{hhk\}_{h\leq k}$ parts of the ⟨110⟩ zones. The stabilization of these orientations can be explained by the formation of dimer bonds between the surface atoms.[34] Other orientations have a rough appearance due to the occurrence of microfacetting. So, no faces or other signs of stabilization appeared for the $\{hhk\}_{h>k}$ parts of the ⟨110⟩ zones which according to the PBC theory are S faces and should be stabilized in one direction.

ACKNOWLEDGMENTS

The authors wish to thank Dr. F. Driessen and S. Olsthoorn for recording the PL spectra. W. Hänni (CSEM), W. Elst, Dr. G. Janssen, and Dr. W. van Enckevort are acknowledged for technical assistance and useful discussions. This work was financially supported by the European Community Brite Euram Project No. BE-5099-92 under Contract No. BRE-2-0147.

[1] G. Janssen, W. Vollenberg, L. J. Giling, W. J. P. van Enckevort, J. J. D. Schaminée, and M. Seal, Surf. Coat. Technol. **47**, 113 (1991).
[2] K. A. Snail and L. M. Hanssen, J. Cryst. Growth **112**, 651 (1991).
[3] J. J. Schermer, W. J. P. van Enckevort, and L. J. Giling, Diamond Related Mater. **3**, 408 (1994).
[4] K. A. Snail and C. J. Craigie, Appl. Phys.Lett. **58**, 1875 (1991).
[5] G. Vogelpohl, in *Landolt-Börnstein*, edited by K.-H. Hellwege and A. M. Hellwege, New Series Vol. 6 (Springer, Berlin, 1955), p. 586.
[6] A. G. Gaydon and H. G. Wolfhard, *Flames: Their Structure, Radiation, and Temperature* (Chapman & Hall, London, 1979).
[7] P. Alers, W. Hänni, and H. E. Hintermann, Diamond Related Mater. **2**, 393 (1993).
[8] K. A. Snail, C. L. Vold, C. M. Marks, and J. A. Freitas, Jr., Diamond Related Mater. **1**, 180 (1992).
[9] P. K. Bachman, D. Leers, and H. Lydtin, Diamond Related Mater. **1**, 1 (1992).
[10] J. J. Schermer, J. E. M. Hogenkamp, G. C. J. Otter, G. Janssen, W. J. P. van Enckevort, and L. J. Giling, Diamond Related Mater. **2**, 1149 (1993).
[11] Y. Hirose, S. Amanuma, and K. Komaki, J. Appl. Phys. **68**, 6401 (1990).
[12] L. M. Hanssen, K. A. Snail, W. A. Carrington, J. E. Butler, S. Kellogg, and D. B. Oakes, Thin Solid Films **196**, 271 (1991).
[13] J. J. Schermer, W. A. L. M. Elst, and L. J. Giling, Diamond Related Mater. (to be published).
[14] F. A. J. M. Driessen, S. M. Olsthoorn, T. T. J. M. Berendschot, H. F. Pen, L. J. Giling, G. A. C. Jones, D. A. Ritchie, and J. E. F. Frost, Phys. Rev. B **45**, 11 823 (1992).
[15] W. J. P. van Enckevort, G. Janssen, W. Vollenberg, J. J. Schermer, and L. J. Giling, Diamond Related Mater. **2**, 997 (1993).
[16] R. Klein-Douwel, J. Spaanjaars, and J. J. ter Meulen (to be published).
[17] K. A. Snail, R. G. Vardinman, J. P. Estrera, J. W. Glesener, C. Merzbacher, C. J. Craigie, C. M. Marks, R. Glosser, and J. A. Freitas, Jr. J. Appl. Phys. **74**, 7561 (1993).
[18] C. M. Marks, H. R. Burris, J. Grun, and K. A. Snail, J. Appl. Phys. **73**, 755 (1993).
[19] B. E. Williams, H. S. Kong, and J. T. Glass, J. Mater. Res. **5**, 801 (1990).
[20] G. Janssen, W. J. P. van Enckevort, W. Vollenberg, and L. J. Giling, Diamond Related Mater. **1**, 789 (1992).
[21] G. Janssen, J. J. Schermer, W. J. P. van Enckevort, and L. J. Giling, J. Cryst. Growth **125**, 42 (1992).
[22] K. A. Snail, Z. P. Lu, R. Weimer, J. Heberlein, E. Pfender, and L. M. Hanssen, J. Cryst. Growth **137**, 676 (1994).
[23] J. G. E. Gardeniers, C. H. Klein-Douwel, and L. J. Giling, J. Cryst. Growth **108**, 319 (1991).
[24] F. C. Frank, K. E. Puttick, and E. M. Wilks, Philos. Mag. **3**, 1262 (1958).
[25] R. E. Clausing, L. Heatherly, L. L. Horton, E. D. Specht, G. M. Begun, and Z. L. Wang, Diamond Related Mater. **1**, 411 (1992).
[26] C. Wild, R. Kohl, N. Herres, W. Müller-Sebert, and P. Koidl, Diamond Related Mater. **3**, 373 (1994).
[27] W. J. P. van Enckevort, G. Janssen, J. J. Schermer, and L. J. Giling, Diamond Related Mater. **4**, 250 (1995).
[28] D. Hull and D. J. Bacon, *Introduction to Dislocations* (Pergamon, New York, 1984).
[29] P. Hartman and W. G. Perdok, Acta Crystallogr. **8**, 49, 521, 525 (1955).
[30] W. J. P. van Enckevort and L. J. Giling, J. Cryst. Growth **45**, 90 (1978).
[31] H. Kanda, M. Akaishi, and S. Yamoaka, J. Cryst. Growth **108**, 421 (1991).
[32] W. J. P. van Enckevort, G. Janssen, W. Vollenberg, M. Chermin, L. J. Giling, and M. Seal, Surf. Coat. Technol. **47**, 39 (1991).
[33] A. Badzian and T. Badzian, Diamond Related Mater. **2**, 147 (1993).
[34] J. J. Schermer, W. J. P. van Enckevort, and L. J. Giling, J. Cryst. Growth **148**, 248 (1995).
[35] P. Hartman, Z. Kristallogr. **121**, 78 (1965).
[36] L. J. Giling and W. J. P. van Enckevort, Surf. Sci. **161**, 567 (1985).
[37] T. Tsuno, T. Imai, Y. Nishihayashi, K. Hamada, and N. Fujimori, Jpn. J. Appl. Phys. **30**, 1063 (1991).
[38] L. F. Sutcu, C. J. Chu, M. S. Thompson, R. H. Hauge, J. L. Margrave, and M. P. D'Evelyn, J. Appl. Phys. **71**, 5930 (1992).
[39] B. V. Spitsyn, L. L. Bouilov, and B. V. Derjaguin, J. Cryst. Growth **52**, 219 (1981).
[40] J. A. Freitas, Jr., K. Doverspike, P. B. Klein, Y. L. Khong, and A. T. Collins, Diamond Related Mater. **3**, 821 (1994).

2.3 The behavior of the molybdenum-CVD diamond interface at high temperatures

This study presents the interface between diamond and molybdenum and its stability at temperatures going from100°C to 800°C. The motivation for this study lies the potential use of molybdenum as electrical contact material on diamond. Chemical modifications owing to temperature increase can modify the electrical properties of this interface and a more fundamental knowledge of this interface is therefore of important.

Molybdenum is also used as a deposition substrate for growing diamond films. Its resistance to the high deposition temperatures and the spontaneous nucleation of diamond on its surface explain why the use of molybdenum is wide spread In this study at temperatures above 550°C hexagonal Mo_2C was detected caused by carbon diffusion from the diamond phase. This Mo_2C is probably the diamond nucleation centre when using molybdenum as deposition substrate. The fact that the present work shows that the Mo_2C formation is probably limited by a carbon diffusion process, implies that effective homogeneous nucleation on molybdenum can only take place if enough carbon was able to diffuse into the molybdenum substrate surface. In practice this phenomena is known when using molybdenum as substrate and often carbon rich pre-deposition conditions are used before switching to the actual diamond deposition parameters.

In conclusion, the findings of the present study are mainly of theoretic interest but also have practical implications.

ELSEVIER

Diamond and Related Materials 4 (1995) 1137–1141

DIAMOND AND RELATED MATERIALS

The behaviour of the molybdenum–CVD diamond interface at high temperature

S.N. Mikhailov [a], D. Ariosa [a], J. Weber [a], Y. Baer [a], W. Hänni [b], X.-M. Tang [b], P. Alers [b]

[a] *Institut de Physique de l'Université, Rue Breguet 1, CH-2000 Neuchâtel, Switzerland*

[b] *Centre Suisse d' Electronique et de Microtechnique (CSEM), Rue Jaquet-Droz 1, CH-2007 Neuchâtel, Switzerland*

Received 26 August 1994; accepted in final form 10 March 1995

Abstract

Molybdenum was deposited onto a H-saturated surface of high quality polycrystalline HF-CVD diamond films in UHV. The interface structure and its composition were studied by XRD and RBS in the temperature range 100 °C–800 °C. Interdiffusion and formation of a hexagonal Mo_2C carbide were detected after annealing at $T \geq 550$ °C. The solid state reaction leading to the bulk carbide formation is, probably, limited by carbon diffusion through the interface.

Keywords: Interface; Structural characterization; Carbide; Diffusion

1. Introduction

One possible way of creating ohmic contact to diamond is to use transition metals which have an affinity for carbon and can form stable carbide phases [1]. Indeed, the ohmic behaviour of metal–diamond contacts is usually attributed to the formation of a carbide phase and electrically active defects associated with it [1–6]. It is therefore important to understand the process involved in the formation of the metal–diamond interface.

Molybdenum can be considered as a candidate for the formation of electrical contacts with diamond. The contact ohmic behaviour and a formation of Mo_2C phase were reported in Refs. [1,5,6]. There is a relatively large difference between the formation temperatures of the first and the second carbide phases [7,8]. There are few experimental data concerning the growth of Mo carbide phases on diamond surfaces and their structures. Cubic structure was observed on naturally occurring boron doped diamond after annealing at $T \geq 850$ °C [1]. On the other hand, growth of hexagonal structure at $T = 700$ °C was reported on polycrystalline CVD diamond [7]. Several types of molybdenum carbides (cubic Mo_2C, hexagonal MoC, β-Mo_2C) were found on metallized diamond powders after deposition of high energy Mo atoms [9].

To our knowledge no data can be found in the literature regarding the kinetics of carbide phase growth on diamond. The basic mechanism for the solid state reaction leading to carbide formation on diamond surface is of importance but still poorly understood. Interfacial reaction or diffusion of material through the interface could be controlling factors in the growth process [10]. Conditions at the interface during carbide growth, its morphology and impurities are all relevant parameters. In particular, the presence of oxygen has been reported in several papers [1,7] and this could be significant for growth kinetics [10,12] as well as for electrical properties [11]. More experimental data are needed to provide insight into the mechanism of carbide phase growth and into correlation of this with electrical properties.

Our recent study [6] showed that a molybdenum carbide forming reaction on H-saturated CVD diamond surface is activated at low temperature $T \geq 400$ °C and that the contact behaviour is ohmic. The present paper reports on our results concerning the evolution of the molybdenum–diamond interface at elevated temperatures, carbon diffusion and growth of a hexagonal Mo_2C bulk phase on polycrystalline diamond surface at $T \geq 550$ °C. We show that growth is probably limited by the diffusion process.

2. Experimental details

Polycrystalline diamond films were grown at CSEM by the HF-CVD method (CH_4 and H_2 atmosphere) on

SSDI 0925-9635(95)00289-8

wafers of polished Si (001) at $T \approx 830$ °C. A pure H_2-atmosphere treatment was used as the final stage of diamond film growth in order to saturate the surface carbon dangling bonds with atomic hydrogen. No further surface treatment was performed.

Molybdenum deposition onto the diamond film surface was carried out in a separate UHV ($p < 10^{-8}$ mbar) chamber by electron beam evaporation at a rate of ~ 0.5 Å s^{-1}, controlled using a quartz crystal resonator. The surface composition during Mo deposition or during annealing was monitored by in situ Auger electron spectroscopy (AES)[6].

3. Results and discussion

3.1. Characterization of diamond films

Characterization of the surface and bulk properties of our CVD diamond films was carried out by several methods.

Micro-Raman spectroscopy demonstrated high quality diamond films: Fig. 1 shows a spectrum for one of our samples. The peak at 1332 cm^{-1} is also seen in spectra recorded from natural diamond. The FWHM of this peak is 8 cm^{-1}, to be compared with an FWHM value of 3 cm^{-1} for natural diamond [13,14].

UHV Atomic force microscopy was used to study the topography of the CVD diamond films (Fig. 2). The average grain was found to be of the order of 500 nm and surface roughness about 300 nm.

No surface contamination was detected on our samples with either Auger or X-ray photoelectron spectroscopy. Direct evidence for hydrogen saturation of our CVD diamond film was given by time of flight scattering and recoil spectroscopy (TOF-SARS) [6].

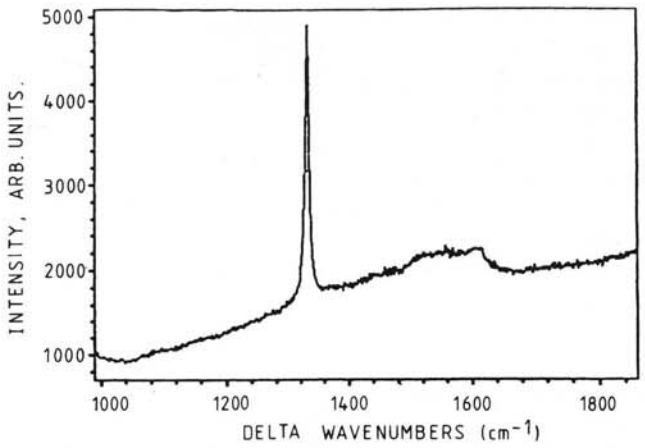

Fig. 1. Raman spectra of HF-CVD diamond film (FWHM is 8 cm^{-1}).

3.2. Solid state reaction leading to Mo-carbide formation

Molybdenum was deposited at low temperature ($T \approx 100$ °C) to a thickness of about 200 nm onto the H-terminated diamond film. The sample was then annealed at different temperatures. Samples were kept at each annealing temperature for 1 h. Interfacial structure evolution and composition were studied by X-ray diffraction (XRD) and Rutherford backscattering (RBS) techniques.

Fig. 3 shows Mo-film XRD spectra after different annealing stages. The peak at $2\theta = 44.0°$, observed in every spectrum, belongs to diamond (111). The peak at $2\theta = 40.5°$ in Fig. 3(a) allows us to deduce that Mo-film is dominantly (110) oriented ($2\theta = 40.5°$) upon deposition. This peak is relatively broad (FWHM $\approx 2°$) and displays an almost flat rocking curve. These characteristics denote a widely spread orientation of small Mo crystallites, the diameter of which could be estimated to be about 60 Å [15]. Upon annealing at 500 °C, the Mo (110) peak increases in intensity and sharpens, thus indicating a growth of the size of surface particles to about 200Å (Fig. 3(b)). Annealing at 600 °C results in the appearance of peaks corresponding to the Mo_2C hexagonal phase. In Fig. 3(c) peaks at $2\theta° = 34.5$, 38.0, 39.6, 52.3 correspond to planes (100), (002), (101), (102) of hexagonal Mo_2C, respectively [16]. At the same time the Mo(110) intensity at $2\theta = 40.5°$ decreases. Finally, after annealing at 800 °C, the Mo_2C peaks dominate the "θ–2θ" scan. No other Mo-phases (Fig. 3(d)) could be observed.

Pole-figure XRD measurements were carried out on Mo(200) reflection. These measurements gave no evidence for preferential orientation for the as deposited nor for the annealed Mo films.

Formation of the Mo_2C phase at elevated temperatures was further characterized by RBS measurements. Fig. 4 shows Mo RBS spectra before and after annealing, under identical conditions and for constant integrated beam current. Analysis [17] of Mo and C RBS spectra shows the following results: annealing at $T \geq 500$ °C for 1 h does not cause any change, indicating no evident interdiffusion or carbide formation at this temperature; annealing at 600 °C leads to the formation of Mo_2C phase approximately 20 nm thick in the region of metal–diamond interface; finally after annealing at 800 °C, nearly the entire 200 nm thick Mo film is transformed into Mo_2C carbide (Fig. 4).

Carbide phase formation might be limited by any one of the following steps: liberation of surface atoms into a reactive state (for instance by C–C bond breaking); interdiffusion through the interface (in particular, through an already formed carbide phase); and reaction on the surface [7].

In order to evaluate the role of interdiffusion through carbide layers, we set up an experiment to find out

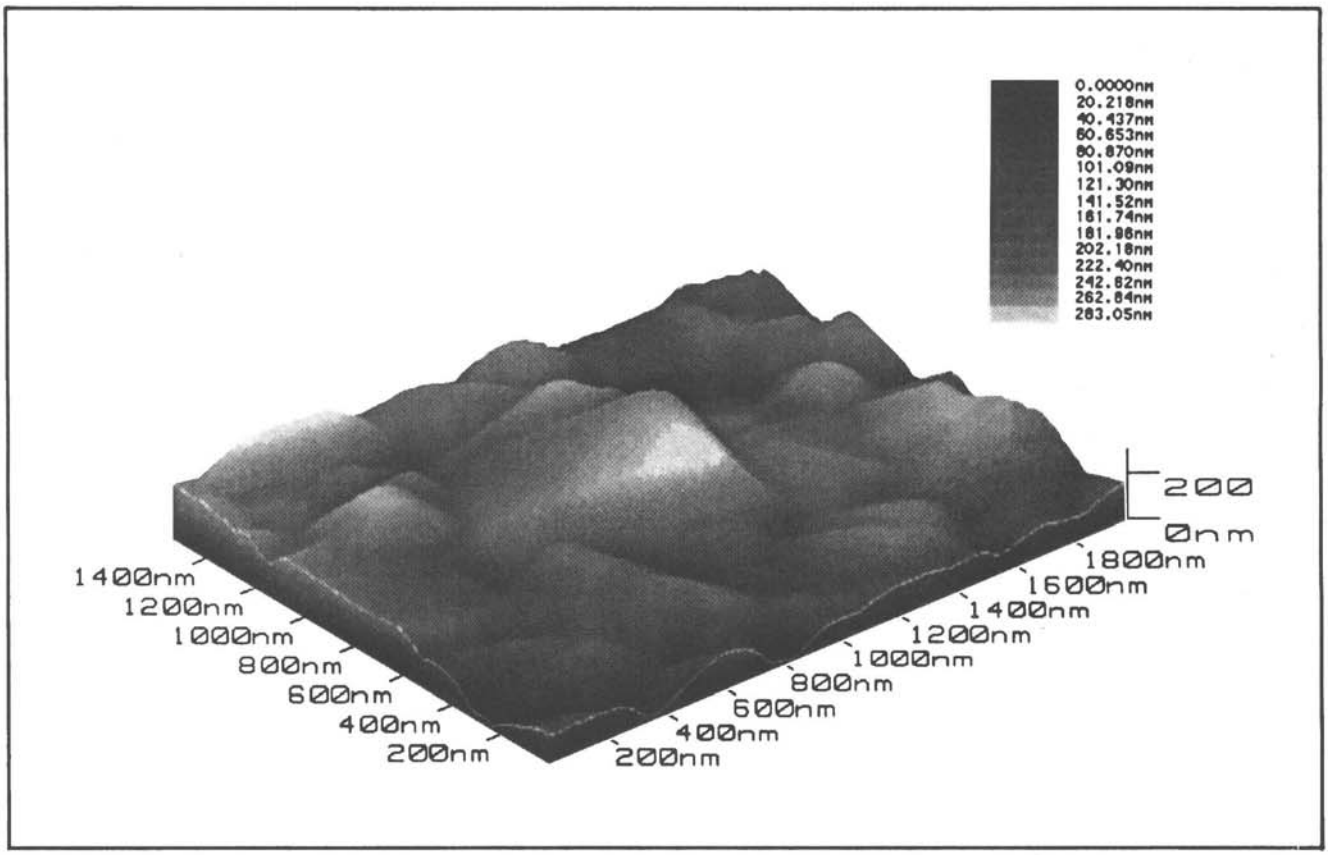

Fig. 2. Atomic force microscopy picture of CVD diamond surface as grown.

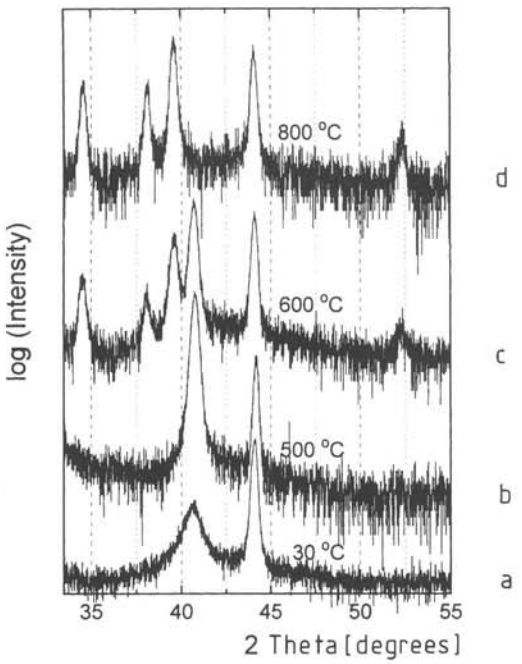

Fig. 3. X-ray (Cu Kα) diffraction spectra of Mo films on diamond after annealing at different temperatures T_a: (a) as deposited; (b) 500 °C; (c) 600 °C; (d) 800 °C.

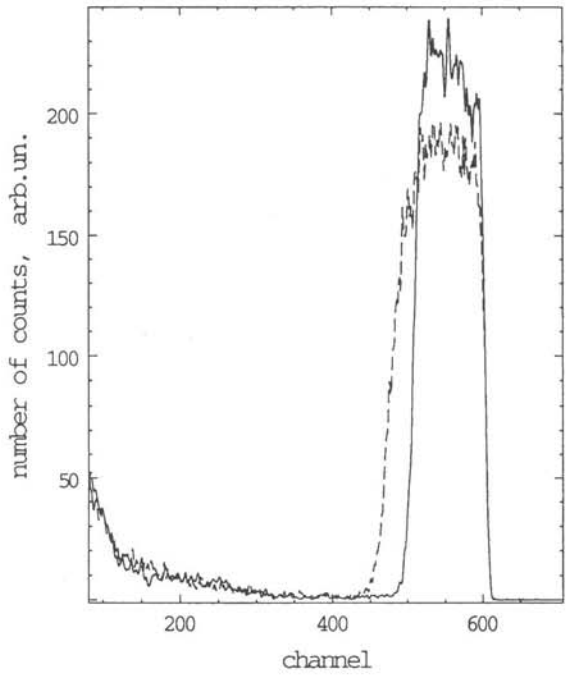

Fig. 4. 2 MeV $^4He^+$ backscattering experimental spectra (E_a = 2.0 MeV, θ_{inc} = 150°, θ_{diff} = 150°) of Mo film deposited on CVD diamond film as deposited (solid line) and after annealing to 800 °C (dashed line).

whether the time needed for molybdenum carbonisation depends on the thickness of Mo_2C carbide interlayers. Carbide layers of three different thicknesses were grown on the diamond films by Mo deposition and annealing at 800 °C in UHV. The carbon KVV Auger line shape and area measured after this process is typical for carbide phase [6]. One or two monolayers (ML) of Mo were then deposited on top of each sample to study the carbonisation kinetics. The samples were heated and the Auger signal of carbon (I_c) and of molybdenum (I_{Mo}) were monitored with AES. Fig. 5 shows the ratio of intensities $(I_C)/(I_{Mo})$ as a function of annealing time for three different initial thicknesses of Mo_2C film (X,ML) annealed at temperature $T_a = 560$ °C. Also shown are data for one thickness of Mo_2C ($X_3 = 20$–28 ML) annealed at three different temperatures T_a. The results show that carbonisation is thermally activated over a relatively large temperature range and that the rate of carbonisation depends on the carbide interlayer thickness. This suggests that the limiting factors are neither reaction at the interface nor liberation processes but, most probably, diffusion processes. If this is indeed the case, growth should be proportional to $\sqrt{t}$, where t is the annealing time, with the constant of proportionality $\sqrt{D}$, D being the diffusion parameter [10]. It is possible to estimate the time t (at the relevant temperature T_a) needed to get the same I_C/I_{Mo} ratio for each sample. At $I_C/I_{Mo} = 0.18$, for exemple, one can estimate from Fig. 5 the sucessive ratio $t_1:t_2:t_3$. Within the uncertainties in the determination of the thicknesses of the initial Mo_2C layers X_i, the ratio $t_1:t_2:t_3$ corresponds through the diffusion relation to $X_1^2:X_2^2:X_3^2$, strengthening the picture where carbide growth is controlled by a diffusion process. Moreover, the fact that the depth analysis with Auger spectroscopy is limited to 2–4 ML suggests that C is diffusing up through the Mo_2C rather than that Mo is diffusing down into the layer. In this latter situation, it would be expected that the Auger ratio I_C/I_{Mo} saturates at the value for Mo_2C (0.5) rather rapidly for all samples. This conclusion is in agreement with other experimental results [7]. By extracting D values at the other temperatures T_a from the curves of Fig. 5 one gets: $D_{560\,°C} \approx 4\times10^{-20}$ m^2 s^{-1}, $D_{580\,°C} \approx 9\times10^{-20}$ m^2 s^{-1}, $D_{600\,°C} \approx 2\times10^{-19}$ m^2 s^{-1}, and $D_{620\,°C} \approx 3\times10^{-19}$ m^2 s^{-1}. Plotting ln$D$ versus $1/T_a$ allows us to estimate the effective carbonisation activation energy E_a to be 1.9 ± 0.4 eV. In accordance with the above conclusion, we associate this energy with the carbon diffusion through the interfacial Mo_2C phase. To the best of our knowledge, there are as yet no published data with which we can compare this estimate. Finally we note that the large difference between the lattice constants for diamond ($a = 3.56$ Å) and for the hexagonal Mo_2C ($a = 2.99$ Å, $c = 4.72$ Å) phases would lead one to expect defect formation at the Mo_2C–diamond interface during carbide growth. Defects in a thin carbide film could play the role of traps, trapping species diffusing through interfacial Mo_2C. Thus, at least, for the beginning of the process, when the carbide film is thin, the formation of hexagonal Mo_2C at the interface could lead to a creation of traps and that could be relevant for the kinetics of carbonisation.

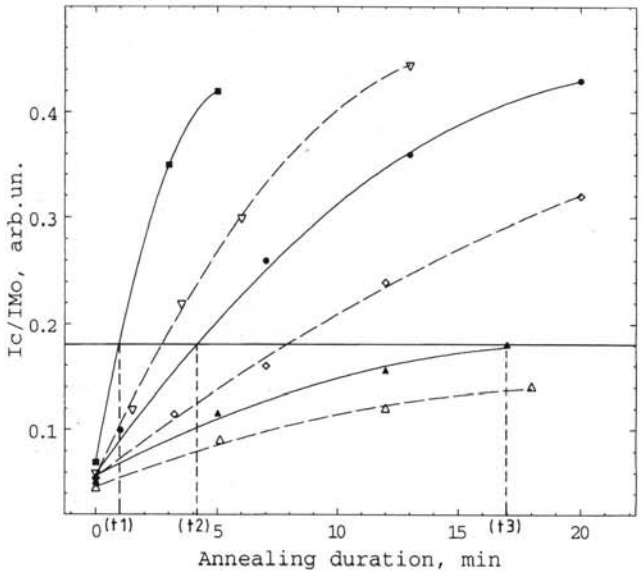

Fig. 5. Carbon to molybdenum Auger signal ratio as a function of the duration of annealing. The solid lines correspond to samples with different initial thicknesses of Mo_2C: 4–6 ML (■), 10–14 ML (●), 20–28 ML (▲), all annealed at 560 °C. The dashed lines correspond to samples with initial Mo_2C thickness of 20–28 ML, annealed at different temperatures: 540 °C (△), 580 °C (◇), 620 °C (▽). These lines are only guides for the eye. The ratio $I_c/I_{Mo} = 0.5$ coincides with Mo_2C surface stoichiometry [6].

4. Summary

It has been shown that the evolution of the molybdenum–CVD diamond interface in the 500 °C to 800 °C range is associated with hexagonal Mo_2C carbide growth controlled by a diffusion process. An experimental method has been developed with which it was shown that carbon is most probably the diffusing species and with which first estimates of the diffusion parameter D of carbon in interfacial Mo_2C have been obtained.

Acknowledgement

The authors gratefully acknowledge the financial support of the Swiss National Science Foundation (Project No. 21-37'655.93) carried out under the auspices of the trinational "D-A-CH" cooperation of Germany, Austria and Switzerland on the "Synthesis of Super hard Materials".

References

[1] K.L. Moazed, J.R. Zeidler and M.J. Taylor, *J. Appl. Phys., 68* (1990) 2246.

[2] T. Tachibana, B.E. Williams and J.T. Glass, *Phys. Rev. B, 45* (1992) 11968 and 11975.

[3] K.L. Moased, R. Nguyen and J.R. Zeidler, *IEEE Electron Device Lett., 9* (7) (1988) 350.

[4] H. Kawarada, M. Aoki, H. Sasaki and K. Tsugawa, *Diamond Relat. Mater., 3* (1994) 961.

[5] G. Kawaguchi, J. Nakainishi, A. Otsuki, T. Oku and M. Murakami, *J. Appl. Phys., 75* (1994) 5165.

[6] S. Mikhailov, J. Weber, Y. Baer, W. Hänni and X.-M. Tang, *Solid State Commun., 93* (1995) 869–873.

[7] A. Bächli, J. S. Chen, R.P. Ruis, M.-A. Nicolet, W. Hänni and H.E. Hintermann, paper presented at *High Temperature Electronic Conference, June 5–10, 1994, Charlotte, NC.*

[8] B. Thaddeus and T.B. Massalski (eds.), C–Mo phase diagram, in *Binary Alloy Phase Diagrams*, ASM International, 2nd edn., 1990.

[9] N.V. Novikov, M.A. Voronkin and I.V. Bondar, *Diamond Relat. Mater., 3* (1993) 61.

[10] M.-A. Nicolet and S.S. Lan, in *Microstructure Science*, VLSI Electronics, Vol. 6, 1983, Chapter 6.

[11] Y. Mori, H. Kawarada and A. Hiraki, *Appl. Phys. Lett., 58* (1991) 940.

[12] D.M. Scott, P.J. Grunthaner, B.Y. Tsaur, M.A. Nicolet and J.W. Mayer, *Proc. Symp. on Thin Film Interfaces and Interactions*, The Electrochemical Society, Pennington, NJ, 1980, p. 148.

[13] D.S. Knight and W.B. White, *J. Mater. Res., 4* (1989) 385.

[14] P.V. Huong. *Diamond Relat. Mater., 1* (1991) 33.

[15] B.D. Cullity, *Elements of X -ray Diffraction*, Addison-Wesley, 1958, p. 262.

[16] Handbook of Powder Diffraction File, N 11-680; Ref. H. Tutiy, *Bull. Inst. Phys. Chem. Res.*

[17] X.-M. Tang, J. Weber, Y. Baer and F. Finger, *Solid State Commun., 74* (1990) 171.

2.4 Morphology and structural characterization of plasma-assisted prepared carbon films

The now presented work is a part of a research program studying the laser arc amorphous carbon deposition. Its importance lies in the extensive way the problem of particle incorporation during deposition has been analysed. By using various analytical means, the authors where not only able to determine the influence of the different deposition parameters on the amount of particles incorporated but also they determined the origin of these particles.

The present study has allowed to optimise the deposition method and offers at the same time a problem solving analytical approach. As common in most deposition methods, the optimisation of the laser arc system at IWS-FHG has been pushed further and the findings presented in this study do therefore no longer reflect the actual deposition set-up or conditions. However, the analytical approach presented remains still valid and is part of the ongoing research at IWS-FHG.

ELSEVIER

Diamond and Related Materials 5 (1996) 968–972

DIAMOND AND RELATED MATERIALS

Morphology and structural characterization of plasma-assisted prepared carbon films

D. Drescher [a], H.-J. Scheibe [a], A. Mensch [b], P. Alers [c], Ch. Dyer [d]

[a] *Fraunhofer-Institut für Werkstoffphysik und Schichttechnologie, Helmholtzstraße 20, 01069 Dresden, Germany*
[b] *TU Dresden, Institut für Werkstoffwissenschaft, 01062 Dresden, Germany*
[c] *CSEM Neuchatel, Maladiere 71, 2007 Neuchatel, Switzerland*
[d] *RENISHAW plc, Old Town, Wotton-under-Edge, Gloucestershire, GL12 7DH, UK*

Received 29 August 1995

Abstract

Since the properties of amorphous carbon films are determined by the structure of the amorphous network and embedded particles, it is necessary to characterize these properties with respect to the deposition conditions. Relating the particle structure to that of the cathode material may provide information on the origin and growth.

The morphology and structure of amorphous carbon films deposited with a pulsed arc source (Laser-Arc) were studied using microscopic (optical, transmission electron microscopy (TEM) and atomic force microscopy (AFM)) and spectroscopic (Raman and electron energy loss spectroscopy (EELS)) investigation methods. The influence of the deposition temperature and annealing after deposition on the structure of the amorphous films was studied. The results of structural analysis show that the homogeneous, very smooth film obtained is amorphous and diamond-like, with a plasmon peak situated at about 28 eV. The influence of the deposition temperature can be seen in the shift of the plasmon peak in the electron energy loss spectrum and the square relation of the fitted D/G peak in the Raman spectrum. Particles with dimensions of several hundred nanometres are embedded in the film. In contrast with the film structure, these particles show graphite-like behaviour in the Raman spectrum corresponding to the polycrystalline graphite target material.

Keywords Raman spectroscopy; Electron energy loss spectroscopy; Transmission electron microscopy; Amorphous carbon films; Structural properties; Deposition process

1. Introduction

Physical vapour deposition (PVD) processes can be used to prepare amorphous carbon (a-C) films revealing a broad spectrum of properties ranging from graphitic or soft to diamond-like (DLC) or hard carbon.

The structure of the amorphous films is characterized by the bonding states of the carbon atoms, especially by the ratio of sp^3 to sp^2 bonds. The diamond likeness depends on the content of sp^3 bonds. a-C films with an sp^3 content up to 85%, also called highly tetrahedral films (ta-C), are obtained by filtered ion beam deposition [1].

Plasma-assisted deposition techniques can produce coatings without hydrogen, homogeneous down to the nanometre level and with smooth and dense surfaces. Plasma sources based on the vacuum arc erosion of graphitic cathode material produce a-C films with the highest content of sp^3 bonds [2]. Conventionally, arc plasma sources are associated with the emission of particles which disturbs the film quality. Several plasma filtering systems have been combined with continuous and pulsed arc sources to separate the particles from the plasma to reduce particle incorporation in the substrate [3,4]. However, such filters lower the deposition rate dramatically and do not eliminate the particles completely.

The Laser-Arc deposition method represents an arc technology in which the erosion of material is controlled using a pulsed laser [5]. By limitation of the arc burning time, the emission of particles is strongly reduced, and by application of high peak current pulses and high repetition rates, a high deposition rate can be reached. In carbon film deposition, the number and size of the particles seems to be dependent on the length of the arc pulses. At a pulse duration of 100 μs, the microparticles

SSDI 0925-9635(95)00438-6

are not completely eliminated; preliminary results indicate that, at pulse lengths below 40 μs, the particle content can be minimized [6].

The mechanical and optical properties are determined by the structure of the amorphous matrix and embedded particles. Hence, it is necessary to characterize these components with respect to the deposition conditions. Relating the particle structure to that of the cathode material may provide information on the origin and growth.

2. Experimental arrangement

The DLC films were prepared with the Laser-Arc arrangement, which is presented in more detail in Ref. [5]. The deposition was carried out with arc current pulses of 100 μs duration, a peak arc current of 1000 A and a repetition frequency of up to 200 Hz. Deposition rates of 6 μm h^{-1} were reached. The target to substrate distance was 120 mm. The deposition was carried out at a base pressure of 5×10^{-4} Pa without using a substrate bias. The films were deposited on crystalline silicon with a thickness varying between 50 and 500 nm. The temperature of the substrate measured by a PT 100 sensor beside the samples did not exceed 100 °C during the normal deposition process. For comparison, some films were deposited at temperatures up to 500 °C.

Particle analysis was performed using an optical microscope coupled with a CCD camera. DLC films, deposited under equal conditions ($T_S = 50$ °C), were used for these measurements. For every sample, 20 different images were taken in order to obtain results with sufficient statistical reliability. The measured integral area was 630 μm^2. The images were digitized in a computer and transmitted into a binary image. From the binary images, the statistics of the particle number and particle size were determined. It should be noted that only particles with a diameter of greater than 350 nm can be detected accurately by this method.

The film morphology was studied by scanning (SEM) and transmission (TEM) electron microscopy combined with electron diffraction and electron energy loss spectroscopy (EELS). The SEM images were taken in a Jeol JSM 640 scanning electron microscope. TEM measurements were obtained with a Zeiss EM 912 Omega transmission electron microscope using thin films up to a thickness of 100 nm. Bright-field images were taken with zero loss filtering. For the electron diffraction pattern, a spot size of 1 μm in diameter was applied. For TEM, the films were separated from the substrate; the thickness of the films was below 100 nm for EELS measurements. Atomic force microscopy (AFM) investigations were carried out with an AFM Rasterscope 3000 and compared with the TEM study.

In addition, the film and particle structure was studied by micro-Raman spectroscopy. The Raman measurements were carried out with a Renishaw Ramascope using an He–Ne laser with an excitation wavelength of 633 μm. The high spatial resolution (1 μm) allows discrimination between the homogeneous DLC film and small incorporated particles. Laser excitation did not cause any structural changes in the film by heating effects.

3. Results and discussion

3.1. Film morphology and statistics of embedded particles

The typical film morphology of Laser-Arc-deposited C films is illustrated in the SEM image in Fig. 1 which shows a cross-section of a 1 μm film on a silicon substrate. In the film, particles with a broad size distribution are embedded. The results of the size distribution are presented in Fig. 2, where the normalized particle frequency vs. the particle diameter is shown at different film thicknesses. The majority (approximately 80%) of the detected particles are smaller than 500 nm. Up to a film thickness of 500 nm, the particle distribution does not depend on the film thickness. This indicates that the deposition conditions during film growth do not change

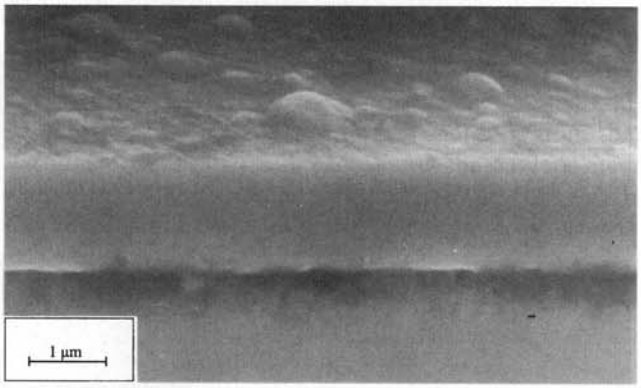

Fig. 1. SEM image of a 1 μm thick DLC film on crystalline silicon.

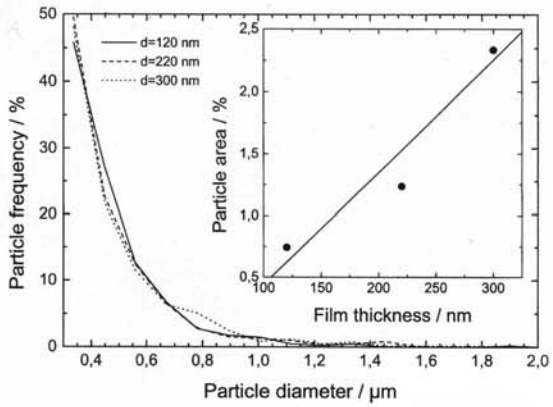

Fig. 2. Particle frequency as a function of the particle diameter at different film thicknesses.

with time. The distribution is also independent of the substrate position in the vacuum chamber during the growth process.

The inset in Fig. 2 shows the area fraction of the particles as a function of the film thickness. As is expected, the area fraction increases proportionally with the film thickness. For an extrapolated thickness of 1 μm, the particles cover about 8%. Because of the increasing particle content with increasing thickness and the constant particle diameter distribution, we can assume that the particles originate from cathode erosion.

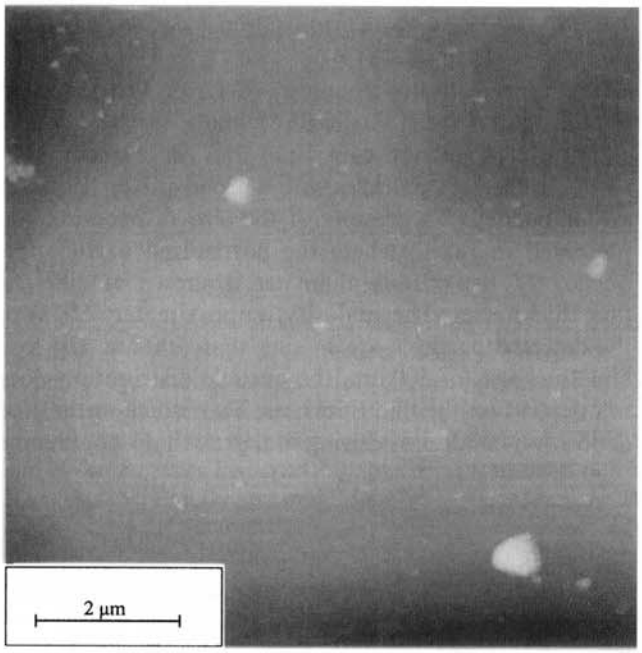

Fig. 3. AFM image of a 100 nm thick DLC film, deposited at 50 °C.

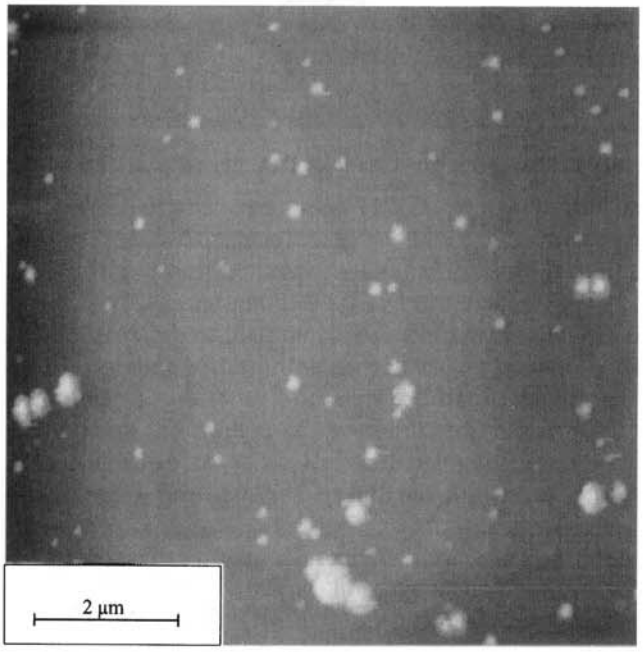

Fig. 4. AFM image of a 100 nm thick DLC film, deposited at 350 °C.

The typical morphology in the submicrometre region of the film was analysed by AFM (Figs. 3 and 4). In Fig. 3, a 100 nm thick DLC film, grown at 50 °C, shows some particles up to a diameter of 700 nm. The average diameter is of the order of 200 nm. The particles have a nearly globular structure. Films with the same thickness and deposited under the same conditions but at a substrate temperature of 350 °C reveal an increased number and size of particles (Fig. 4). Large particles and "clusters" up to a diameter of 1 μm are observed. The clusters consist of smaller particles with a size of several hundred nanometres.

This result indicates that the particle content is dependent on the deposition temperature. Furthermore, the number and size of the particles increase at higher substrate temperatures. It can be concluded that the particles emitted from cathode erosion and incorporated in the growing film are centres of particle growth during deposition. At low temperatures, the growth rate is much smaller than at higher temperatures.

This is in contrast with the results of particle analysis by optical measurements discussed above. The particle size distribution should change with the film thickness due to growth. Obviously, the growth rate at room temperature and the thickness of the coatings are too small to show any evidence in the particle statistics determined by optical means. We can conclude from these results that the particle content is a mixture of particle incorporation by arc spot emission and particle growth in the film, strongly influenced by the deposition temperature.

3.2. Structure of the film matrix and particles

The film morphology can also be demonstrated by TEM images. Fig. 5 shows a representative TEM image for a film grown at 50 °C. A smooth, dense film with a "random" noisy background is observed, characteristic of amorphous films. Distinct non-random image features superimposed on the background are observed. Such structures have been reported in Ref. [7] and are called lattice fringes. Due to the image resolution, the characteristic size of these fringes could not be determined. In the images some embedded particles are found. These particles have an average size of 50 nm.

The corresponding diffraction pattern reveals diffuse haloes indicating an amorphous structure. No sign of crystalline structure is observed. The haloes are well separated from each other. The distance between the two inner circles indicates a short-range order of 0.36 nm. This value is close to the lattice constant of diamond (0.355 nm).

The structure of the particles in the film is not detectable in the diffraction pattern. This means that

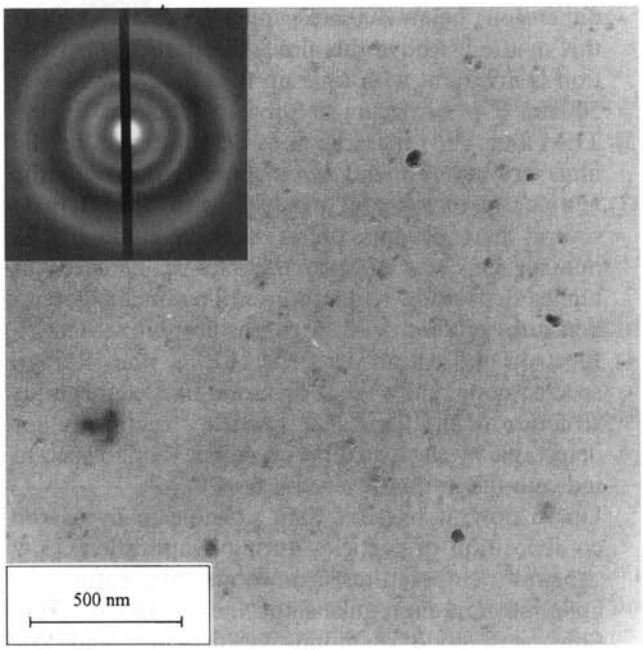

Fig. 5. TEM image and diffraction pattern of a 100 nm thick DLC film, grown at 50 °C.

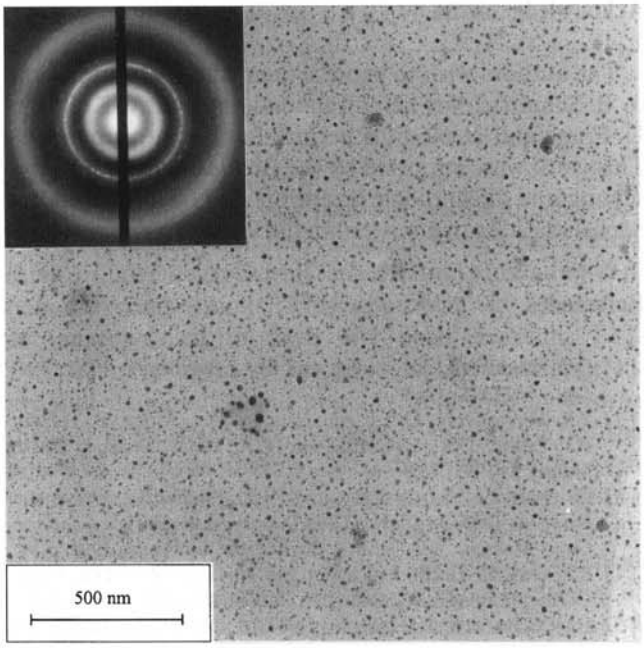

Fig. 6. Graphitization effect, starting at a temperature of 700 °C.

they possess the same amorphous structure as the bulk film or their content in the spot region is too low to cause any crystalline features. Fig. 6 shows the same sample after annealing by the electron beam in the microscope up to about 700 °C. Black areas are observed which have grown during the heating process and can be identified by the electron diffraction pattern as crystalline graphite particles. The amorphous film structure seems to be preserved.

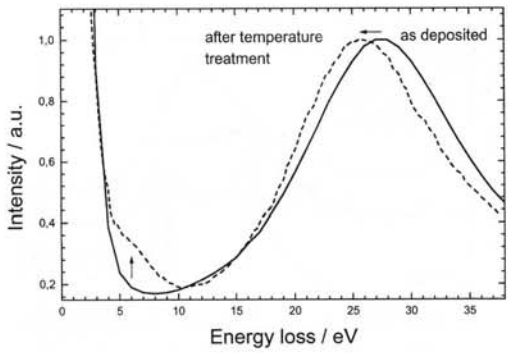

Fig. 7. Plasmon peak shift caused by temperature treatment.

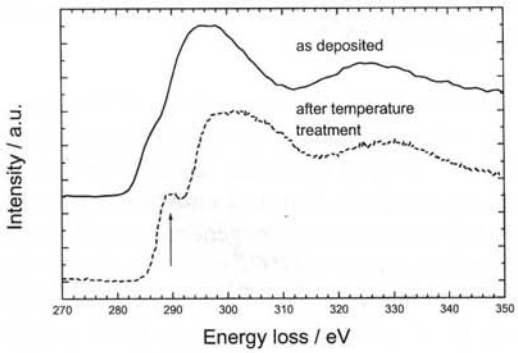

Fig. 8. High energy part of the electron energy loss spectra of an as-deposited sample and after temperature treatment.

This graphitization effect is also evident in the electron energy loss spectra, measured for the same sample and shown in Figs. 7 and 8. In the low energy region, the plasmon peak shifts from 27.5 eV for the as-deposited sample to 25.5 eV for the annealed sample. The latter also reveals additional excitations around 6 eV caused by transitions of π electrons, indicating an increased number of sp^2 bonds. The high energy part of the electron energy loss spectrum shows no specific features in the absorption edge for the as- deposited film, but a peak for the temperature treated sample which is due to antibonding π^* electron states (sp^2). For films revealing a sufficient π plasmon excitation near an energy loss of 6 eV, an estimation of the sp^3/sp^2 ratio is possible. This is not the case for our films. To obtain a value of the sp^3 to sp^2 bonding fraction, the correlation with the intrinsic stress and mass density was used. Intrinsic stress measurements of films grown at 50 °C reveal values of about 4 GPa at a mass density of 2.6 g cm^{-3}. Using the correlation given in Refs. [8] and [9], about 30% of the bonds are of sp^3 type. This result is also in agreement with the data in Ref. [10], where the bonding fraction is derived from the mass density.

The annealing experiment indicates the thermal stability of the deposited carbon films up to a temperature of about 700 °C. For hydrogen-containing films, the graphitization effect has been reported at a temperature of 300 °C [11].

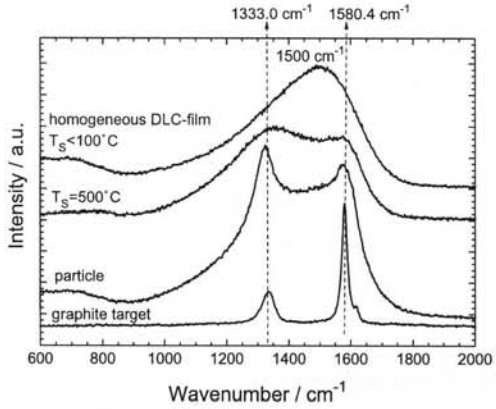

Fig. 9. Raman spectra of the target material, homogeneous film and incorporated particle.

Additional structural investigations of the homogeneous film and particles were carried out by micro-Raman spectroscopy. In Fig. 9, typical Raman spectra of the homogeneous carbon film and embedded particles are displayed. The ordinary homogeneous film, deposited at a temperature below 100 °C, reveals a broad Raman peak which indicates a disordered amorphous structure. The peak is not symmetric and can be fitted well by two gaussian distributions, situated at 1350 cm^{-1} (D peak) and 1500 cm^{-1} (G peak). The area relation of the peaks I_D/I_G is near unity. At higher substrate temperatures, e.g. 500 °C, the Raman spectrum is divided into two pronounced peaks with an area relation above four. In agreement with Ref. [12], this behaviour indicates a transition from a diamond-like structure at low substrate temperature to an increased graphitic structure at higher temperature. The highest content of sp^3 bonds is exhibited at room temperature.

Furthermore, the particles embedded in the homogeneous film exhibit two strongly pronounced Raman peaks at nearly the same positions as the fitted gaussian peaks for the spectrum of the homogeneous film. The spectrum can only be fitted well by using four gaussian distributions. Two of the peaks are very similar to those of the polycrystalline graphitic target material and the other two are similar to those of the homogeneous film. This indicates the graphitic nature of the particles which are probably covered or grown by diamond-like deposition.

4. Conclusions

(1) The morphology and structure of a-C films and their particle inclusions, deposited by a pulsed arc produced plasma (Laser-Arc), were studied by optical, electron and atomic force microscopy and Raman spectroscopy as a function of the deposition parameters.

(2) Quantitative particle analysis by optical microscopy shows that the particle content increases with the film thickness and deposition temperature. Particle dimensions below 400 nm cannot be determined by this method. Above this limit, the particle distribution is invariant with time up to a film thickness of 500 nm. The maximum size of the particles is 1.5 μm.

(3) TEM and AFM investigations demonstrate that the films are smooth and homogeneous down to the nanometre region and particles with diameters of several tens of nanometres can be studied. The number and size of such particles is increased at higher deposition temperatures. Treatment at temperatures of about 700 °C causes graphitization.

(4) Electron diffraction patterns, EELS and Raman spectroscopy show the diamond-like amorphous structure of the films. The particle structure is not detectable by electron diffraction, but Raman spectra indicate the graphitic structure.

(5) Up to now, it has not been possible to avoid the co-deposition of particles during evaporation. Low substrate temperatures near room temperature are an important prerequisite for the growth of DLC films with good diamond-like structure and low particle content. Further investigations concerning the particle formation and growth are under way.

Acknowledgements

The authors wish to express their sincere appreciation to B. Schultrich for helpful discussions and A. Kolitsch, U. Franz and L. Neef for performing the measurements. This work was supported by the Bundesminister für Forschung und Technologie (grant no. 13 N 5951A) and the Sächsisches Staatsministerium für Wirtschaft und Arbeit.

References

[1] D.R. McKenzie, D. Muller and B.A. Pailthorpe, *Phys. Rev. Lett., 67* (1991) 1286.
[2] V.S. Veerashamy, G.A.J. Amaratunga, W.I. Milne, P. Hewitt, P.J. Fallon, D.R. McKenzie and C.A. Davis, *Diamond Relat. Mater., 2* (1993) 782.
[3] I.I. Aksenov, S.I. Vakula and V.E. Strel'nitskij, *Proc. 1st European Conf. on Diamond and Diamond-Like Carbon Coatings, Crans-Montana, September, 1990*, Elsevier, Lausanne, 1991, p. 98.
[4] B.F. Coll, G. Hecht, F. Richter and J. Hahn (eds.), *Thin Films*, DGM Informations-Gesellschaft, Oberursel, 1994, p. 3.
[5] H.-J. Scheibe and P. Siemroth, *IEEE Trans. Plasma Sci., 18* (1990) 917.
[6] H.-J. Scheibe, D. Ristau and M. Rahe, *Diamond Relat. Mater., 2* (1993) 1424.
[7] K.W.R. Gilkes, P.H. Gaskell and J. Yuan, *Diamond Relat. Mater., 3* (1994) 369.
[8] D.R. McKenzie, Y. Yin, N.A. Marks, C.A. Davis, B.A. Pailthorpe, G.A.J. Amaratunga and V.S. Veerashamy, *Diamond Relat. Mater., 3* (1994) 353.
[9] J. Robertson, *Diamond Relat. Mater., 3* (1994) 361.
[10] T. Frauenheim, U. Stephan, P. Blaudeck and G. Jungnickel, *Diamond Relat. Mater., 3* (1994) 462.
[11] A.P. Rubshtein, I.Sh. Trakhtenberg and V.B. Vykhodets, *Diamond Relat. Mater., 3* (1994) 688.
[12] R.O. Dillon, J.A. Woolam and V. Katkanant, *Phys. Rev. B, 29* (1984) 3482.

2.5 Raman characterization of amorphous carbon films

The present study is using Raman analysis in an attempt to characterise the diamond likeliness of amorphous carbon films as deposited by the laser arc method. It uses the shape and intensity of the so-called D and G band in the a-c spectrum to compare the properties of a-c films deposited under different conditions. The results indicate a great potential for this approach and subsequent further research by the authors and others have led to a systematic classification method of a-c films.

Although the now following publication only contributed in a small way reaching this goal, its contribution has been of use and helped the authors in the development of the laser arc deposition method.

Fresenius J Anal Chem (1995) 353 : 695–697

Fresenius' Journal of
Analytical
Chemistry

Raman characterization of amorphous carbon films

H.-J. Scheibe[1], D. Drescher[1], P. Alers[2]

[1]Fraunhofer-Institut für Werkstoffphysik und Schichttechnologie, Helmholtzstrasse 20, D-01069 Dresden, Germany
[2]CSEM Neuchatel, Maldiere 71, CH-2007 Neuchatel, Switzerland

Received: 27 February 1995 / Accepted: 13 March 1995

Abstract. Amorphous carbon films, deposited with the LASER-ARC technique, have been characterized using Raman scattering experiments at an excitation wavelength of 633 nm provided by a He-Ne laser. To distinguish between the homogeneous amorphous film and incorporated particles area resolved measurements have been carried out due to the laser spot diameter of 1 μm. Typical diamond-like (DLC) films, grown near room temperature, show a broad Raman band between 1000 cm^{-1} and 1800 cm^{-1} fitted very well by two gaussian distributions. Films deposited at higher substrate temperatures reveal more graphitic features in the spectra. The spectra of particles consists of a graphite-like portion originated from the graphitic structure of the particle and a diamond-like portion caused by the covering DLC film. The degree of disorder and diamond-likeness in the film structure is quantified by the peak position, the full width at half maximum (FWHM) and intensity relation of the fitted "D"- and "G"-peaks.

1 Introduction

Raman scattering of carbon materials such as graphite, diamond and amorphous carbon has been analyzed in great detail [1], [2], [3]. It offers a relatively easy and unique tool to characterize the structure of carbon films without destroying the sample and without the necessity of removing the film from the substrate. For the investigations only a small area in the order of mm^2 is needed. Using a small excitation spot it is possible to distinguish between different structures, e.g. microparticle embedded in the homogeneous matrix.

Raman spectra are very sensitive to changes in the translational symmetry of the solid, in amorphous carbon they provide information about the level of microstructural disorder. Furthermore, Raman scattering depends on number and size of graphitic bonded clusters (sp^2, threefold coordinated) and the amount of fourfold coordinated (sp^3) carbon atoms [4].

In opposite to graphite and diamond with a crystalline structure that is connected with narrow Raman lines amorphous carbon reveals broad bands caused by the structural disorder with an unsymmetrical Raman band in the wavenumber region between 900 cm^{-1} and 1800 cm^{-1}. Its shape is formed by two more or less significant features, originating from the graphitic "G"-line at about 1580 cm^{-1} and the "D"-line near 1350 cm^{-1}. Analyzing the intensity relation I_D/I_G, the peak position and their FWHM one gets information about the diamond-likeness of the films.

In this paper the Raman investigation of DLC-films, deposited with a pulsed arc technique is reported and the results are compared with those found in literature.

Correspondence to: H.-J. Scheibe

2 Experimental

The DLC-films were prepared with the LASER- ARC setup, published in detail elsewhere [5]. The deposition was carried out with arc current pulses of 100 μs duration, a peak arc current of 1000 A and a repetition frequency of up to 200 Hz. Deposition rates of 6 μm/h have been reached at a target substrate distance of 120 mm. The deposition was carried out at a base pressure of 5×10^{-4} Pa without substrate bias. The temperature of the substrate was measured by a PT 100 sensor beside the sample.

The films have been deposited on crystalline silicon. The film thickness varied between 50 nm and 500 nm.

The Raman characterization was carried out with a Renishaw Ramascope. A He-Ne laser with a wavelength of 633 nm was used. The light intensity (< 10 mW) did not degrade the sample by heating effect. A spot diameter of about 1 μm allows to take high spatial resolution spectra and to distinguish between different structures in the DLC film.

The spectra were evaluated (background subtraction and peak-fit) with the software ORIGIN.

3 Results and discussion

Typical film morphology of the LASER-ARC deposited C-films is shown in Fig. 1 as a cross section of an 1 μm film SEM image on a silicon substrate. In the film particles with a broad size distribution are embedded. Typical Raman spectra of the homogeneous film is shown in Fig. 2a. The films, deposited at a temperature below 100° C, show a broad Raman peak without specific features. The peak is not symmetric and can be well fitted by two gaussian dis-

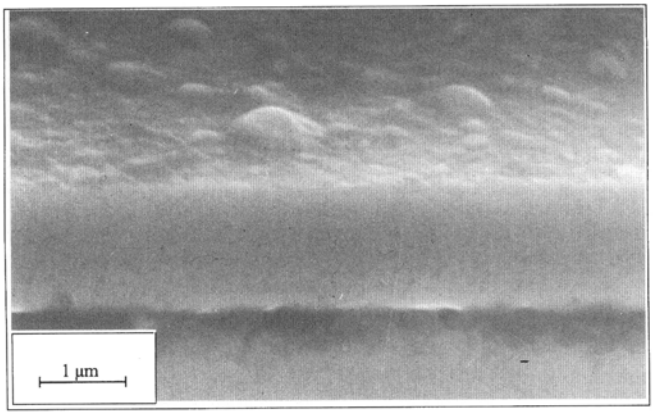

Fig. 1. SEM image of a 1 µm thick DLC film on crystalline silicon (cross section)

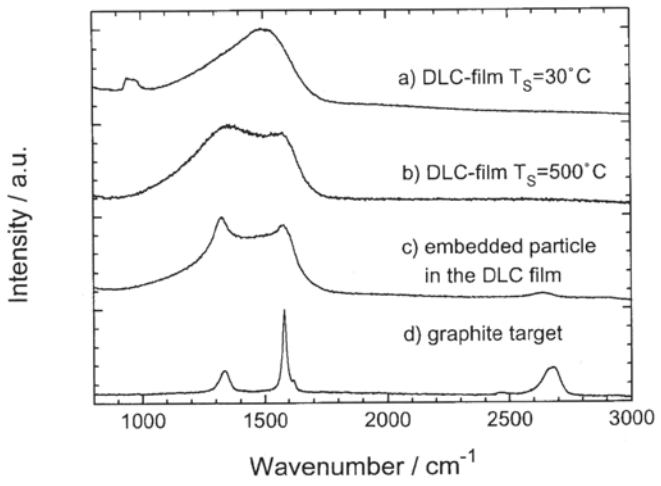

Fig. 2 a–d. Typical Raman spectra of DLC films, embedded particle and graphite target

tributions, situated at 1350 cm^{-1} ("D"-peak) and 1530 cm^{-1} ("G"-peak).

Figure 2 b belongs to a film, deposited at a substrate temperature of 500° C. The shape of the spectrum is divided into two peaks.

In the homogeneous DLC-film particles and clusters of smaller particles up to a diameter of 1.5 µm are embedded. A Raman spectrum of a particle incorporated in a DLC film grown at 30° C is shown in Fig. 2 c. The Raman spectrum of the graphite target (Fig. 2 d) shows the significant "D" and "G" peak typical for a graphitic structure [1].

By fitting procedures, the parameters I_D/I_G, FWHM and peak position were determined and listed in Table 1.

Dillon et al. [4] showed that the intensity ratio I_D/I_G of "D"- to "G"-peak is proportional to the structural order in the carbon film. This ratio increased with annealing temperature and reached a maximum at 800° C, after which the ratio decreases. That is explained as follows: For amorphous carbon films graphitic (sp^2) crystallites are probably too small in size and number to couple effectively to the incoming laser beam, and thus they contribute little to the Raman spectrum. As the film is annealed, the crystallites grow and begin to contribute to the increase of I_D/I_G. Above 800° C, at crystallite sizes of about 20 Å, I_D/I_G decreases, because of the important increase in the momentum conservation effects. For graphitic carbon I_D/I_G is inversely proportional to the effective crystallite size, L_a, in the direction of the graphite plane [6]. In amorphous carbon I_D/I_G is proportional to the crystallite size up to 25 Å [7]. For $L_a > 25$ Å the ratio behaves like in graphite. Comparing the spectra and the fitted data with the literature, film a in Fig. 3 reveals the most disordered structure and highest sp^3 bonding fraction characterized by $I_D/I_G = 0.9$ and high FWHM.

At higher deposition temperature (500° C) the spectrum b shows a less disordered nature with less fraction of sp^3 bonds by $I_D/I_G = 6.4$ and a narrower "D" peak. Comparing to the data of Dillon, high temperatures during deposition and post treatment promote the formation and growth of graphitic bonded (sp^2) clusters. During the film growth the highest fraction of sp^3 bonds are formed at room temperature.

The two significant peaks in the spectrum of the particle already observed in Fig. 2 b are much more pronounced. The Raman band can only be well fitted by using 4 peaks (Fig. 3). We explain this property by the model that the spectrum is a superposition of a graphitic part and an amorphous part. The particle consists of a graphitic center covered by the amorphous film. Since the Raman scattering cross section of graphitic structures differs from that of the amorphous film, an exact quantification of the fitted peak parameter is not possible, but the model is supported by the data. Thus, the covering film reveals a structure similar to sample *a* and the center is of graphitic nature similar to the graphite target d. The second one can be even a particle from the target that was emitted during the arc spot erosion and incorporated in the growing film.

Table 1. Peak fit parameter of the Raman spectra

Sample	"D" peak position	"D" peak FWHM	"G" peak position	"D" peak FWHM	I_D/I_G
a) 30° C	1355 cm^{-1}	250 cm^{-1}	1530 cm^{-1}	178 cm^{-1}	0.9
b) 500° C	1367 cm^{-1}	320 cm^{-1}	1581 cm^{-1}	103 cm^{-1}	6.4
c) Particle graphitic cluster	1320 cm^{-1}	64 cm^{-1}	1586 cm^{-1}	70 cm^{-1}	0.8
covering film	1335 cm^{-1}	318 cm^{-1}	1511 cm^{-1}	199 cm^{-1}	0.6
d) Target	1333 cm^{-1}	43 cm^{-1}	1580 cm^{-1}	22 cm^{-1}	0.5

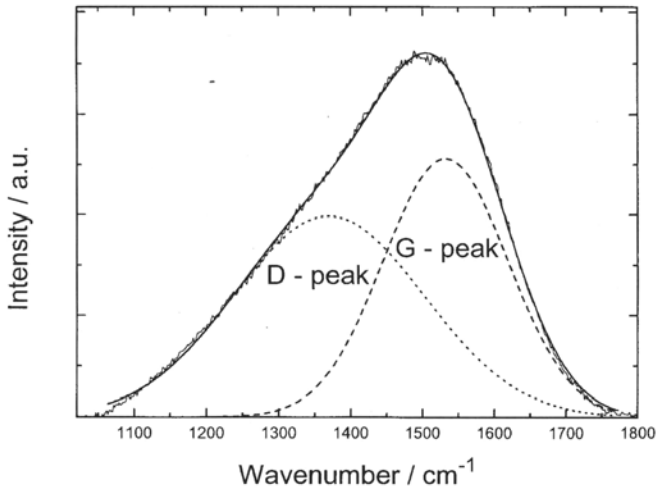

Fig. 3. Peakfit of Fig. 2 a

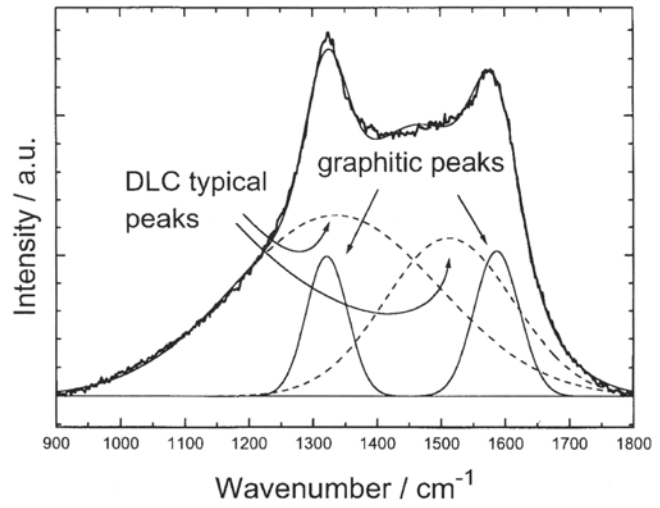

Fig. 4. Peakfit of a particle embedded in the homogeneous film

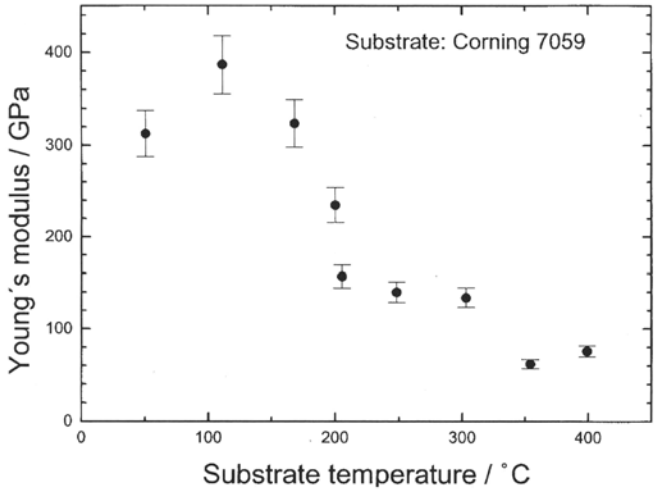

Fig. 5. Temperature dependence of the Young's modulus

In the wavenumber region above 2000 cm^{-1} second order Raman peaks are observable in spectra c and d but not in a and b. This is a second evidence of the crystalline graphitic structure of the particle.

The results of the Raman measurements are in agreement with optical and mechanical properties like the optical gap energy E_G and Young's modulus J. At room temperature the value of E_G = 2.0 eV and J = 400 GPa have been reached. With increased substrate temperature, at 500° C, these properties degrade to E_G = 0.3 eV and J = 50 GPa (Fig. 5).

Additional to Raman investigations, the morphology of the DLC film and embedded particles were carried out by AFM, TEM, electron diffraction and EELS and are reported in the previous article [8].

4 Summary

1. Correlating the specific parameter of the Raman spectra to mechanical and optical properties this method could be a quick and easy method for the film quality.

2. The heat treatment after deposition and the substrate temperature during film growth strongly influence the film structure. Films with diamond-like structure and highest sp^3 content are deposited at room temperature. In order to specify the temperature dependence of film structure during the growth process further experiments are in progress.

3. The particles incorporated in the homogeneous DLC film are of graphitic nature. They could form during the arc erosion on the target surface.

Acknowledgements. The autors wish to express their sincere appreciation to B. Schultrich for helpful discussions and L. Neef and Ch. Dyer of RENISHAW for supporting the measurements. The work was supported by the Bundesminister für Forschung und Technologie, grant no. 13 N 5951A and by the Sächsisches Staatsministerium für Wirtschaft und Arbeit.

References

1. Tuinstra F, Koenig JL (1970) J Chem Phys 53:1126
2. Bachmann PK, Wiechert DU (1992) Diamond Related Mat 1: 422–433
3. Wagner J, Ramsteiner M, Wild C, Koidl P. Phys Rev B 40: 1817
4. Dillon RO, Woolam JA, Katkanant V (1984) Phys Rev B 29: 3482
5. Scheibe H-J, Siemroth P (1990) IEEE Trans Plasma Sci 18:917
6. Cho N-H, Krishnan KM, Veirs DK, Rubin MD, Hopper CB, Bhushan B, Bogy DB (1990) J Mater Res 5:2543
7. Prawer S, Ninio F, Blanchonette I (1990) J Appl Phys 68:2361
8. Scheibe H-J, Drescher D, Kolitsch A, Mensch A, Alers P (1995) Fresenius J Anal Chem (this issue)

2.6 Correlations between Raman scattering and thermal expansion behaviour for CVD and natural diamond

The thermal expansion behaviour of diamond is a difficult property to measure. Owing to the very low thermal expansion coefficient of diamond the required precision of measuring the expansion of a diamond crystal at different temperatures is not easily obtainable. The measurement becomes even more complicated for thin CVD diamond films and nearly impossible when these films are deposited onto a substrate. Since thermal expansion behaviour of a material is linked to the bonding length of its atoms, as is the Raman shift, the authors have studied the use of the Raman shift of diamond, at different temperatures, as a measure for its thermal expansion.

The in this study proposed method is based on a modified Grüneisen theory which has been developed by the authors. The resulting method is easy to apply and a good correlation between the Raman shift of diamond and its thermal expansion behaviour was found. It can be applied to natural diamond as well as to CVD diamond films. Especially its potential use on thin diamond films still attached to there substrate shows an important field of use where conventional methods did not provide satisfactory results.

The method has proven its validity for diamond but is in principle not limited to this material. The authors have done preliminary work on a similar correlation for other cubic crystalline materials such as Silicon and Germanium. The results of this study (unpublished) gave similar results as presented in the now following article, and show therefore a great potential for the proposed modified Grüneisen theory.

In conclusion, the importance of the publication lies in the proposed modified Grüneisen theory as developed by its authors. Further research in this field would be of great scientific value but due to time constrains the authors where not able to extend the study beyond the results here presented.

ELSEVIER

Thin Solid Films 259 (1995) 14–17

thin solid films

Correlations between Raman scattering and thermal expansion behavior for CVD and natural diamond*

P. Alers[a], H.E. Hintermann[a], I. Hayward[b]

[a]*CSEM, Swiss Center for Electronics and Microtechnology, P.O. Box 41, 2007 Neuchâtel, Switzerland*
[b]*Department of Physics, University of Leeds, Leeds LS2 9JT, UK*

Received 29 April 1994; accepted 21 July 1994

Abstract

To successfully use chemical vapour deposition (CVD) diamond thin films in high temperature applications it is important to know their thermal expansion properties. The thermal expansion properties of natural single crystalline diamond have been the subject of many studies. However measuring these properties can be very difficult, especially for CVD diamond films due to the polycrystalline nature of these films.

In this article it is proposed to use Raman shift measurements to determine the linear thermal expansion coefficient of diamond. A theoretical relation, based on the Grüneisen basic definition, to correlate high temperature Raman scattering data and linear thermal expansion data, will be derived. The verification of this relation, using literature data on Raman shifts and linear thermal expansion of natural diamond, is presented. The results will be applied to a series of new Raman shift measurements, obtained on flame and hot filament CVD diamond films, in the temperature range 20–600 °C.

Keywords: Diamond; Raman scattering; Stress; Structural properties

1. Introduction

Because of the potential applications of natural and chemical vapour deposited (CVD) diamond at temperatures up to 1000 °C in electronics and mechanics, it is of considerable interest to know more about their high temperature properties. Thermal expansion is one of these properties and provides information on stresses which can occur upon heating and cooling if diamond is combined with, or deposited on, other materials. These stresses can, for instance, cause cracking and flaking of CVD diamond films deposited on sintered carbide cutting and drawing tools.

The thermal expansion is normally determined by techniques such as X-ray diffraction or dilatometry; data for natural and CVD diamond can be found in the literature [1–5]. However, these measurements can be quite difficult, especially in the case of CVD diamond layers only a few microns thick.

Thermal expansion, like material properties, is in principle related to basic physical properties such as normal vibrational modes. These normal vibrational modes are also found in Raman spectroscopy measurements and can be expressed in the form of Raman peak shifts and peak widths. If one can define the relationship between these Raman data and the thermal expansion over a temperature range, the latter, as a consequence of this, can be determined through Raman spectroscopy measurement.

To find the relation between Raman data and thermal expansion, a theoretical approach based on the classic Grüneisen theory is proposed. It will be demonstrated that a satisfactory relation between Raman data and thermal expansion can be found.

The Raman data used in this paper for natural diamond at elevated temperatures are taken from the literature [6, 7] and the CVD diamond data were measured by the authors.

* Presented at the 21st International Conference on Metallurgical Coatings and Thin Films, San Diego, CA, USA, April 25–29, 1994.

SSDI 0040-6090(94)06442-3

2. Theory

The theoretical approach is based on the classical Grüneisen theory. The definition of the Grüneisen constant is used,

$$\frac{d\omega}{dV} = -\gamma \frac{\omega}{V} \tag{1}$$

where ω is a phonon frequency, V is the atomic volume and γ is the Grüneisen constant. It has been demonstrated by Parsons [4] that it is possible to use the Grüneisen basic assumption to derive an isothermal pressure dependency. For this the atomic volumes of Eq. (1) are replaced by

$$K = \frac{(P_2 - P_1)/(V_1 - V_2)}{V_1} \tag{2}$$

which leads to Eq. (3):

$$\ln\left(\frac{\omega_2}{\omega_1}\right) = -\gamma \ln\left(1 - \frac{P_2 - P_2}{K}\right) \tag{3}$$

where ω_1 and ω_2 are Raman shift expressed in cm^{-1} at pressures P_1 and P_2 ($N\,m^{-2}$) respectively, and K is the bulk modulus expressed in $N\,m^{-2}$. The Raman shift difference between ω_1 and ω_2 relates to ΔP $(P_2 - P_1)$ which in fact represents the stress σ present in the material at a given temperature. Parsons demonstrated a good agreement between Raman and pressure measurement data up to 2.5 GPa, using a Grüneisen constant of 1.19 ± 0.09.

At the same time Parsons proposed to use the complete Grüneisen relation (Eq. (4)), containing the isothermal compressibility χ_T, the temperature-dependent heat capacity $C_v(T)$, and a temperature-dependent Grüneisen parameter $\gamma(T)$, to determine the temperature-dependent linear thermal expansion coefficient $\alpha(T)$:

$$\alpha(T) = \gamma(T) \frac{\chi_T C_v(T)}{V} \tag{4}$$

However, if one looks at the result obtained in such a way on diamond and if one considers materials with negative linear thermal expansion coefficients at low temperatures, e.g. Si and Ge, one finds that the complete Grüneisen theory is not easily applied and the Grüneisen parameter changes drastically with temperature. In the Si and Ge case, the Grüneisen parameter even becomes negative at low temperatures. This makes the practical use of the proposed method difficult and unreliable.

To overcome these difficulties, the authors propose to develop the Grüneisen definition (Eq. (1)) introducing the linear temperature-dependent thermal expansion coefficient $\alpha(T)$, at constant pressure, in a slightly different way, as proposed by Krishnan [5]. In expressing the atomic volume in Eq. (1) as a function of α_T [1]

$$V = V_0(1 + \alpha(T)T)^3 \tag{5}$$

Eq. (6) can be derived,

$$\ln \frac{\omega_T}{\omega_0} = -3\gamma \ln(1 + \alpha(T)T) \tag{6}$$

where ω_T and ω_0 are Raman shifts at temperature T and 0 K respectively expressed in cm^{-1} and $\alpha(T)$ is expressed in K^{-1}. This relation, however, is only applicable on stress-free materials. In the case of stress a supplementary shift would be noticed which is described by Parsons' relation (Eq. (3)).

In Section 4 it will be shown that Eq. (6) holds well for diamond and that γ for natural diamond is a temperature-independent Grüneisen constant with a value of 1.04 ± 0.05. Preliminary work on Si and Ge shows that Eq. (6) holds equally well for these materials, including a good agreement at low temperatures.

3. Experimental

Diamond films were grown by hot filament and combustion flame chemical vapor deposition. The hot filament films were deposited on (100) Si wafers and made freestanding by etching the silicon substrate away [8]. The resulting diamond membrances were ≈ 1 μm thick and exhibited a fine columnar grain structure with an average crystallite size of ≈ 500 nm. The combustion flame films were deposited on molybdenum and became freestanding upon cooling [9]. These films exhibited columnar grains of ≈ 5 μm and were ≈ 30 μm thick. Both film types showed negligible amounts of non-diamond carbon in their Raman spectra.

The Raman spectroscopy measurements were performed with a Renishaw Ramascope 2000 μ-Raman system using the 514.5 nm radiation of an air cooled Ar-ion laser. The 546.07 nm radiation of a mercury lamp was used as an internal standard for the measurements. The precision of the measurements was $\pm 0.5\ cm^{-1}$. A Linkam PU1500 microscope furnace was used to heat the sampes up to 600 °C in air. The temperature stability during the measurements was ± 2 °C. The upper temperature limit of 600 °C is in principle low enough to prevent significant oxidation of the diamond films.

4. Results and discussion

To verify the relationship proposed above the case of natural diamond is presented using Raman spectroscopy and thermal expansion data taken from the literature [1, 2, 6]. In Table 1 the results of a cross fit of two sets of Raman data and two sets of thermal expansion data are shown. For each combination of data the

Table 1
Cross fit of Raman and thermal expansion data using Eq. (6)[a]

	$\omega_0 = 1333.8\ \text{cm}^{-1}$		$\omega_0 = 1333.2\ \text{cm}^{-1}$	
	ω_1, α_1	ω_1, α_2	ω_2, α_1	ω_2, α_2
γ	1.05	1.04	1.05	1.02

[a] α_1, Thermal expansion data [1]; α_2, thermal expansion data [2]; ω, Raman shift data [6]; ω_2, Raman shift data [7].

fitted Grüneisen constant is given. An example of these fitting results is shown in Fig. 1.

It should be noticed that in the literature Raman data used in this article, there exists a difference of about 1 cm^{-1} between the data obtained by Zouboulis and Grimsditch [6] and those from Herchen and Cappelli [7]. This difference however is roughly constant and thus, because γ gives the slope between the Raman and thermal expansion data, has no significant influence on the fitted γ value. However, a small change in the value chosen for ω_0, in both cases, creates a great difference in the linear thermal expansion coefficient, calculated from Eq. (6), at low temperatures. It was found that the best fits were obtained using a value for ω_0 of 1333.8 cm^{-1} in the Zouboulis and Grimsditch case and a value 1333.2 cm^{-1} for Herchen and Cappelli. The literature value [6] of 1333.5 cm^{-1} shift is proposed for ω_0 at 0 K. Considering the experimental error of $\pm 0.5\ \text{cm}^{-1}$ in the literature-proposed value, the values used in the fit for ω_0 are well within this range.

In Fig. 2, the Raman results obtained on two stress-free flame diamond films (flame #1 and flame #2) and one tensile stressed, hot filament membrane (hot filament #1) are shown. The fact that the hot filmament membrane was under tensile stress could easily be determined from its tendency to roll up after the Si had been etched away. The stress was subsequently induced by unrolling the film between the two quarts windows of the hot stage sample cell. The literature data from Zouboulis and Grimsditch [6] and Herchen and Capelli [7] are also plotted.

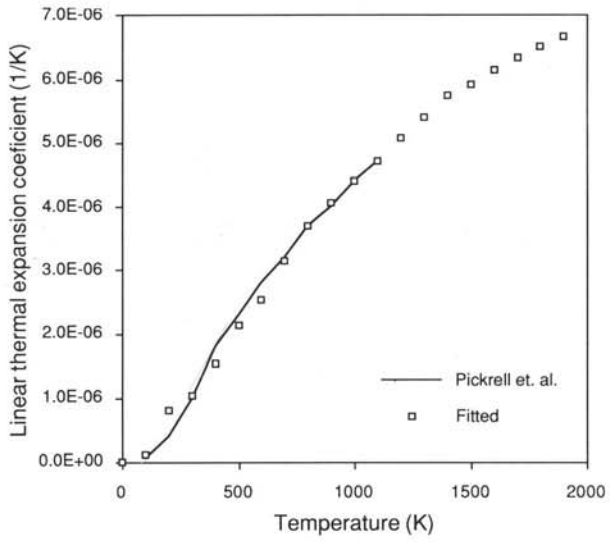

Fig. 1. Experimental linear thermal expansion coefficient data taken from Pickrell et al. fitted using Eq. (6) with $\gamma = 1.04$ and $\omega_0 = 1333.8\ \text{cm}^{-1}$; Raman data from Zouboulis and Grimsditch [6].

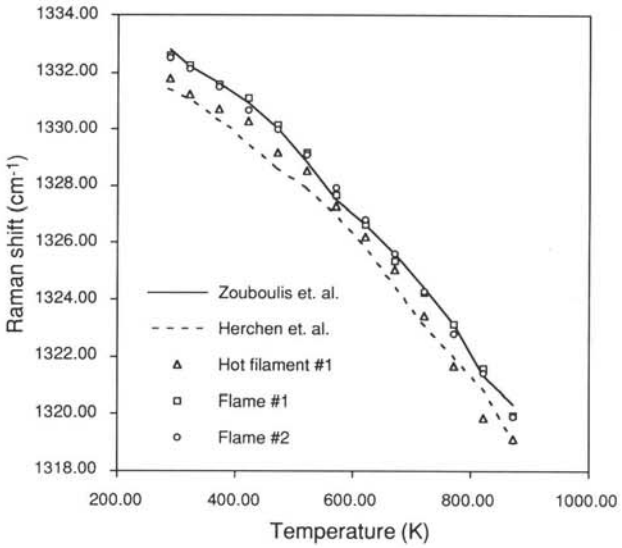

Fig. 2. Temperature behavior of the Raman shift for natural and CVD diamond.

One can see straight away that the data as obtained by Herchen and Capelli somewhat different from those of Zouboulis and Grimsditch and this work. Only the hot filament film, which is known to be under tensile stress comes close to the data of Herchen and Cappelli. We propose that the difference in their measurements might come from the fact that they used a diamond-containing tensile stress, and will therefore use the results from fitting the Zouboulis and Grimsditch data ($\omega_0 = 1333.8\ \text{cm}^{-1}$ and $\gamma = 1.04$) in the discussion of the CVD diamond results.

To verify whether the proposed Eq. (6) is valid for the case of CVD diamond, we calculated the linear thermal expansion coefficient $\alpha(T)$ using the Zouboulis and Grimsditch fitting data ($\omega_0 = 1333.8\ \text{cm}^{-1}$ and $\gamma = 1.04$) and the measured Raman shift. The results of these calculations and the linear thermal expansion data of natural and CVD diamond as obtained by Pickrell et al. [2] are displayed in Fig. 3.

It can be seen that the calculated data for the flame-deposited diamond are in good agreement with the literature data. The slightly lower values, calculated for the flame-deposited diamond, are well within the experimental error of $\pm 0.30 \times 10^{-6}\ \text{K}^{-1}$. If we look now at the linear thermal expansion coefficients calculated for the hot filament film we see that there is a significant discrepancy between the calculated data and literature

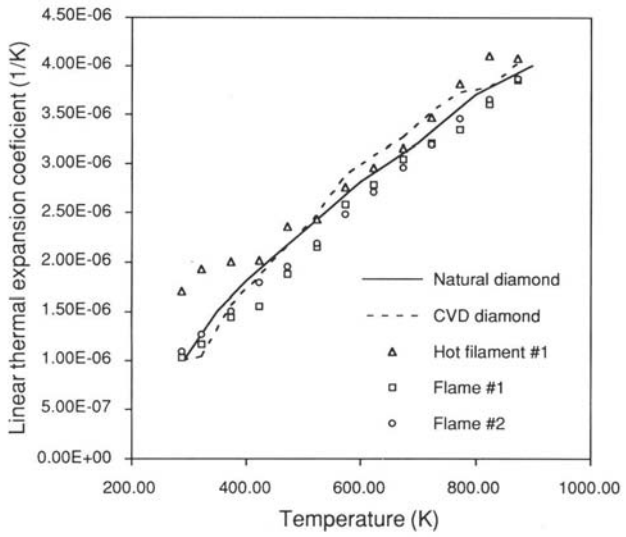

Fig. 3. Experimental linear thermal expansion coefficient data on natural (——), and CVD (– – –) diamond taken from Pickrell et al. [2]. □, ○, △, fits using Eq. (6) with $\gamma = 1.04$ and $\omega_0 = 1333.8\ \mathrm{cm}^{-1}$ and Raman data obtained by the authors.

at low temperatures. Taking into account that the data on the thermal expansion of hot filament CVD diamond films, as obtained by Pickrell et al., are within the experimental error as for natural diamond, and bearing in mind that out hot filament films have similar qualities as those used by Pickrell et al., we believe that the difference in thermal expansion predicted by our calculations is caused by the fact that the film is under tensile stress rather than by the fact that this film shows a different thermal expansion behavior at low temperatures. However, to verify this assumption more measurement results on thermal expansion and Raman shift of CVD diamond films are needed.

4. Conclusions

The Raman shifts of a number of CVD diamond films are measured over temperature range of 20–600 °C. A relation between Raman shift temperature dependence and linear thermal expansion temperature dependence was derived from the Grüneisen basic assumption. This relation was shown to be valid for natural diamond as well as for CVD diamond films.

Acknowledgements

We gratefully acknowledge Renishaw and Linkham Scientific for making the presented measurements possible.

References

[1] G. A. Slack and S. F. Bartram, *J. Appl. Phys.*, *46* (1) (1975) 89.
[2] D. J. Pickrell, K. A. Kline and R. E. Taylor, Thermal expansion of polycrystalline diamond produced by chemical vapor deposition, *Appl. Phys. Lett.*, *64* (1994) 18.
[3] S. B. Quadri, C. Kim, E. F. Skelton, T. Han and J. E. Butler, *Thin Solid Films*, *236* (1993) 103.
[4] B. J. Parsons, *Proc. R. Soc. Lond.*, *A*, *352* (1977) 397.
[5] R. S. Krishnan, *Proc. Ind. Acad. Sci.*, *24* (1946) 45.
[6] E. S. Zouboulis and M. Grimsditch, *Phys. Rev. B*, *43* (15) (1991) 12490.
[7] H. Herchen and M. A. Cappelli, *Phys. Rev. B*, *43* (14) (1991) 11740.
[8] M. Bingelli, J.-P. Dan, A. Grisel, W. Hänni, H. E. Hintermann, P. Krebs and C. Müller, *Proc. 2nd Int. Conf. on Applications of Diamond Films and Related Materials*, MYU, Tokyo, 1993, p. 51.
[9] P. Alers, W. Hänni and H. E. Hintermann, *Diamond Related Mater.*, *2* (1992) 393.

2.7 Friction properties of ta-C and a-C:H coatings under high vacuum

The present study is using a high vacuum tribology testing instrument, used to analyses the friction behaviour of carbon films under high vacuum conditions. The results obtained clearly demonstrate the big influence of environmental conditions on the frictional behaviour of carbon films.

The research done for this publication introduces new ways of modifying carbon films in order to enhance their frictional properties under high vacuum conditions.

Available online at www.sciencedirect.com
SCIENCE DIRECT
Surface & Coatings Technology 200 (2005) 1976 – 1981
SURFACE & COATINGS TECHNOLOGY
www.elsevier.com/locate/surfcoat

Friction properties of ta-C and a-C:H coatings under high vacuum

C. Meunier [a,*], P. Alers [b], L. Marot [c], J. Stauffer [c], N. Randall [d], S. Mikhailov [c]

[a] FEMTO-ST/CREST, 4 place Tharradin, BP 71427, 25211 Montbéliard, France
[b] Vacotec SA, 1 Allée des Défricheurs, CH-2304 La Chaux de Fonds, Switzerland
[c] CAFI, 8A rue Jambe Ducommun, CH-2400 Le Locle, Switzerland
[d] CSM-Instruments Inc., Needham, MA 02494, USA

Available online 15 September 2005

Abstract

The tribological behaviour of ta-C and a-C:H carbon films was analysed by pin-disc tests under high vacuum ($<10^{-3}$ Pa). The tests were executed on a commercial High Vacuum Tribometer (CSM-Instruments) and compared with results obtained under controlled atmospheric pressure conditions.

In this work, we present the comparison of the friction coefficients under high vacuum and under controlled atmosphere conditions of two sets of carbon films, one prepared by Filtered Cathodic Vacuum Arc (FCVA; giving rise to hydrogen-free carbon), the other by Plasma Enhanced Chemical Vapour Deposition (PECVD; leading to hydrogenated carbon). The structure of these films was analysed by Raman and Rutherford BackScattering (RBS) spectroscopy and Elastic Recoil Detection (ERD) as well as by X-rays reflectometry (XRR).

We will demonstrate that under vacuum, FCVA carbon layers do not slide ($\mu=0.5-0.7$) but PECVD carbon films can have a good sliding behaviour ($\mu=0.1-0.3$). An inverse behaviour was observed under controlled atmospheric conditions.

These first results indicate a predominant role of the structure of the films, as analysed by Raman and RBS-ERD spectroscopy as well as by XRR, on the tribological characteristics of the carbon films. In particular, the influence of hydrogen concentration seems to be directly linked to the vacuum tribological behaviour of the coatings.

Keywords: FCVA; PECVD; Carbon DLC; Hydrogen

1. Introduction

Diamond-like carbon films (DLC) offer several unique properties. By varying the ratio between the threefold sp^2 and fourfold sp^3 carbon atoms, the range of the properties of the DLC films can be tailored and the possibility of hydrogenated materials offers an extended range of properties. Then, soft or hard carbon can be obtained, chemically inert with good tribological properties. Extensive reviews on the preparation and properties of these carbon films can be found in [1–4]. The most widespread uses of DLC films are in wear and corrosion protection of magnetic storage media. However, DLC films provide a good flexibility and may find applications in bearings, gears, seals and engine components. They can also be used in oils [5]. However, their friction behaviour is complex and depends on several parameters such as the parameters relevant of the film itself, as well as those relevant to friction test, like the contact pressure, the sliding speed, the materials of the counterparts and their geometry, the composition and the pressure of the atmosphere. Recently, superlubricity of these kinds of films has been reported [6]. In this paper, we compared ta-C prepared by Filtered Cathodic Vacuum Arc (FCVA) and a-C:H prepared by Plasma Enhanced Chemical Vapour Deposition (PECVD) in friction tests with different atmosphere conditions.

2. Experimental

The hard carbon films (ta-C) were prepared by arc discharge in a laboratory system with a commercial source (RHK Technology Company) where the arc was controlled by the trigger voltage (10–25 kV) and filtered. The films

* Corresponding author. Tel.: +33 3 819 946 76; fax: +33 3 819 946 73.
E-mail address: cathy.meunier@pu-pm.univ-fcomte.fr (C. Meunier).

0257-8972/$ - see front matter © 2005 Elsevier B.V. All rights reserved.
doi:10.1016/j.surfcoat.2005.08.013

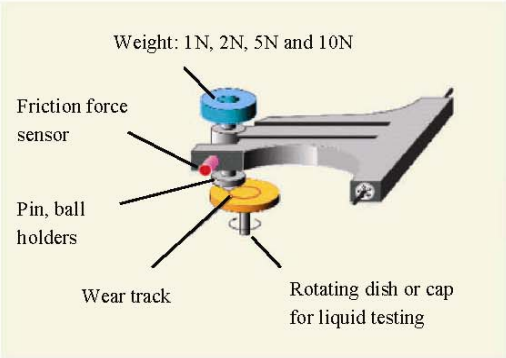

Fig. 1. Schematic diagram of pin (ball) on disk tester.

were deposited onto a titanium alloy TA6V4, mirror-polished discs in 8 mm diameter and 2 mm thickness and titanium coated.

With varying the trigger voltage (12, 15, 20 kV) and keeping constant the bias voltage on the substrate to −2500 V, we obtained three carbon films called ta-C1, ta-C2 and ta-C3. The pulse frequency is kept constant at 1 Hz and 2000 pulses are counted for all the depositions. The starting pressure in the chamber before arc discharge was around 10^{-5} Pa. Roughnesses (Ra) were in the 1–2 nm range for all the FCVA carbon films.

The soft films were prepared by a conventional r.f. PECVD device (13.56 MHz) in methane pressure (kept constant at 1 Pa), the starting pressure was around 10^{-3} Pa. The films were deposited on 440C and 316L steels, mirror-polished discs in 24 mm diameter and 3 mm thickness. The self-bias voltage was the main control parameter of the deposition. Using values of −520 V and −1450 V for self-biased discharges during 2 h, two films were obtained called a-C:H1 and a-C:H2. These deposition conditions lead to good compromise between adhesion and mechanical properties [7]. Roughnesses (Ra) were in the 0.5–1.5 nm range for all the PECVD carbon films.

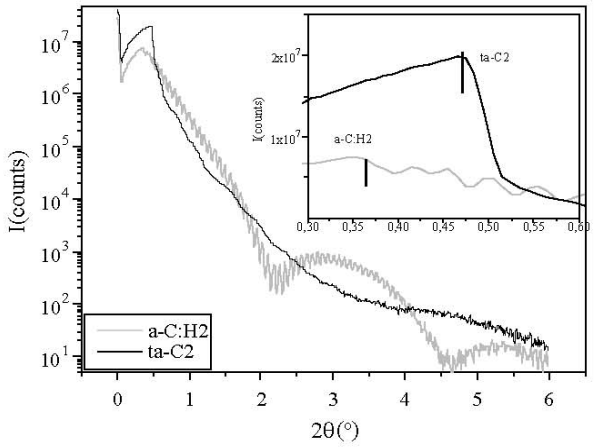

Fig. 2. XRR curves for a-C:H and ta-C films. In the insert, the shift of the critical angle is shown and revealed the difference in density between ta-c and a-C:H.

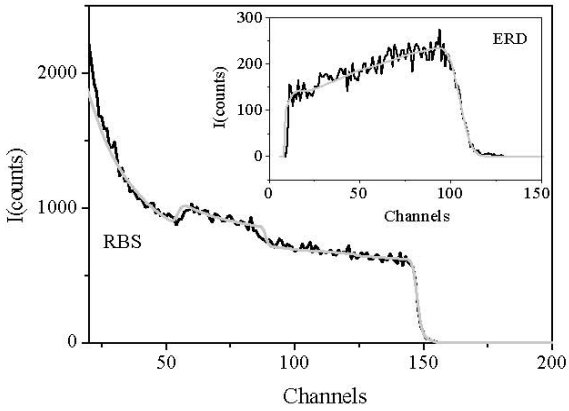

Fig. 3. Some examples of RBS and ERD spectra used for the determination of the hydrogen concentration in the DLC films.

X-rays reflectometry (XRR) measurements were made on a commercial device (X'Pert MPD) with the λCuKα1 radiation (40 kV, 30 mA). The RBS-ERD measurements were performed with a He^{+} 2 MeV ion beam energy and an ion current of 8 nA. Nanoindentation testing on the samples was carried out using a CSM™ nanohardness tester (NHT) to measure hardness and Young's modulus. A maximum load of 1.5 mN was used in order to avoid substrate effects for ta-C samples and the loading and unloading rates were maintained at 3 mN/min. Due to the small thicknesses of the PECVD films, this maximum load ranged between 0.5 mN and 1.5 mN and even in these conditions, substrate influence cannot be avoided. The hardness and Young's modulus were determined by the Oliver and Pharr method [8]. At least five measurements were made at each load on the coated samples.

Wettability tests were done by sessile drop and surface energy has been evaluated by linear extrapolation of the wettability coefficients cosθ with three liquids (diiodomethane, ethylene glycol and water).

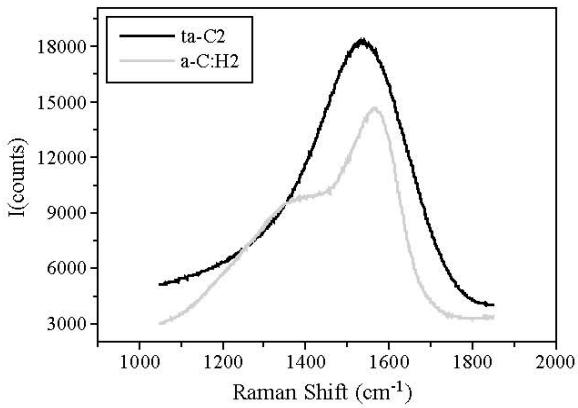

Fig. 4. Comparison of the Raman shift for the two carbon films a-C:H2 and ta-C2.

Table 1
Physico-chemical characteristics of the two sets of films used for the tribological tests

Sample	%H	XRR density	I_D/I_G	γ (mJ/m^2)	θ_{water} (°)	H (GPa)	E (GPa)	t (nm)
a-C:H 1	25	1.55	1.65	40.2	70±4	23	173	190
a-C:H 2	21.5	1.60	1.05	40.6	72±4	21	149	140
ta-C1	1	2.05	0.92	36.5	89±4	27	230	800
ta-C2	1	2.45	0.45	38.5	83±4	38	296	800
ta-C3	1	2.42	0.31	40.2	80±4	45	260	800

Tribological behaviour of the coatings is tested under pin-on-disk measurements with two commercially available unidirectional pin-on-disk tribometers (CSM Instruments), one is a conventional unidirectional tribometer, the second one is a high vacuum tribometer ($<10^{-3}$ Pa). These two devices are in the same geometry and allow a direct comparison of the friction results. All the tests were carried out with a constant load of 2 N at a temperature of 24 °C with a linear speed of 0.02 m/s in ambient air (Relative Humidity 40% RH), in dry nitrogen (4% RH) and under vacuum (10^{-3} Pa, 0% RH). All tests were conducted with 6 mm diameter balls (100Cr6), in order to eliminate differences due to the contact area. The dynamic coefficient of friction values were recorded as a function of sliding distance. A schematic representation of the used head is shown in Fig. 1.

3. Results and discussion

Three aspects of the film were chosen, assumed to be representative of the main properties implied in the friction behaviour, i.e. the diamond-like or graphite-like structure of the carbon film and its hydrogen content, its hardness and its surface energy. The first aspect was studied by determining the density of the film, its composition and the sp^2 tendency. X-rays reflectometry is a powerful technique for the determination of the density of a film. In X-ray measurements, the angle where the absorption by a material begins is called θ_c for critical angle, and some examples of these angles are illustrated in the insert in Fig. 2.

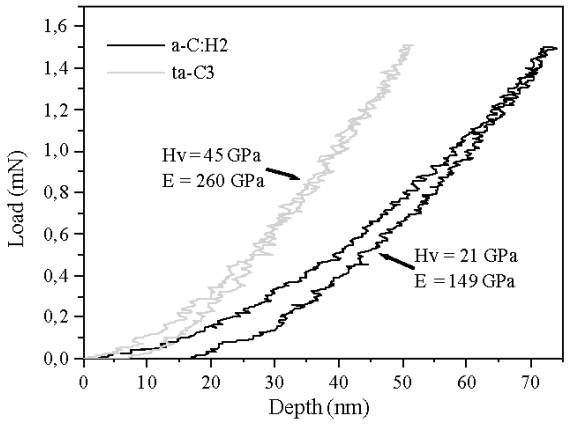

Fig. 5. Comparison of load–unload curves used in the hardness and Young's modulus determination for a-C:H2 and ta-C3 DLC samples.

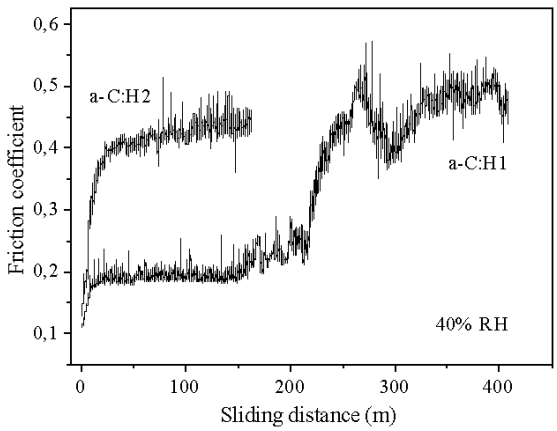

Fig. 6. a-C:H friction coefficient in air (40% rate of humidity RH).

By applying in a first approximation the following relation:

$$\theta_c^2 = \frac{\lambda^2 r_0}{\pi}|\rho| = \frac{4\pi r_0}{k_0^2} N_A |\rho_m| \frac{\sum_j c_j \left(Z_j + \Delta f_j' - i\Delta f_j''\right)}{\sum_j c_j A_j}$$

where θ_c is the critical angle, r_0 is the Thomson radius for the electron, λ_0 is the used wavelength, c_j is the concentration of the element (Z_j, A_j) and $\Delta f_j'$, $\Delta f_j''$ are the correction factors for the dispersion, a value of the average electron density ρ can be extracted. If c_j is known, an average mass density ρ_m can be calculated. This c_j determination is the purpose of the ERD measurements, in the carbon film the hydrogen content is determined. An example of ERD spectra is presented in Fig. 3 for the a-C:H1 deposition conditions onto a silicon substrate. This ρ_m density is an average value of the density, really poorly defined, of the film but can act well as a comparative value between the films [9,10]. In Fig. 2, oscillations are due to the interferences between the surface and the substrate

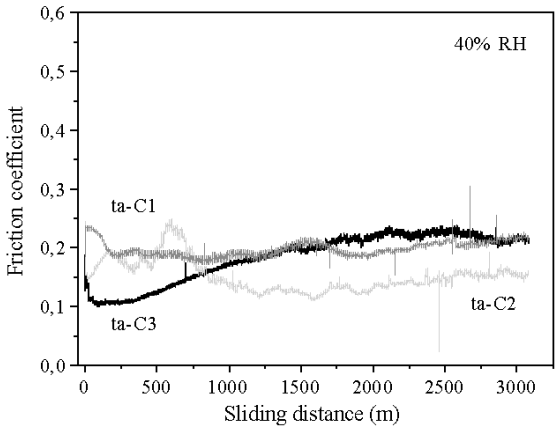

Fig. 7. ta-C friction coefficient in air (40% rate of humidity RH).

Table 2
Friction coefficients for the DLC films for different sliding distances

	μ (starting)		μ (2 m)		μ (5 m)		μ (25 m)	
	Vac.	40% RH	Vac.	40% RH	Vac.	40% RH	Vac.	40% RH
a-C:H1	0.19	0.11	0.17	0.11	0.78	0.15	1.20	0.21
a-C:H2	0.15	0.13	0.12	0.19	0.48	0.19	0.79	0.38
ta-C1	0.27	0.19	0.51	0.23	0.51	0.23	0.49	0.23
ta-C2	0.28	0.24	0.43	0.19	0.61	0.16	0.34	0.15
ta-C3	0.31	0.19	0.60	0.15	0.44	0.15	0.41	0.12

interface and these oscillations can be seen for a film with a thickness below 400 nm if the flatness is good (less than 3 nm roughness). A very thin top surface layer is pointed out in all samples (3–4 nm). This top layer gives rise to the modulation of the interference fringes on PECVD films. The Raman bands are located around 1500 cm^{-1} corresponding to the sp^2 bonding states of the carbon atoms in the film (Fig. 4) and are decomposed in two Gaussian parts called I_D and I_G. The ratio I_D/I_G indicates the sp^2 tendency [11,12] (high value for high Csp^2 content). The values of the hydrogen content, the average mass density and I_D/I_G ratios are grouped in Table 1. One can see that a good range of I_D/I_G value can be achieved by FCVA by modulating the arc striking voltage, translating a good range for the sp^2 tendency in the film structure [13]. By increasing the trigger voltage, the shift of the ion energy provides also a good range for the hardness, which can be decreased by 60% (to 45 GPa–27 GPa to 20 kV–12 kV) for the negative bias voltage of 2.5 kV. An example of hardness test is illustrated in Fig. 5, on these curves we observed higher maximum and residual penetration depths for a-C:H sample due to the sp^3/sp^2 bonding ratio. The highly sp^3-bonded tetrahedral carbon provides a high hardness value of ta-C and therefore give its high elastic behaviour (only 7 nm remaining plastic deformation). We characterized the surface energy for these films by sessile drop and we found the slightly hydrophilic behaviour of these films with a contact angle for water varying between 70° and 89°. But these water angles

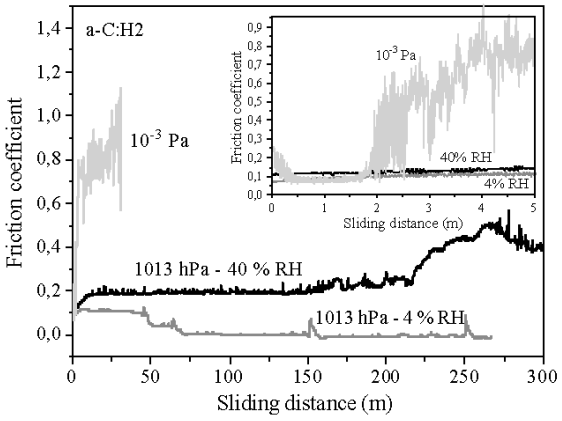

Fig. 8. Influence of the atmosphere conditions on the a-C:H1 friction coefficient.

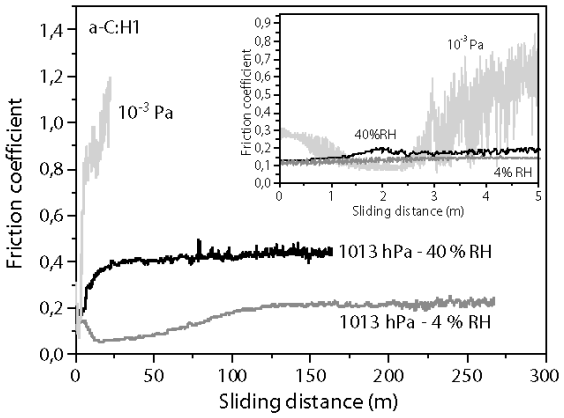

Fig. 9. Influence of the atmosphere conditions on the a-C:H2 friction coefficient.

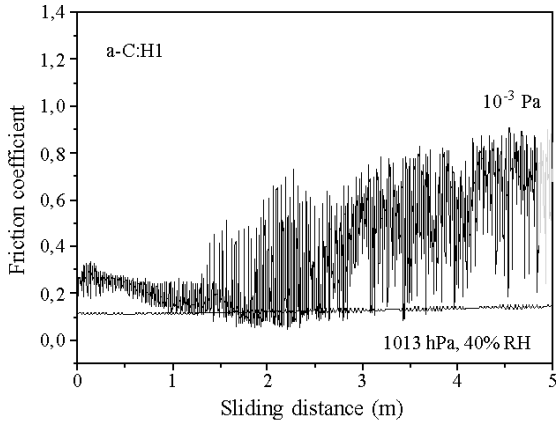

Fig. 10. Comparison of the behaviour of the a-C:H1 film under vacuum and air.

showed also a not so good wettability of the carbon surfaces by the liquid water, so poor adsorption of water can be expected. However, the surface sensitivity of the wettability

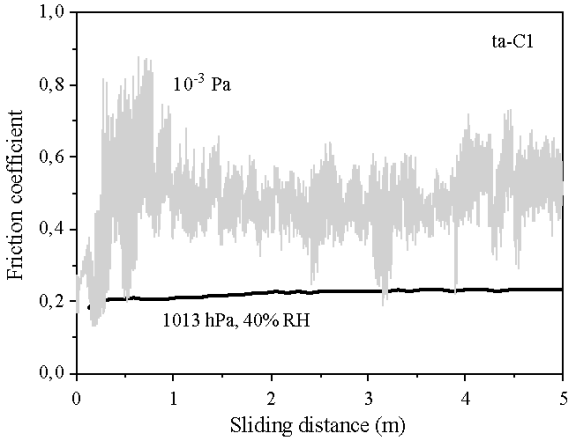

Fig. 11. Comparison of the behaviour of the ta-C1 film under vacuum and air.

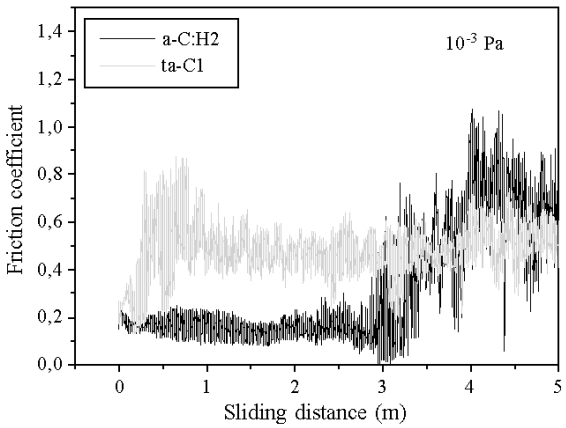

Fig. 12. Comparison of the behaviour of the ta-C1 and a-C:H2 under vacuum and air.

test is about one monolayer and does not correspond to the whole thickness of a film. Some little differences can be found between ta-C and a-C:H sets and we showed that the surface energies of the ta-C films can reach those of the hydrogenated films (Table 1). We can expect a better variability of the water wettability for the unhydrogenated carbon films than for hydrogenated films.

In Figs. 6 and 7, we compared the friction behaviour in air (40% RH) as a function of a sliding distance for the two sets of films. In Table 2, we extracted some friction coefficients during the ball-disk tests at different sliding distances. Firstly in accordance with the water wettability, the friction coefficient for the DLC films are lower on the first sliding meters when surface energy is higher (40% RH). However, the fracture of the a-C: H film occurs earlier than in the ta-C film, the metal–metal friction coefficient is found after 170 and 220 m for a-C:H1 and a-C:H2, respectively, partially due to the weak thickness of PECVD films. In the case of ta-C films, this phenomenon is not observed even after 3 km. Secondly, the fact that the friction is better when dry nitrogen is used (4% RH) for all the samples is in agreement with Zhang et al. [14] and Miyoshi et al. [15] (example for a-C:H films; Figs. 8 and 9). The inert nitrogen gas in the environment might be beneficial to the formation of a transfer layer on the ball, which subsequently acts as lubricating layer, resulting in little wear debris formation. Finally, in vacuum, for a-C:H films (Fig. 10), a friction coefficient below 0.1 can be achieved after 50 cm path whereas the ta-C films cannot slide below 0.15 (Fig. 11), but the general behaviour is a rapid failure of all the coatings. Under vacuum, a better sliding distance is obtained with a-C:H films rather than ta-C. ta-C films showed similar behaviour than diamond [16]. These results are in good accordance with others works [17–22]. Low friction of such DLC films can be attributed to a different viscoplastic behaviour of the films leading or not, to a transfer layer that has weak chemical or physical interaction with the sliding counterparts [23]. Fukui et al. showed that high-order mass fragments of hydrocarbons could be found in the wear track as well as in the transfer layer [24].

In vacuum, the difference between ta-C and a-C:H films (Fig. 12) can be explained by the hydrogen desorption from the film during friction as proposed by Fontaine et al. [25]. This hydrogen motion can lubricate the surfaces in contact and so reduces the adhesion and friction.

4. Conclusions

We have shown that the sliding behaviour of the studied DLC films can be linked to both their material composition as well as to the experimental environmental conditions. More specifically, it was found that changes in humidity of the environmental conditions, the initial friction coefficient of a-C:H films decreases with decreasing percentage of RH. However, the sliding lifetimes of the a-C:H films show an initial increase going to lower humidity, but are extremely reduced at 0% RH (under vacuum). For ta-C films, the initial friction coefficient is higher under vacuum conditions and moreover its sliding lifetime is nearly inexistent for these thicknesses. We believe that the fact that the ta-C films, under vacuum conditions, have an extremely short sliding lifetime, as compared to the a-C:H films, can be directly linked to the material composition, especially the hydrogen content. Hence, under vacuum conditions, when no surface absorbant can act as lubricant, film composition will be the predominant factor in sliding behaviour. With respect to sp^2/sp^3 ratio and thus resulting hardness and modulus of the films, it was found that in the presence of lubricant (water), hardest films show a better sliding lifetime whereas under vacuum conditions, due to material composition, the soft films (a-C:H) show better sliding lifetimes. The authors therefore believe that the combination of highly hydrogenated DLC with hard ta-C opens new opportunities for improving DLC sliding behaviour on extreme environmental conditions.

Acknowledgements

We want to thank VACOTEC SA for their technical support in the vacuum devices.

This work was partially supported by the FEDER grant PIC INTERREG3 no. A21AJ/9.3/1.

References

[1] J. Robertson, Mater. Sci. Eng., R Rep. 37 (4–6) (2002) 129.
[2] A. Grill, Diamond Relat. Mater. 8 (2–5) (1999) 428.
[3] R. Hauert, U. Muller, Diamond Relat. Mater. 12 (2003) 171.
[4] C. Donnet, A. Grill, Surf. Coat. Technol. 94–95 (1997) 456.
[5] H. Ronkainen, S. Varjus, K. Holmberg, Wear 222 (1998) 120.

[6] A. Erdemir, Tribol. Int. 37 (2004) 577.
[7] E. Tomasella, L. Thomas, M. Dubois, C. Meunier, Diamond Relat. Mater. 13 (2004) 1618.
[8] W.C. Oliver, G.M. Pharr, J. Mater. Res. 7 (1992) 1564.
[9] L.G. Parrat, Phys. Rev. 95 (1954) 359.
[10] C. Meunier, E. Tomasella, S. Vives, S. Mikhailov, Diamond Relat. Mater. 10 (2001) 1491.
[11] F. Tuinstra, J.L. Koening, J. Chem. Phys. 53 (1970) 1126.
[12] A.C. Ferrari, J. Robertson, Phys. Rev., B 61 (2000) 14095.
[13] C. Meunier, F. Munnik, J. Stauffer, E. Germann, S. Mikhailov, Thin Solid Films 482 (2005) 197.
[14] W. Zhang, A. Tanaka, K. Wazumi, Y. Koga, Thin Solid Films 413 (2002) 104.
[15] K. Miyoshi, B. Pohlchuck, K.W. Street, J.S. Zabinski, J.H. Sanders, A.A. Voevodin, R.L.C. Wu, Wear 225–229 (1999) 65.
[16] K. Miyoshi, D.H. Buckley, Appl. Surf. Sci. 6 (1980) 161.
[17] A.K. Gangopadhyay, P.A. Willermet, M.A. Tamor, W.C. Vassell, Tribol. Int. 1 (1997) 9.
[18] C. Donnet, T. Le Mogne, L. Ponsonnet, et al., Tribol. Lett. 4 (1998) 259.
[19] R. Gilmore, R. Hauert, Surf. Coat. Technol. 133–134 (2000) 437.
[20] J. Andersson, R.A. Erck, A. Erdemir, Wear 254 (2003) 1070.
[21] Se Jun Park, Jong-Kuk Kim, Kwang-Ryeol Lee, Dae-Hong Ko, Diamond Relat. Mater. 12 (2003) 1517.
[22] H. Ronkainen, S. Varjus, J. Koskinen, K. Holmberg, Wear 249 (2001) 260.
[23] J.C. Sanchez-Lopez, C. Donnet, J.L. Loubet, M. Belin, A. Grill, V. Patel, C. Jahnes, Diamond Relat. Mater. 10 (2001) 1063.
[24] Haruyo Fukui, Miki Irie, Yoshiharu Utsumi, Kazuhiko Oda, Hisanori Ohara, Surf. Coat. Technol. 146–147 (2001) 378.
[25] J. Fontaine, C. Donnet, A. Grill, T. Le Mogne, Surf. Coat. Technol. 146–147 (2001) 286.

3 Conclusions and outlook

The present thesis is the result of a long process of research and publications alternated by pauses in the ongoing work resulting from the changing professional environment of its author. During the years past the first publications some of the initial conclusions prepared for this final chapter have become reality. The author therefore decided to present the in their initial form with added comments indicating their present value and status.

"The field of diamond and diamond like carbon materials has been under continues development over the last decade. From the discovery of diamond and DLC synthesis towards its applications a continuing progress is being made. Along with the increasing importance a revival of Raman spectroscopy, a particularly powerful method for carbon deposit analysis, has taken place."

These were the basic observations made by the author reflecting the early part of his thesis work. Each of the above point were developed as follows:

"DLC has become a widely used industry coating technique, with its application in area's ranging from car engines to computer hard disks. Progress is being made in this field especially on the reliability of the deposition processes and the adhesion of DLC on different substrate materials. Due to its relative ease of deposition, DLC is becoming one of the principal thin film coatings used in industry's high tech applications. The properties of the deposit can be tuned to range from graphite towards almost pure diamond and therefore a number of new applications are to be expected."

DLC is presently still a very important coating material. Major progress has since been made in the price of the coating (became much cheaper, comparable to already existing hard coatings like TiN etc.). The application field has also expanded from the initial field of material wear protection into optical and electronic applications. The variety of different DLC compositions has widened and a great number of doped coatings (Metal, electronic) are now available. The DLC coating (and other carbon form derivatives) is now an industry wide standard, the ongoing research effort in this field remains very strong and is now mainly application driven. Some of those recent developments are reflected in the last publication "Friction propertie**s** of ta-C and a-C:H coatings under high vacuum" presented in this thesis.

"Diamond deposition is only now producing its first commercial applications. Its future lies in the unique properties of diamond. To be able to exploit them, major technical progress is still needed. At the moment diamond produced by synthesis is as expensive as natural diamond. The added advantage comes from the fact that by CVD method the diamond can be deposited as a thin film. To become of real use problems like adhesion on different materials and deposition on large areas have to

be solved. Nevertheless, diamond will create its place in the industry field of coatings. Its applications will probably stay limited, due to the high expense involved and the relatively complicated technology. Especially DLC will be a concurrent due to its comparable properties and its more accessible technology."

The above is presently still true. Although progress has been made in both deposition methods as well as in practical application of the coatings, the use of diamond coatings has remained limited to a few successful applications (cutting tools, heat sinks, electrodes, AFM tips etc.). Although for those applications diamond gives superior results, in main stream use DLC and other coatings mostly prove to be more economic and easier applicable.

"Raman spectroscopy has come a long way over the last few years. This is mainly due to a remarkable technical progress, which has makes the technique more accessible. Slow equipment which required a skilled operator and a considerable capital investment, has been replaced by easy to operate installations which provide quick results at a reasonable price. The parallel development of these new Raman instruments and the diamond and DLC deposition methods has greatly helped to make Raman spectroscopy increasingly popular. It has proven to be the most powerful tool to characterise diamond and DLC.

Future development is to be expected in two fields. First even easier and less expensive equipment will be introduced to the market. These systems will be dedicated to a limited number of applications and do thus not require all elements of a full Raman system. On the other hand the understanding of Raman results has been greatly improved and automated expert libraries, like the ones used in IR spectroscopy, are being developed. The properties of DLC can already be automatically evaluated by computer software routines. Other applications are being developed for automatic drug detection to be used in airports. Over the next couple of years Raman spectroscopy will be probably become as important as IR spectroscopy is at present for modern industry."

The conclusions presented have become reality, Raman equipment has even more come down in price and has also been extended by a range of new, small and inexpensive instruments. The new generation of Raman instruments are often as small as a cigarette box and used fibre optic probes dedicated to their application. The field of industry applications has widened greatly (chemical process monitoring, environmental monitoring, new science applications including near field optical microscopy) and automated software for results analysis is now readily available. A new range of combined instruments is now also offered (Raman combined with UV/VIS or NIR, Raman combined with SEM of AFM).

Since the start of this thesis a great number of new developments in the field of diamond, DLC coatings and their analysing by Raman and other methods have occurred. These developments will continue for quite some more time since the potential of all subjects presented has not by far been covered yet.

Further development can be expected especially in the field of diamond coatings. Here the author expects new technologies related to semiconductor applications, which will finally open the market for large scale diamond film usage.

DLC has already established itself as a main stream coating technology. In this field further specialization and enhancement of certain properties can be expected. The author does not expect many new applications for DLC but more a consolidation and steady growth of the existing market. The research in this area is therefore expected to be aiming at cost and yield improvements and not so much on fundamental properties.

Finally in the field of Raman spectroscopy, further miniaturization and cost reduction is expected. The application field will further expand and the method will probably become as widely used as IR and UV/VIS spectroscopy.

The presented thesis has proven to be an ongoing challenge, which has been able to count on a great number of very supportive friends, colleagues and relatives. The author believes it illustrates well the fact that, although the period in which the work has been completed has been long, the content of even the starting part is still relevant to today's scientific community. The subjects discussed in this document are presently being pursued by many research groups world wide. The Author hopes that they find the same passion and joy he experience working on these subjects.